# CASE STUDY ON GEOLOGICAL HAZARD IN KARST AREAS



**by**

**The Malaysia-Thailand Working Group**

**A joint project carried out by**
**Minerals and Geoscience Department, Malaysia**
**and**
**Department of Mineral Resources, Thailand**

**The Malaysia-Thailand Border Joint Geological Survey Committee (MT-JGSC)**
**2022**

# CASE STUDY ON GEOLOGICAL HAZARD IN KARST AREAS

## CASE STUDY 1: SINKHOLES GEOLOGICAL HAZARD IN KINTA VALLEY, PERAK, MALASIA

## CASE STUDY 2: ROCK FAILURE ASSESSMENT ON PALEO-COLLAPSE IN CASE THE PRASAT HIN PAN YOD TOURIST SITE, SATUN GEOPARK, THAILAND


**By**

**The Malaysia-Thailand Working Group**



**A joint project carried out by**

**Department of Mineral and Geoscience, Malaysia**

**and**

**Department of Mineral Resources, Thailand**

**The report is submitted to the Malaysia-Thailand Border Joint Geological Survey Committee**

**(MT-JGSC)**

**August 2022**

# PREFACE

This report on the Case Study of Geological Hazard in Karst Area is the result of close co-operation between the Department of Mineral and Geoscience Malaysia and the Department of Mineral Resources, Thailand. The study was carried out independently by both the Malaysia and Thailand Working Groups specifically in karst areas on each side of the countries.

This report is focused on the geological hazard in Kinta Valley Perak, Malaysia and Phang Nga Province, Satun, Thailand, and the result of this study is reported with the title Case Study on Geological Hazard in Karst Area, "Case Study 1 Case Study - Sinkholes Geological Hazard in Kinta Valley, Perak" and "Case Study 2: Case Study - Rock Failure Assessment on Paleo-Collapse in Case the Prasat Hin Pan Yod Tourist Site, Satun Geopark".

Based on the findings, the occurrence of sinkhole of Kinta Valley was contributed by several factors which is lithology, land use / land cover, slope, elevation, landform, groundwater acidity, distance to fault, topographic wetness index and groundwater level and mostly triggered by far field earthquake and climate change, while the rockfall and rockslide hazard of Prasat Hin Pan Yod tourist site, Phang Nga Province is dominate by the wedge failure and mostly triggered by heavy rain and ground shaking. Based on the SMR analysis, a new safe route is recommended for the tourist.

It is hope that the findings of both study cases could be used to aid local government and related agencies in development planning and geological disaster mitigation and will be published to local people for knowledge sharing.

Mr. Hisamuddin bin Termidi
Director General
Department of Mineral and Geoscience
Malaysia
August 2022

Dr. Pongboon Pongtong
Director General
Department of Mineral Resources
Thailand
August 2022

# ACKNOWLEDGEMENTS

The Malaysia and Thailand Working Groups would like to thank the Director-General of the Minerals and Geoscience Department Malaysia (JMG) and the Director-General of the Department of Mineral Resources, Thailand (DMR) for their encouragement, support and funding of this project.

Thanks also to all officers and staffs of the Minerals and Geoscience Department Malaysia and Department of Mineral Resources, Thailand for their involvement in this project either directly or indirectly.

We extend special thanks to Dr. Che Aziz Ali, Geology Program, Faculty of Science and Technology, National University of Malaysia (UKM), for helpful advice, valuable suggestion, and encouragement in completing this study.

We also would like to thank the Department of National Parks, Wildlife and Plant Conservation, Thailand, for facilitating access to site of Prasat Hin Pan Yod. We also thank the Bureau of Environmental Geology, Department of Mineral Resources (DMR), Thailand, for providing facilities during the fieldwork in Satun.

# EXECUTIVE SUMMARY

In Malaysia, sinkhole occurrence has been a hindrance to development and caused considerable loss to the economic and local authorities. There have been 270 cases recorded since 1970 in the developed region of Kinta Valley, primarily consisting of Kinta Limestone. This study aims to identify contributing and triggering factors of sinkhole occurrence in Lembah Kinta from the literatures, meteorological data, geological data and statistical analysis by using the Frequency Ratio (FR) Method and Analytical Hierarchy Process (AHP). Method by producing susceptibility index map. This susceptibility index map is aimed to be used by the authority or local government for development planning and geological hazard management.

Four main factors were identified which are topographical, geological, anthropological, and hydrogeological consisting of 9 conditioning factors: elevation, gradient, topographic wetness index, lithology, fault density, landform, groundwater level, land use/land cover index (LU/LC) and groundwater alkalinity. All conditioning factors were analyzed and translated into spatial layers using GIS software. A total of 58 sample point consisting of a 1970's-2020's sinkhole record was used for the sampling. FR analysis results show that the lithology factor has the highest prediction rate (4.597105), follow by land use/land cover (3.670758), slope (2.991155), elevation (2.96571), landform (2.931122), groundwater alkalinity (1.972701), distance to fault (1.738532), topographic wetness index (1.259796) and groundwater level (1.00). Validation assessment shows that high and very high susceptibility classes represent 93.10% occurrence of sinkholes combined with the previous study's findings, it is concluded that the formation of a sinkhole in Lembah Kinta is triggered by a far-field earthquake and seasonal changes.

Rockfall and rockslide incident is currently the severe geohazard affecting marine tourism in Thailand. Two years ago, some tourist sites, located both in the Gulf of Thailand and the Andaman Sea, were prohibited to access. The tourist site of Prasat Hin Pan Yod chamber, developing from a paleo-collapse sinkhole on Koh Khao Yai island of Satun province, is now confronting unsafe caused by rockfall and rockslide hazards as well. The study applied the integration of simple multi-criteria in GIS, traditional stereographic projection analysis, and Slope Mass Rating (SMR) to determine rock mass instability of Ordovician limestone and to find a safe route entrancing the Prasat Hin Pan Yod limestone chamber. Various discontinuities on natural outcrop slope relating to geomorphological features were investigated and assessed the stability: sea cliff, sea cave, and also a former broken block of the rockslide.

The study result was found that the dominant wedge failure of rock fall can occur in many places of the Prasat Hin Pan Yod tourist site. Small pieces of broken limestone hanging at high places and also filling in rock niches are often found in the field investigation. Rock fragments splitting off rock face may fall away down whenever it is triggered by heavy rain or ground shaking. Direct toppling failure is the comparative subordinate of the rock fall hazard. Its negative impact is similar to wedge failure and difficulty to perform risk management as well. Planar failure and

toppling failure seem to be low scores and rarely occur the two big severe events happened from that failure modes and revealed obviously field evidence of broken blocks. The precedent event was caused by toppling failure and the latest, February 20, 2021, was originated by planar failure. The traditional way is now not suitable for getting through the Prasat Hin Pan Yod chamber. Depending on the high SMR score and a few joint intersections causing the geohazard, a narrow strait located between the former broken block and sea cliff is determined as the new safe route for tourists. Moreover, Kayak should be adopted to use for moving over that narrow place and also permit a one for in and out. The tourist numbers to visit attractive places should be controlled. For more safety, helmet is one of the simple essential tools for tourists and it will help them to protect the hanging rock fallen from sea cliffs or high places.

# CONTENT

# LIST OF FIGURES

CASE STUDY 1: SINKHOLES GEOLOGICAL HAZARD IN KINTA VALLEY, PERAK, MALASIA



CASE STUDY 2: ROCK FAILURE ASSESSMENT ON PALEO-COLLAPSE IN CASE THE PRASAT HIN PAN YOD TOURIST SITE, SATUN GEOPARK, THAILAND

# LIST OF TABLE

CASE STUDY 1: SINKHOLES GEOLOGICAL HAZARD IN KINTA VALLEY, PERAK, MALASIA



CASE STUDY 2: ROCK FAILURE ASSESSMENT ON PALEO-COLLAPSE IN CASE THE PRASAT HIN PAN YOD TOURIST SITE, SATUN GEOPARK, THAILAND

# GLOSSARY OF FOREIGN WORDS

## MALAYSIA WORDS

| WORDS | MEANING |
|---|---|
| *Bandar* | Town |
| *Bukit* | Hill |
| *Daerah* | District |
| *Gempa bumi* | Earthquake. Earth = bumi, quake = gempa |
| *Kampung* | Village |
| *Keterancaman* | Susceptibility |
| *Lembah* | Valley |
| *Lubang benam* | Sinkhole. sink = benam, lubang = hole |
| *Sungai* | River |

## THAILAND WORDS

| WORDS | MEANING |
|---|---|
| *Koh* | Island |
| *Mu Koh* | Group of island |
| *Khao* | Mountain |
| *Prasat* | Castle |
| *Hin* | Rock |
| *Pan* | Thousand |
| *Yod* | Peak |
| *Yai* | Great / Large |

# CASE STUDY 1: SINKHOLES GEOLOGICAL HAZARD IN KINTA VALLEY, PERAK, MALASIA


## ABSTRACT

In Malaysia, sinkhole occurrence has been a hindrance to development and caused considerable loss to the economic and local authorities. There have been 270 cases recorded since 1970 in the developed region of Kinta Valley, primarily consisting of Kinta Limestone. This study aims to identify contributing and triggering factors of sinkhole occurrence in Lembah Kinta from the literatures , meteorological data, geological data and statistical analysis by using the Frequency Ratio (Bieniawski and Metallurgy) Method and Analytical Hierarchy Process (AHP). Method by producing susceptibility index map. This susceptibility index map is aimed to be used by the authority or local government for development planning and geological hazard management. Four main factors were identified which are topographical, geological, anthropological, and hydrogeological consisting of 9 conditioning factors: elevation, gradient, topographic wetness index, lithology, fault density, landform, groundwater level, land use/land cover index (LU/LC) and groundwater alkalinity. All conditioning factors were analyzed and translated into spatial layers using GIS software. A total of 58 sample point consisting of a 1970's-2020's sinkhole record was used for the sampling. FR analysis results show that the lithology factor has the highest prediction rate (4.597105), follow by land use/land cover (3.670758), slope (2.991155), elevation (2.96571), landform (2.931122), groundwater alkalinity (1.972701), distance to fault (1.738532), topographic wetness index (1.259796) and groundwater level (1.00). Validation assessment shows that high and very high susceptibility classes represent 93.10% occurrence of sinkholes combined with the previous study's findings, it is concluded that the formation of a sinkhole in Lembah Kinta is triggered by a far-field earthquake and seasonal changes.



**Keyword:** Kinta Valley, Sinkhole, Susceptibility, AHP, Frequency Ratio

# 1. INTRODUCTION

Sinkholes are prominent disasters that commonly take place in karst areas, as it was defined as a hole formation that is caused by the natural erosion (dissolution) process which is active in the tropical environment (Fournier, 1962; Douglas, 1969 in Ahmad Khairut Termizi et al., 2018). Since 1970, there are numerous cases of sinkholes formation have been recorded in Peninsular Malaysia, especially in Kinta Valley, Perak (270 cases, Ahmad Khairut Termizi et al, 2018), Kuala Lumpur and Ampang Jaya, Selangor (33 cases, Banks et al., 2020) and Perlis and Kedah (6 cases, Yunus Abdul Razak et al., 2003) causing economic distress to the government, as well as a landowner and local authorities. Some properties and infrastructural losses are reported, involving residential houses, government premises and roads. The sinkholes occurrence became worse in densely populated and rapidly developed susceptible karst areas.

Although there is no loss of lives had ever been reported, it is crucial for the government to take relevant measures in reducing the risk to the environment and communities, as stated in the Eleventh Goals of Sustainable Development Goal by United Nation – *'Make cities and human settlements inclusive, safe, resilient, and sustainable, by Disaster Risk Reduction (DRR)'* (United Nations, 2015). This paper will summarize the affecting factors that contribute and trigger the sinkhole incident locally and regionally, susceptibility maps of sinkholes, and mitigation measures to reduce the risk of sinkholes.

# 2. OBJECTIVES

The objectives of this study are as follows:

i) To identify the local and regional factors that contribute to and trigger the sinkhole formation in the study area
ii) To generate the sinkhole susceptibility model for the study area by considering local and regional factors

## 3. LOCATION AND GEOGRAPHY OF STUDY AREA

The study area is located in the Kinta Valley,Perak, covering three (3) districts (Ipoh, Batu Gajah and Kampar) which are geographically charaterised by populated lowlands valleys and mountainous areas of Titiwangsa Ranges in the east and Kledang Ranges in the west (Figure 3.1). The study area is well-connected by rail track and highways which span from the Thailand-Malaysia Border in the north of Peninsula Malaysia until Johor Bharu, Johor in the southern part of Peninsula Malaysia. The Kinta Valley is also a part of Kinta Valley Geopark which has been established since 2017 and are well-known for its karst landscape and karst features such as caves, lakes, and limestone pillars. This spectacular landscape could be attributed to the extreme tropical climates of the area; humid season with all year-round rainfall accumulation. Most of the caves can be seen from the highways and are used as temples and recreational areas.

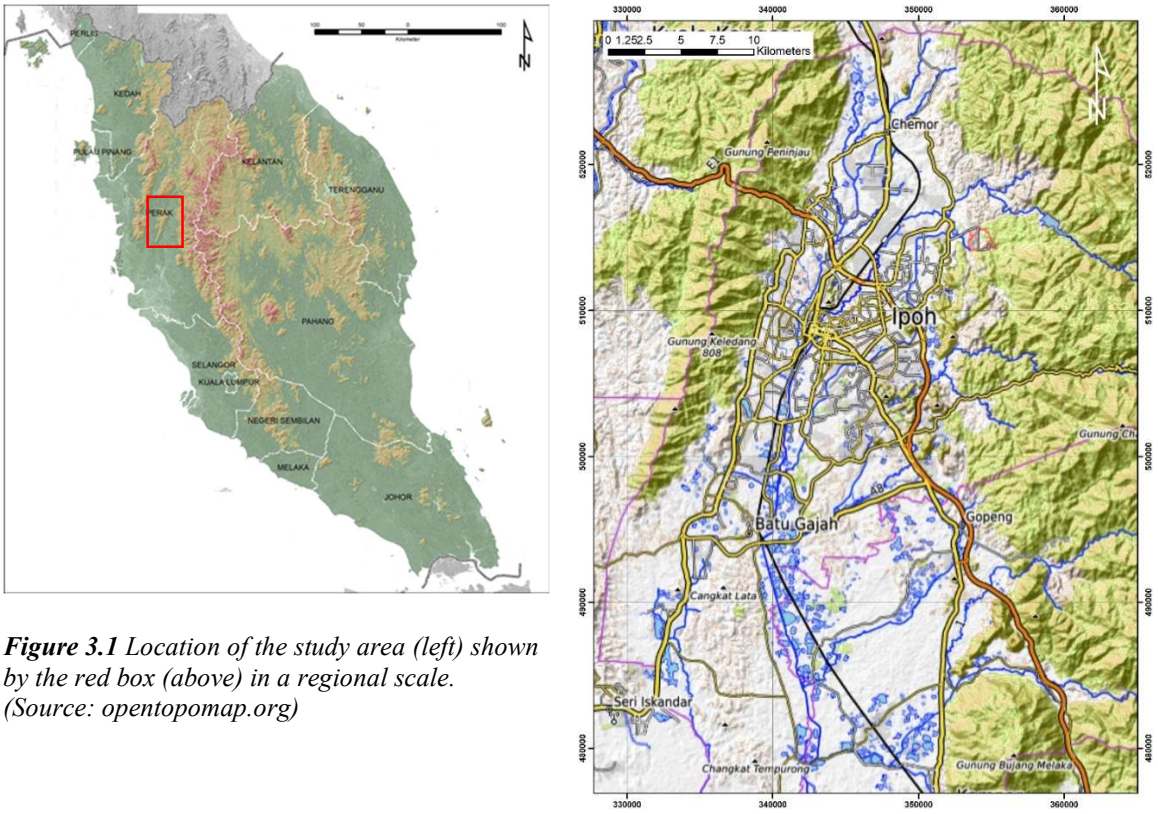


***Figure 3.1*** *Location of the study area (left) shown by the red box (above) in a regional scale. (Source: opentopomap.org)*

In terms of land use, 48% of Kinta Valley has been subjected to the tin mining activities since the colonial times as early as 1850's and most of the ex-mine area has been reclaimed as residential, commercial, and agricultural sites (Ahmad Khairut Tarmizi et al., 2018). At present, the Kinta Valley is a main area for limestone resources in Malaysia.

# 4. GEOLOGY AND GEOLOGICAL HAZARD

## 4.1. Geology of Study Area

Kinta Valley is situated in the Western Belt province of Peninsular Malaysia. The lowlands of the Kinta Valley consist of clastics and limestone bedrocks known as the Kinta Limestone dated Devonian to Permian age (Suntharalingam, 1968), while the mountainous area consist of Kledang Granite forming the western boundary of Kinta Valley and Main Range Granite at the eastern site of the valley (Figure 4.1). The age of Kledang Granite is estimated to be ranging from 213-193 Ma, while the age of Main Range Granite is ranging between 205-193 Ma based on radiometric dating (Krahenbuhl, 1991) and both lithodemic units are made up of coarse-grained porphyritic biotite granite (Ros Fatihah, 2018).

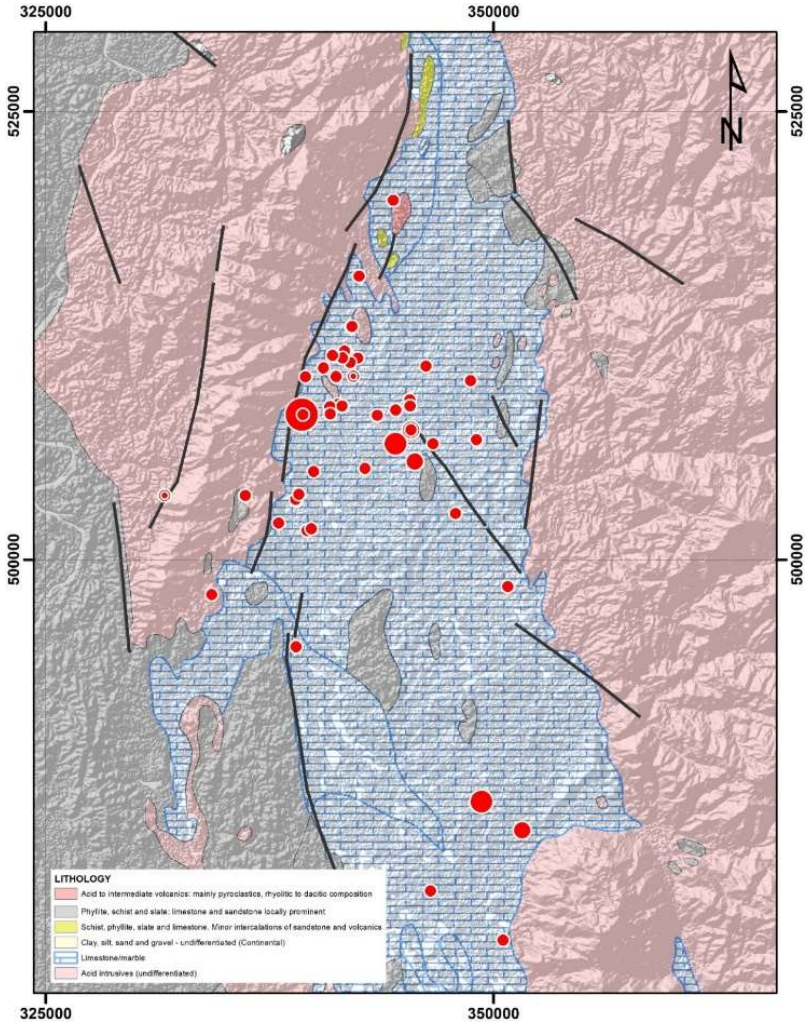


***Figure 4.1*** *Geology of Kinta Valley, Perak (JMG, 2008) and the recorded occurrence of sinkholes*

Tectonically, structural styles of the Kinta Valley were controlled by regional meso-tectonic NNE-SSW compression, causing the development of N-S Kledang Fault along the contact boundary and NE-SW drainage anomalies from the fracture system (Meng & Pubellier, 2015) and the local intrusion process of both granitic bodies that took place during Triassic. The late intrusion of both granitic bodies caused the limestone body near the contact undergone thermal and regional metamorphism and metamorphosed into marble and schist (Figure 4.2).

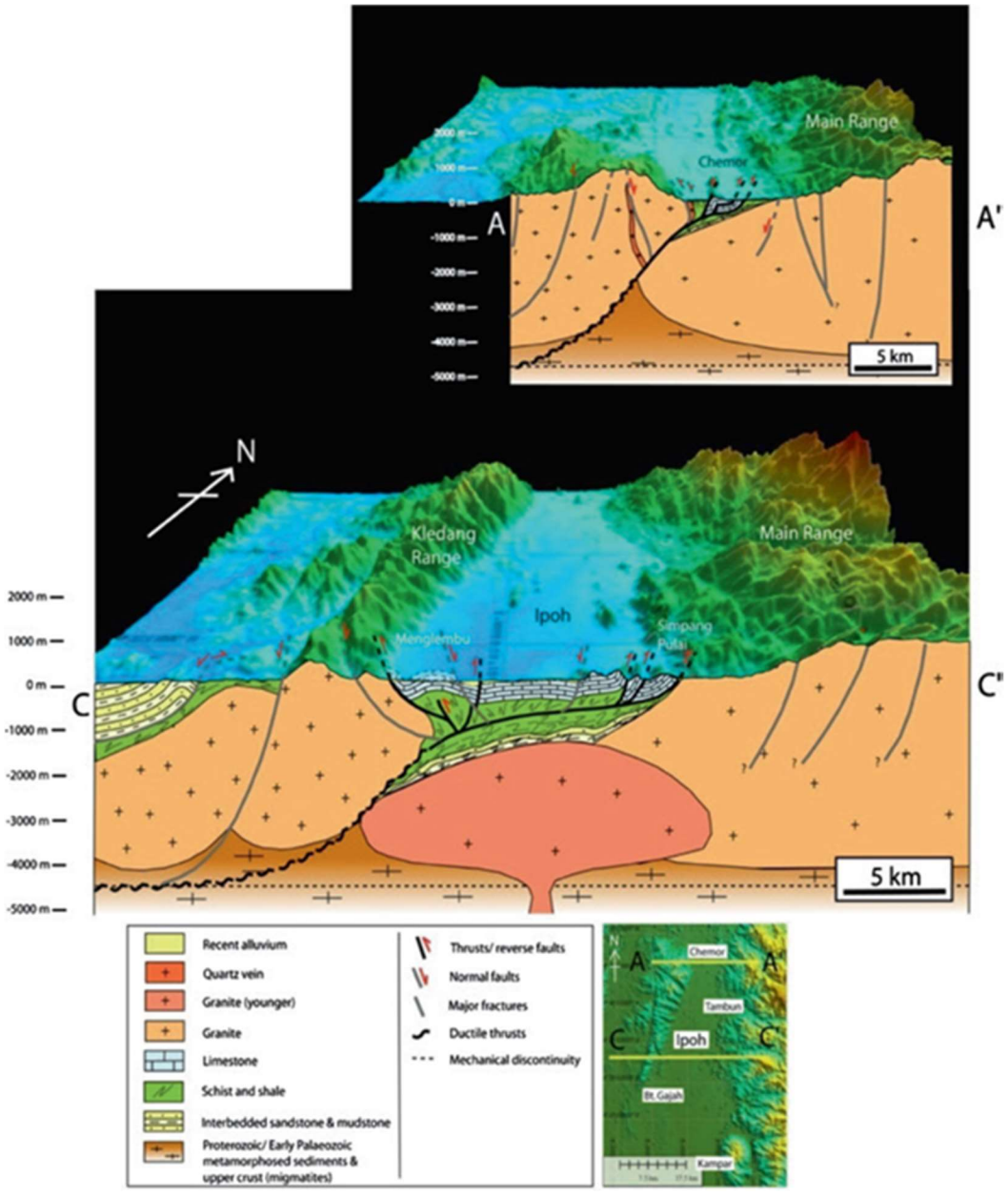


***Figure 4.2*** *Tectonic evolution phases of Kinta Valley suggested by Meng & Pubellier, 2015.*

Kinta Limestone is consisting of massive, greyish white, fine-grained limestone with occasional black carbonaceous patches and intercalated with carbonaceous shale or phyllite (Anua & Zabidi, 2018) and was underlained by poorly stratified schist which indicates regressive, stable continental shelf (Lee Chai Peng, 2009). However, the relationship between these two lithological facies is poorly correlated by the previous researchers due to a lack of evidence. This formation is overlained by shallow Quaternary alluvial deposits with a thickness not exceeding 30 m (Ingham & Bradford, 1960 in Meng & Pubellier, 2015) based on the drilling records and sandy mine tailings or deposits (Chow, 2005).

The karst morphology of Kinta Limestone, developed by the extreme karstification process due to the tropical climate and weathering which has been classified as 'extreme karst kV' by Ros Fatihah, (2018) who studied some selected parameters and karstification classification based on Waltham & Fookes (2005). The results of the karstification process can be seen as a tower karst, cavities, ponds and cave in the area. Only 30% of limestone in Kinta Valley occurs as limestone hills while the rest are burried in the subsurface (Ros Fatihah et al., 2011).

### 4.2. Geological Hazards of Study Area

The occurrence of the sinkhole in Kinta Valley has been reported since the early 1970's and was documented by the Department of Mineral and Geoscience Malaysia, consisting of 161 incidences with 288 dimples features which are unsystematically distributed throughout the area (Ahmad Khairut Tarmizi et al., 2018) (Figure 4.3). Sinkholes diameter is varying between 1 m to 20 m (JMG, unpublished) and from the geometry and shapes, producing 3 main sinkhole types i.e. dropout sinkhole, suffosion sinkhole and buried sinkhole as characterized by Waltham & Fookes (2005). The formation of sinkholes in Ipoh is related to its geological condition as it was developed on limestone bedrock overlain by mostly sandy mine tailings, which such as to have a higher potential for the formation the sinkholes (Chow, 2005).

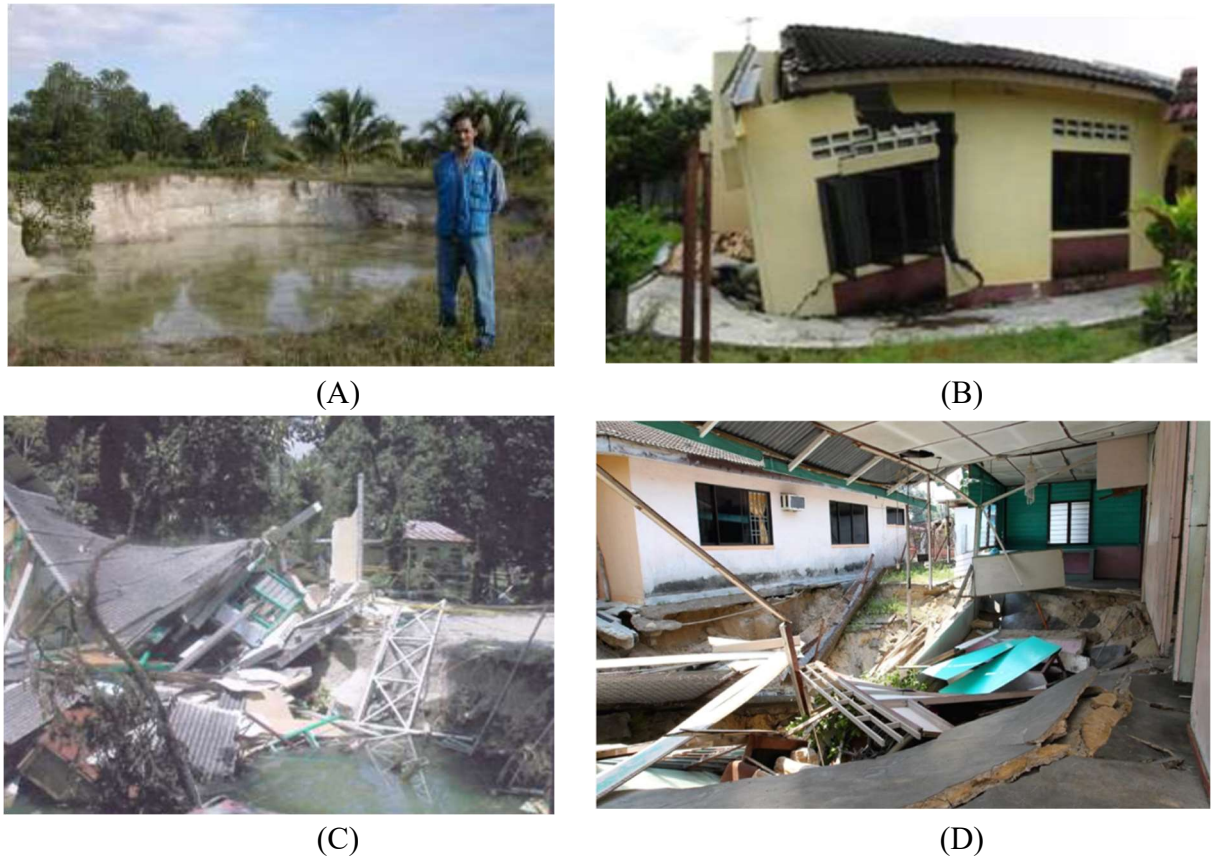

(A) (B)

(C) (D)

***Figure 4.3*** *Sinkhole occurrence in various areas in Kinta Valley, Perak. Explanation (A) sinkhole occurrence in Kg. Kuboi, Gopeng after Acheh earthquake with a diameter of depression around 50 m, (B) major damage of the house caused by the sinkhole on 26 Feb 2008, (C) collapsed house in Kuala Dipang, Kampar with a diameter of depression around 25 m in 2008, (D) several houses damaged by the sinkhole with 8 m diameter of depression in Lahat, Perak.*

The data provided by JMG shows that the frequency of the sinkhole occurrence in the study area is increasing from 1970 until 2007 with the highest annual reported between 2003 and 2007 and after which the trend decreases (Figure 4.5). This period of high occurrence can be correlated with the tremors felt from far-field earthquake incidences that happen during the same period, such as Acheh Earthquake on 26$^{th}$ December 2004 (Mw = 9.1) (Figure 4.4(A)) and Laut Sinabang- Silarut Earthquake on 2$^{nd}$ November 2002 (Mw = 7.4), Nias-Simeulue Earthquake on 28$^{th}$ March 2005 (Mw = 8.6) (Figure 4.4(B)) and West Sumatran Earthquake on 13$^{th}$ September 2007 (Mw = 7.8). In total, 11 incidences of tremor felt in study area has been recorded since 1984 and the same year the tremor recorded is aligned with the higher occurrence of the sinkhole, compared with the non-recorded year.

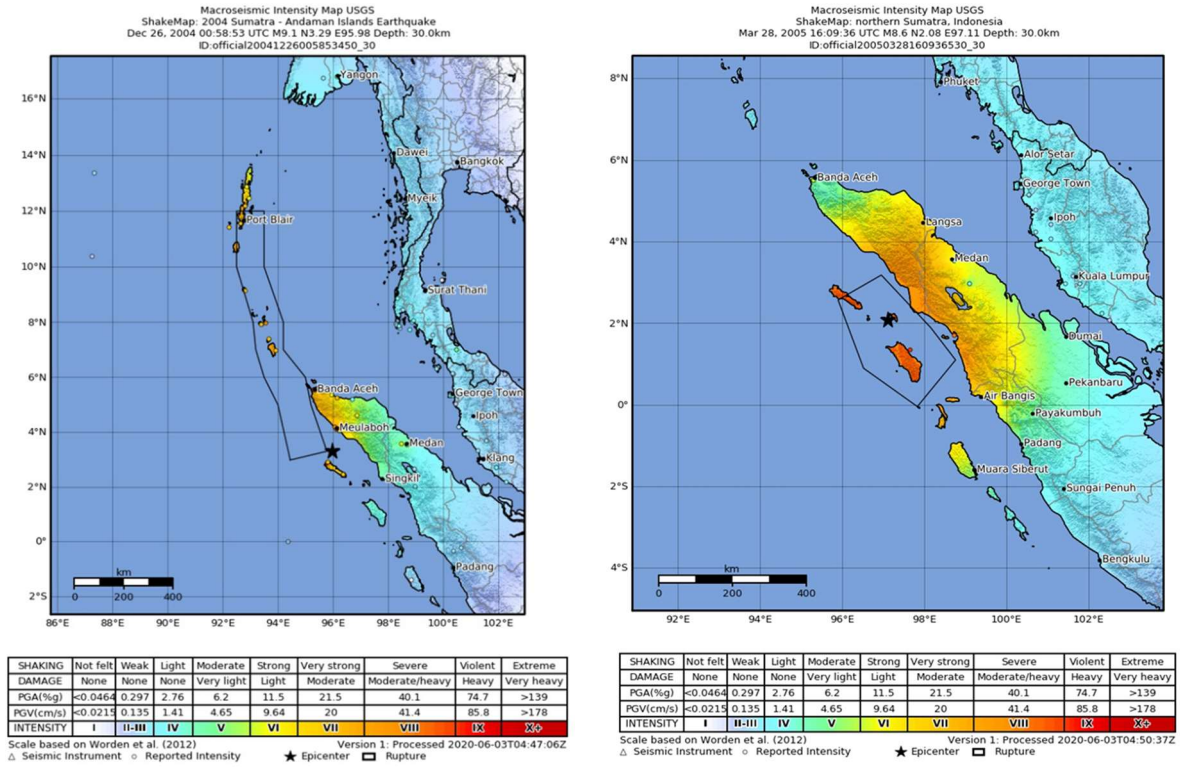


A B

***Figure 4.4*** *Shakemap of (A) Acheh Earthquake, and (B) Nias – Simeulue Earthquake from United States Geological Survey website (https://www.usgs.gov/programs/earthquake-hazards/earthquakes). Both earthquakes caused light shaking in the study area, which triggered sinkhole.*

The declining frequency of sinkhole after 2007 might suggest that most of the pre-existing shallow cavities and voids in the area has been stabilized or had collapsed after the major earthquake event. The same cases of sinkhole plague occurrence after earthquake also happen worldwide, such as Petrinja Earthquake in Croatia in December 2020 (Mw = 6.2) causing 90 sinkhole appearances, mostly in Mecencani and Borojevici area (Bacic et al., 2021), and Bohol Earthquake in Philippine on 15$^{th}$ October 2013 (Mw=7.2) causing the 100 incidents of a sinkhole in Bohol Island Philippine (Manzano et al., 2013).

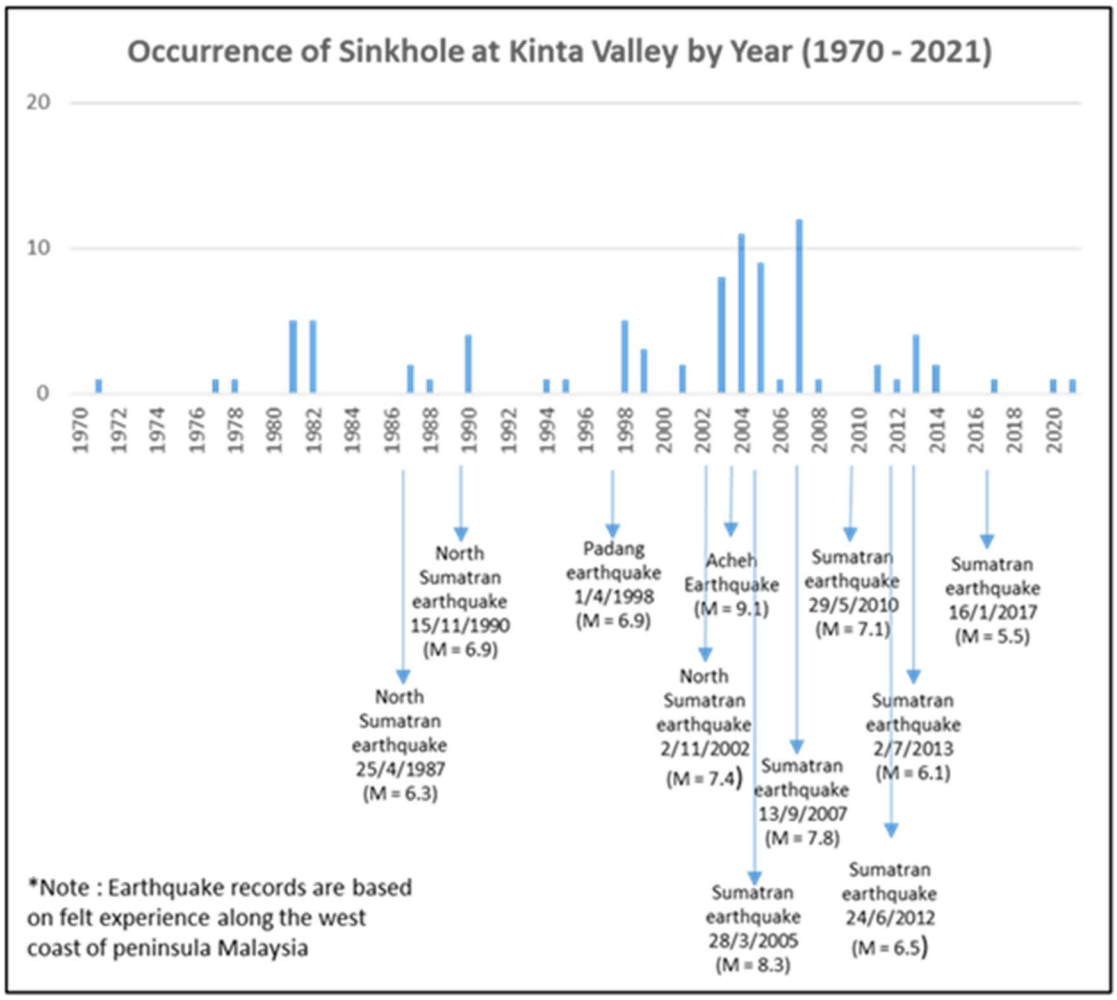


***Figure 4.5*** *Correlation between the felt far-field earthquake event and the intensity of sinkhole occurrence in the study area.*

The cause of the sinkhole occurrence might be mainly contributed by the subsurface karstic features such as the existing pinnacle profiles, cavities and linear trenches, and human activities such as dewatering of groundwater and deep excavations and open cast mining (Kong, 2002), as the pattern of the incident sinkhole is accordingly aligned with the density of mining activity (Ahmad Khairut Tarmizi et al., 2018). In terms of subsurface karstic features, a survey conducted based on borehole data shows that the cavities size in the study area is mostly less than 3 m. in thickness and commonly less than 1 m (Kong, 2002).

Other than the contributing factors mentioned above, climate also contributes to the formation of cavities at the karst area on a regional scale by affecting the fluctuation of groundwater by seasonal change, rainfall acidity and surface temperature over a long period of

time. According to the meteorological data, the western part of Peninsular Malaysia is having a dry season (minimum monthly rainfall accumulation) during February and the wet season (maximum monthly rainfall accumulation) is recorded in October and November are separated by the transition phase (Figure 4.6). During the transition phase, downpours usually occurred locally at certain place with unexpected amount of daily accumulation, causing the rate of groundwater level fluctuations to be drastically higher compared to the other period (Figure 4.7).

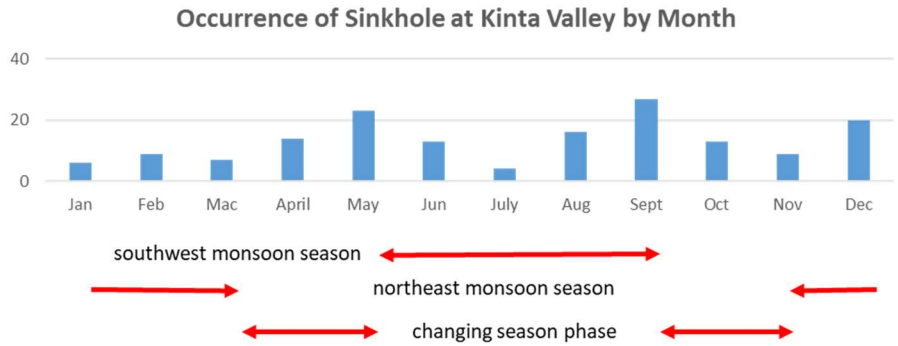


***Figure 4.6*** *Correlation between frequency of sinkhole occurence by month and the seasonal changing phase of West Peninsular Malaysia.*

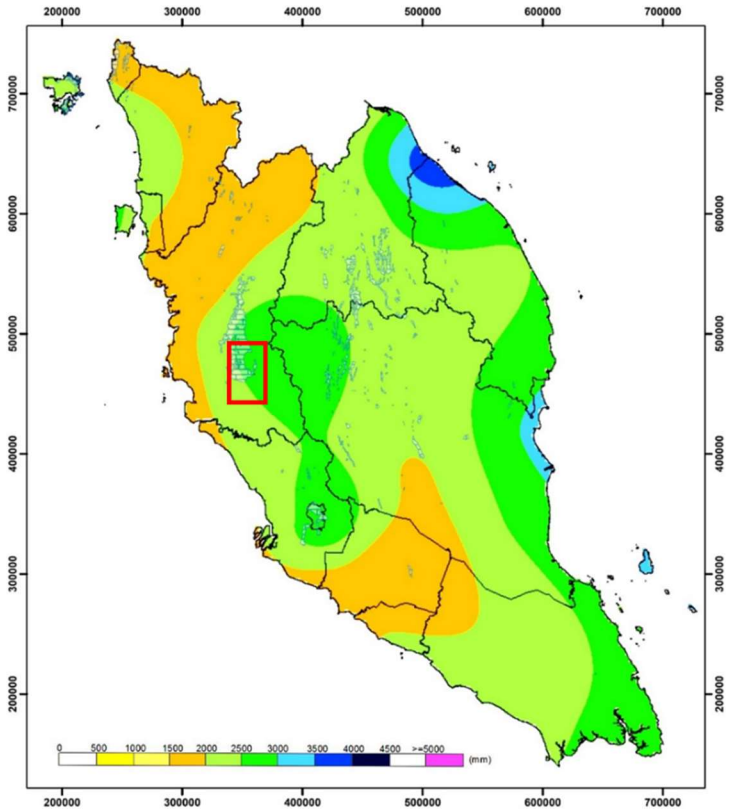


***Figure 4.7*** *Mean rainfall distribution of Peninsular Malaysia. (Source: MetMalaysia website)*

The fluctuations of the groundwater level are related to the formation of cavities in the limestone bedrock whereas most cavities developed within the zone of groundwater level fluctuation (Kong, 2002). Groundwater would act as a filler for the existing cavities and caves, causing the hydrostatic pressure that withstand the loads on upper surface without collapsing. The pressure generated from the high groundwater velocity due to the rise of the groundwater level would also accelerate the erosion process of limestone bedrock and forming cavities and void's structure (Bell, 1999). When the groundwater level declined, the cavities became 'empty' and lose the hydrostatic pressure and causing it to collapse (Ahmad Khairut Tarmizi et al., 2018) and that explains the occurrence of sinkhole in study area are frequently reported during the transition of seasons.

The formation of the cavities also can be related to the groundwater acidity, which are directly impacted by the land use and rainfall acidity. Rainfall acidity distribution obtained from Department of Meteorological Malaysia (Met-Malaysia) shows the decrease of rainfall acidity from 2002 to 2020 (Figure 4.8). The decrease in the rainfall acidity might decrease the groundwater acidity, thus decelerates the dissolution process of the karst.

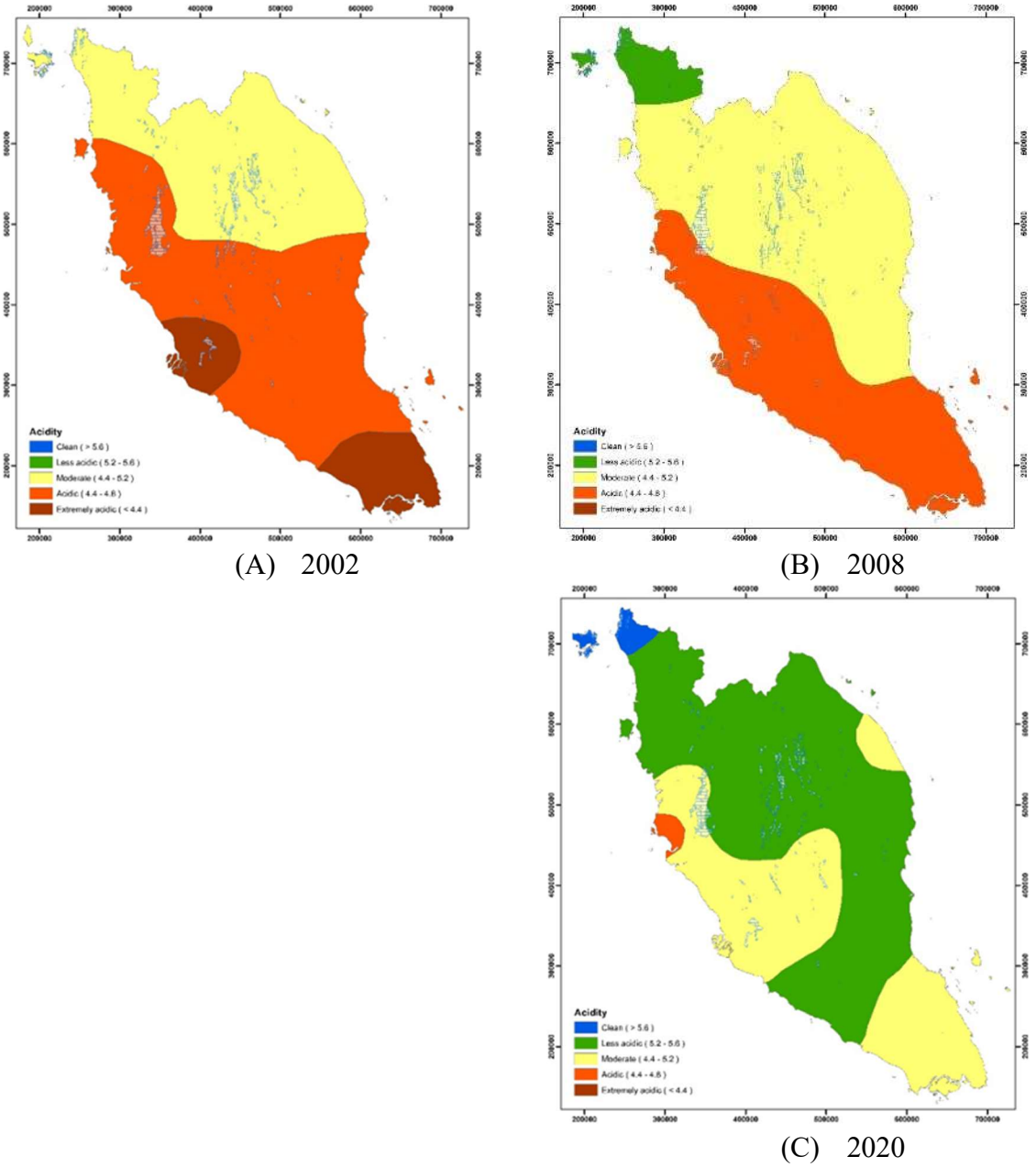


(A) 2002 (B) 2008

(C) 2020

***Figure 4.8*** *Rain acidity distribution on limestone formation in Peninsula Malaysia based on selected years. (Source: MetMalaysia website)*

### 4.3. Sinkhole Susceptibility Modelling

Sinkhole susceptibility modelling, or land subsidence hazard modelling has been conducted previously in the study area by Pradhan et al. (2014) through bivariate statistical analysis methods (frequency ratio methods) and multivariate statistical analysis methods (evidential belief function) using 11 main parameters; altitude, slope, aspect, lithology, distance from fault, distance from river, Normalized Difference Vegetation Index (NDVI), soil type, stream

power index (SPI), topographic wetness index (TWI) and land use/landcover (LU/LC). Al-Kouri et al. (2013) use multi criteria evaluation approaches and considering 8 parameters; lithology, lineament, soil cover, slope, land use mining, urban area features, ponds, and river. In other sinkhole susceptible area such as Kuala Lumpur, the susceptibility map of sinkhole was produced by Rosdi et al. (2017) using multi-decision method, which is analytical hierarchical process using 5 main parameters: lithology, soil type, land use, water level decline (WLD) and proximity to groundwater. The same method was also used by Taheri et al. (2015) for the susceptibility sinkhole mapping at Hamdan Province, Iran while frequency ratio methods has been used by Ozdemir (2015) using different parameters for sinkhole susceptibility mapping at Karapinar, Turkey.

All the studies mentioned above shows different parameters and statistical approaches. Pradhan et al. (2014) research is more into the use of index map related to the sinkhole occurrence while Rosdi et al. (2017) using the parameter weighted to the groundwater and geology condition of the study area. All the considered parameters by Al-Kouri et al. (2013) can be regarded as a causative factor for limestone instability. In term of analysis methods uses, frequency ratio analysis methods show a lower success percentage than evidential belief methods (Pradhan et al., 2014). Other similar research such as Doctor (2008) suggest that the sinkhole density is an important factor for sinkhole potential analysis, based on the research by Zhou (2003) while Qiu et al. (2020) suggest three types of sink attributes namely morphological, imagery and contextual to be used for the sinkhole susceptibility mapping.

## 5. METHODOLOGY

The detailed methodology of this study can be simplified as below:

a) Literature Study and Data Collection

The first step was to put together all the available and relevant data on the study area and arrange it appropriately to help facilitate the rest of the work. This involved desktop study of previous literature, base maps (topographic and geological), sinkhole location, acquiring rainfall and meteorological and groundwater data, land use and land cover data of study area from satellite imagery, collecting records of historical sinkhole, and several other related technical and non-technical documents. In these stages, the regional and local factors contribute to the sinkhole formation will be discussed and correlated.

b) Data processing and analysis

Remote sensing analysis involving two main steps, which is remote sensing interpretation and statistical modelling analysis. Remote sensing interpretation involved the use of appropriate satellite data such as i) imagery data from ESRI Imagery and Google Earth Satellite Imagery, and ii) digital elevation data from Shuttle Radar Topography Mission (SRTM) and Advanced Land Observing Satellite-1 (ALOS). The objective of remote sensing analysis is to outline the geological structure such as fault, fracture system, drainage, and land use/land cover index and to generate relevant index map such as topographical wetness index and topographical openness index. The output of the remote sensing analysis will be used for the statistical and 2-D modelling analysis.

The collected data will be filtered and processed by correlating the incident data with other parameters or factors, such as rock formation, geological structure, climate, groundwater, drainage, elevation, and topographical inclination. All the parameters will be translated into raster factor maps. All the factors are regarded as a contributing factor and will be used to produce sinkhole susceptibility map by two approaches, which is i) multi criteria method – analytical hierarchy process (AHP) and ii) frequency ratio methods by using GIS software, such as QGIS 3.16.10 and ArcMAP 10.8.1 (together with the related software extension). Both susceptibility map will be summarized, checked for errors, and will be compared for the next stage.

c) Field investigation and output verification

Field investigation will be conducted by visiting the latest sinkhole location and comparing the site's condition with the susceptibility map produced.

d) Discussion and conclusion

During this stage, all the data and results from current and previous work are used to endorse the triggering factors and contributing to the sinkhole formation at the study area and suggesting the best remedial and mitigation procedures to reduce the sinkhole risk.

## 6. RESULTS AND DISCUSSION

From a geologist's perspective, the use of different statistical methods and parameters should be determined by studying the environmental condition of the sinkhole and naturality of its occurrence. In the study area, the occurrence of sinkhole is mostly unpredictable, and its frequency

can be correlated with the mining activities/density, geological structure, elevation, sediment thickness and layers inclination, and climate of the area, which are represented by the groundwater level and temperature. Furthermore, the size of sinkhole, represented by the diameter of the sinkhole cannot be related to its frequency.

### 6.1. Incident Data and Conditioning Factors

For the modelling, a total of 58 sinkhole location, occurred between 1977-2020 obtained from Department of Mineral and Geoscience Malaysia will be used. Four main factors are taken into consideration (topographical, geological, anthropological, and hydrogeological) and processed into 8 factor maps using GIS software, namely i) elevation, ii) gradient, iii) topographic wetness index, iv) lithology, v) fault density, vi) landform, vii) groundwater level, viii) land use/land cover index (LU/LC) and ix) groundwater alkalinity (Figure 6.1).

i) Elevation, gradient, topographic wetness index (TWI) and landform

Topographical factor map consists of elevation map, gradient map, and topography wetness index. Elevation map is derived from the digital terrain model (DTM) of ALOS-PALSAR and the final output resolution for the map is defaulted at 12.5 m per pixel. Gradient map was also produced using the same input and resolution. In this study, topographical wetness index (TWI) is produced to demonstrate sediment thickness condition and flow accumulation. Low number of TWI indicates thinner sediment layer and low flow accumulation. The landform conditioning factors is produced statistically using the elevation data from DTM and classified accordingly using classification from Moss (2016).

ii) Lithology and fault distance

Lithology maps are derived from geological map of Peninsular Malaysia by JMG (2014) while the fault is derived from the DTM of ALOS-PALSAR and previous works. The distance of the fault was calculated in ArcGIS software and both lithology factor map and fault distance map are converted into raster format.

iii) Land use/Land Cover (LU/LC) Index

Land use/landcover index map 2020 edition was downloaded from ESRI and resample from 10 m to 12.5 m resolution for analysis. LU/LC conditioning factors represent the anthropological conditioning factors to express human interaction with the environment.

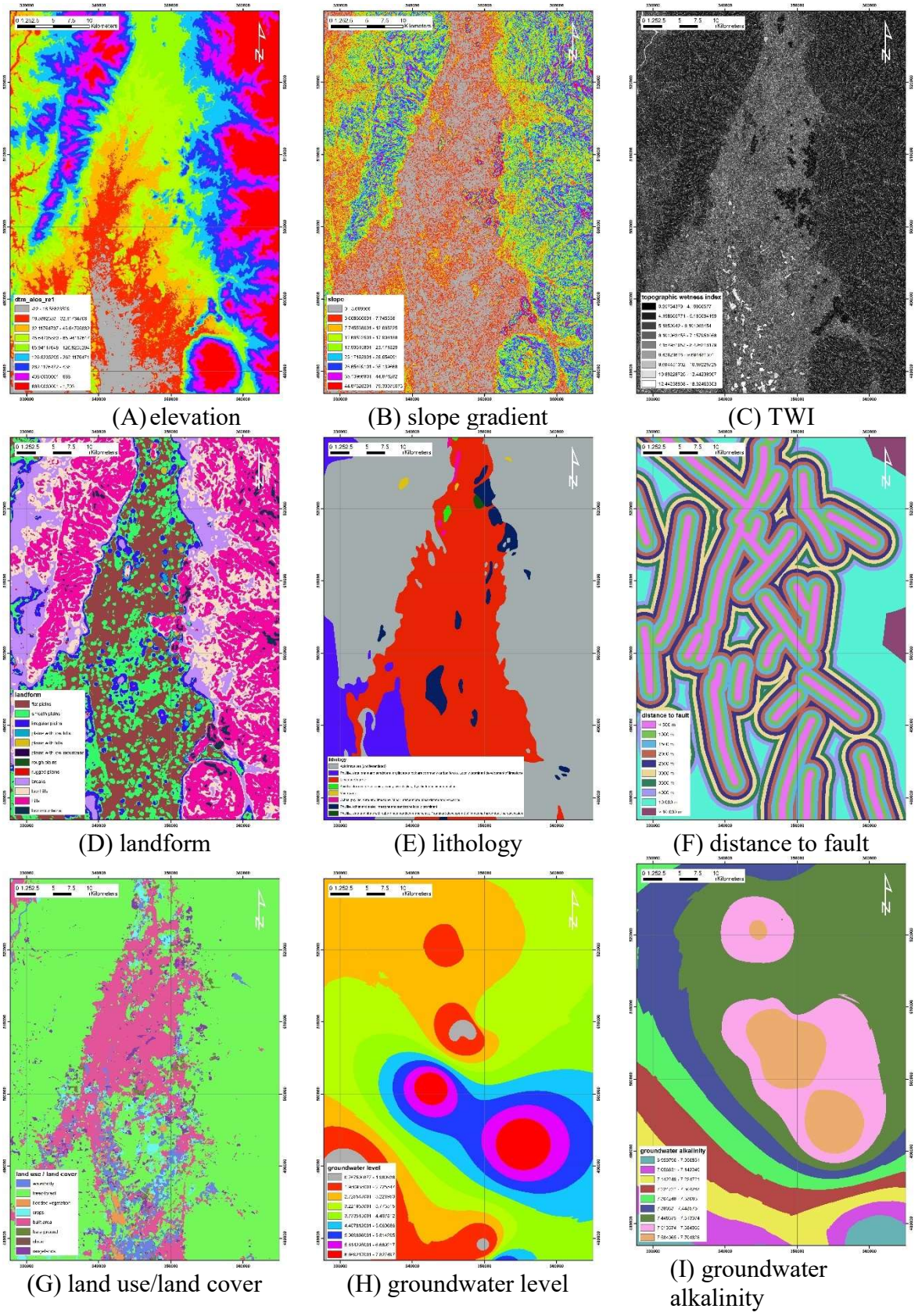


***Figure 6.1*** *Factor map (conditioning factor) used for the analysis.*

iv) Groundwater level and groundwater alkalinity

Both factors above are derived from the collected well data in Perak from 2001 to 2021. Most of the data are incomplete and need to be filtered from errors and transformed into raster format. Higher groundwater level in the study area might be causing the formation of cavities in alluvial soils and induced groundwater fluctuation.

All the conditioning factors are processed to minimize heuristical effect, all the conditioning factor's class will be divided automatically using natural breaks method accordingly except for lithological factor. Some of the potential conditioning factors, such as mining density and slope curvature are ignored in this study as the mining density factors are represented by the distance to fault factors and LU/LC factors which has better coverage within study area and better information, while the slope curvature is almost irrelevant to the sinkhole occurrence.

### 6.2. Frequency Ratio (Bieniawski and Metallurgy) Model

From the naturality of the sinkhole, frequency ratio methods seem to be the best methods to analyze the susceptibility of the sinkhole as it is straightforward method based solely on the occurrence (frequency) ratio. Frequency ratio is the ratio of occurrence to none-occurrence probability for a specific event (Lee & Pradhan, 2006b in Pradhan et al., 2014). In comparison to the other statistical methods, frequency ratio is widely used to establish the relationship between conditioning factors and the occurrence of the geological hazard (Oh & Pradhan, 2011).

In this study, the weight for each of the conditioning factors are calculated manually based on the occurrence in the table and reclassified accordingly in the GIS software. All the conditioning factors (factor map) will be summed using the equation as follows:

$$\text{Sinkhole susceptibility index} = Pr_1fr_1 + Pr_2fr_2 + \ldots. + Pr_nfr_n$$

where '$Pr_n$' refers to prediction rate of the occurence (Figure 6.2) while '$fr_n$' refers to the weighted condition factors based on the relative frequency value acquired (Table 6.1). The generated sinkhole susceptibility index map is shown in Figure 6.3(A).

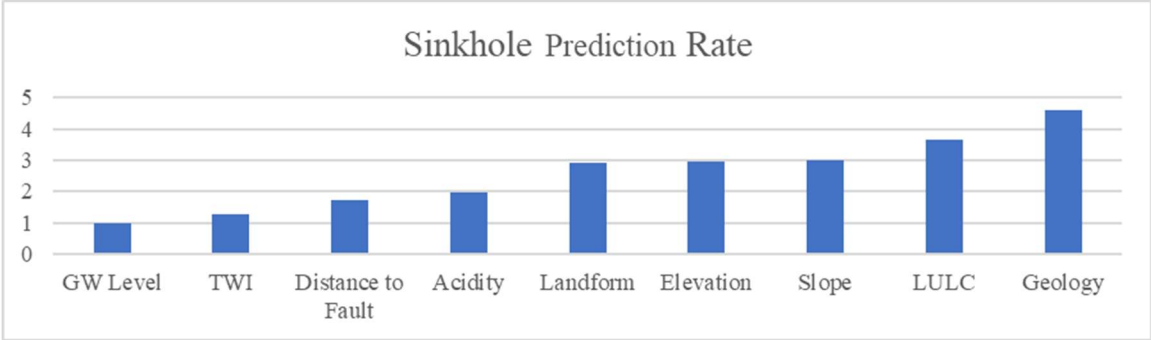


***Figure 6.2*** *Sinkhole prediction rate resulted from FR Method.*

**Table 6.1** Frequency ratio analysis for each conditioning factors and classes.

| No | Data Layers | Class | % Class Pixels | % Sinkhole Pixels | % Relative Frequency | Prediction rate |
|---|---|---|---|---|---|---|
| 1 | Topographic Wetness Index (TWI) | 0.957544 – 4.198666 | 10.6368498 | 0 | 0 | 1.259796 |
| | | 4.198666 – 5.185094 | 24.2354464 | 13.79310345 | 5.349014764 | |
| | | 5.185094 – 6.101063 | 24.4078144 | 20.68965517 | 7.966860048 | |
| | | 6.101063 – 7.157951 | 19.18105 | 24.13793103 | 11.82743287 | |
| | | 7.157951 – 8.426216 | 9.94190147 | 15.51724138 | 14.66924927 | |
| | | 8.426216 – 9.694481 | 6.16129995 | 17.24137931 | 26.30040773 | |
| | | 9.694481 – 10.892287 | 2.83378047 | 5.172413793 | 17.15496694 | |
| | | 10.892287 – 12.442389 | 1.93693568 | 3.448275862 | 16.73206838 | |
| | | 12.442389 – 18.924633 | 0.66492188 | 0 | 0 | |
| | Total | | 100 | 100 | | |
| 2 | Elevation (m) | -22 m - 18 m | 8.4617709 | 1.724137931 | 2.600841043 | 2.96571 |
| | | 18 m – 32 m | 13.1142691 | 10.34482759 | 10.06890476 | |
| | | 32 m – 45 m | 12.7963697 | 62.06896552 | 61.91427526 | |
| | | 45 m – 65 m | 13.3108041 | 22.4137931 | 21.49384605 | |
| | | 65 m – 126 m | 12.1247648 | 1.724137931 | 1.815104985 | |
| | | 126 m – 262 m | 10.444912 | 1.724137931 | 2.107027907 | |
| | | 262 m – 438 m | 9.97265082 | 0 | 0 | |
| | | 438 m – 668 m | 9.91776475 | 0 | 0 | |
| | | 668 m – 1703 m | 9.85669384 | 0 | 0 | |
| | Total | | 100 | 100 | | |
| 3 | Groundwater Alkalinity (pH) | 6.950796 – 7.056831 | 3.71293648 | 0 | 0 | 1.972701 |
| | | 7.056831 – 7.142249 | 6.04773231 | 0 | 0 | |
| | | 7.142249 – 7.224721 | 8.59319066 | 3.448275862 | 5.427626057 | |
| | | 7.224721 – 7.304248 | 8.27288961 | 0 | 0 | |
| | | 7.304248 – 7.38083 | 11.4649628 | 8.620689655 | 10.17025225 | |

| No | Data Layers | Class | % Class Pixels | % Sinkhole Pixels | % Relative Frequency | Prediction rate |
|---|---|---|---|---|---|---|
| | | 7.38083 – 7.448575 | 12.5861665 | 5.172413793 | 5.558558153 | |
| | | 7.448575 – 7.513374 | 29.8669801 | 46.55172414 | 21.08175795 | |
| | | 7.513374 – 7.584065 | 12.6600982 | 15.51724138 | 16.5782928 | |
| | | 7.584065 – 7.704828 | 6.79504332 | 20.68965517 | 41.18351279 | |
| | Total | | 100 | 100 | | |
| 4 | Slope (degree) | 0 – 3.668666 | 29.3936067 | 74.13793103 | 62.44547791 | 2.991155 |
| | | 3.668666 – 7.745538 | 19.8981975 | 20.68965517 | 25.7426307 | |
| | | 7.745538 – 12.665225 | 11.5812822 | 3.448275862 | 7.371549221 | |
| | | 12.665225 – 17.906158 | 10.5280201 | 0 | 0 | |
| | | 17.906158 – 23.171829 | 9.61322214 | 1.724137931 | 4.440342175 | |
| | | 23.171829 – 28.654091 | 8.7099523 | 0 | | |
| | | 28.654091 – 35.139668 | 6.37736713 | 0 | | |
| | | 35.139668 – 44.876282 | 3.16958919 | 0 | | |
| | | 44.876282 – 79.300751 | 0.72876282 | 0 | 0 | |
| | Total | | 100 | 100 | | |
| 5 | Groundwater Level (m) | 0.767501 – 1.980938 | 5.92271559 | 5.172413793 | 10.25283117 | 1 |
| | | 1.980938 – 2.725547 | 10.9156149 | 15.51724138 | 16.68928514 | |
| | | 2.725547 – 3.221953 | 27.2052779 | 36.20689655 | 15.6246234 | |
| | | 3.221953 – 3.773515 | 23.9805901 | 12.06896552 | 5.908559378 | |
| | | 3.773515 – 4.407812 | 11.4001243 | 8.620689655 | 8.877769123 | |
| | | 4.407812 – 5.069686 | 7.32624164 | 6.896551724 | 11.05152428 | |
| | | 5.069686 – 5.814295 | 6.78702304 | 12.06896552 | 20.87671421 | |
| | | 5.814295 – 6.669217 | 3.77686604 | 3.448275862 | 10.7186933 | |
| | | 6.669217 – 7.827497 | 2.68554658 | 0 | 0 | |
| | Total | | 100 | 100 | | |
| 6 | Geology | Acid intrusives | 50.926893 | 6.896551724 | 4.02754765 | 4.597105 |
| | | Phyllite / slate | 19.7868341 | 0 | 0 | |
| | | Limestone / marble | 28.8519416 | 93.10344828 | 95.97245235 | |
| | | Acid to intermediate volcanics | 0.10732871 | 0 | 0 | |
| | | Quartz vein | 0.13976302 | 0 | 0 | |
| | | Schist / Phyllite | 0.17207772 | 0 | 0 | |
| | | Clay, silt and gravel | 0.01516181 | 0 | 0 | |
| | Total | | 100 | 100 | | |
| 7 | Distance to Fault (m) | < 500 m | 10.4425243 | 10.34482759 | 10.91597845 | 1.738632 |
| | | 1000 m | 11.3890573 | 12.06896552 | 11.67688965 | |
| | | 1500 m | 11.5151571 | 37.93103448 | 36.29691608 | |
| | | 2000 m | 10.8672519 | 34.48275862 | 34.96448818 | |
| | | 2500 m | 9.7092486 | 3.448275862 | 3.913463495 | |
| | | 3000 m | 8.51081853 | 1.724137931 | 2.232264136 | |

| No | Data Layers | Class | % Class Pixels | % Sinkhole Pixels | % Relative Frequency | Prediction rate |
|---|---|---|---|---|---|---|
| | | 3500 m | 7.04575172 | 0 | 0 | |
| | | 4000 m | 5.61570834 | 0 | 0 | |
| | | 10000 m | 22.6979997 | 0 | 0 | |
| | | > 10 000 m | 2.20648271 | 0 | 0 | |
| | Total | | 100 | 100 | | |
| 8 | LU/LC (Land use / Land cover) | Waterbody | 4.27908124 | 3.448275862 | 12.24027401 | 3.670758 |
| | | Trees / Forest | 71.2693645 | 8.620689655 | 1.837294583 | |
| | | Flooded vegetation | 0.72640431 | 0 | 0 | |
| | | Crops | 2.81929238 | 1.724137931 | 9.28905553 | |
| | | Built area | 17.0869175 | 86.20689655 | 76.63337588 | |
| | | Bare ground | 0.60843887 | 0 | 0 | |
| | | Cloud | 0.0077543 | 0 | 0 | |
| | | Rangelands | 3.20274683 | 0 | 0 | |
| | Total | | 100 | 100 | | |
| 9 | Landform | flat plains | 19.6867571 | 68.96551724 | 61.19219861 | 2.931122 |
| | | smooth plains | 18.0679963 | 18.96551724 | 18.33550785 | |
| | | irregular plains | 9.29067246 | 6.896551724 | 12.96650978 | |
| | | plains with low hills | 0.41916821 | 0 | 0 | |
| | | plains with hills | 0.24017209 | 0 | 0 | |
| | | plains with low mountains | 0.00086854 | 0 | 0 | |
| | | rough plains | 0.00169505 | 0 | 0 | |
| | | rugged plains | 0.15988125 | 0 | 0 | |
| | | breaks | 12.0374766 | 5.172413793 | 7.505783755 | |
| | | low hills | 14.8924629 | 0 | 0 | |
| | | hills | 24.171284 | 0 | 0 | |
| | | low mountains | 1.03156538 | 0 | 0 | |
| | Total | | 100 | 100 | | |

As predicted, lithological conditioning factors shows the most significant effect on the occurrence of the sinkhole in the study area(Table 1). Almost 93.1% (54 cases) of the sinkhole incident are developed in the karst area, or the area which are underlined by limestone bedrock.

In term of gradient, the sinkhole incident shows a high possibility to occurred in low gradient terrain and shows a decreasing rate of occurrence as the increasing terrain gradient, which 94.83% comprises lower than 7.74$^{o}$ terrain while the rest (5.17%) are lower than 23.17$^{o}$ terrain. Most of the low gradient terrain are comprises populated area of Kinta Valley and the karst region. Lower gradients indicate slow groundwater movement (Al-Kouri et al., 2013) but higher rate of

fluctuations. The rate of fluctuation might also be affected by the type of the landforms of the area, as demonstrated by the landform conditioning factors. A total of 55 sinkholes occurred in plain areas which represent low gradient terrain while the rest of occurrence happens to be at the boundary between mountainous and plain areas (slope breaks).

The value of prediction rate for gradient and elevation factors shows an almost similar number. Elevation of 32 m-45 m from the sea level shows a highest occurrence (61%) percent and gradually decreased towards higher elevation region. No occurrence recorded at the region with the gradient higher than 23$^{o}$ and elevation higher than 262 m. The trends for elevation and gradient proved that both conditioning factors play a significant role in controlling the groundwater saturation, flow and fluctuations (Gao et al., 2021).

Groundwater alkalinity, express in pH demonstrates a mild effect on the sinkhole formation. The trend produced from the analysis shows a lower occurrence below than pH 7.3 and gradually increasing with the increasing groundwater alkalinity. The highest occurrence is recorded between pH 7.4-pH 7.5, might indicate the most suitable environment for the sinkhole occurrence. Groundwater alkalinity may indicate total concentration of bicarbonates which are the product of balance reaction and indicate extensive dissolution of carbonate rocks and limestone (Taheri et al., 2015).

For the case of distance to fault, the highest probability of sinkhole is located within 2 km from the fault, comprising of 64.82% or 55 incidents. Intense faulting can contribute to the formation of secondary porosity and acting as a presential pathways for ascending deep sourced fluids, thus making the weathering reaction to be more aggressive (Taheri et al., 2015). Furthermore, the faulting zone in the study area also contributed to the tin mineralization which catalysed development of tin mining activities along the faulting areas (Rajah, 1979) and indirectly contributes to the development in the area, as represented by the high number of sinkhole occurrences in built area based on land use/land cover conditioning factors.

Groundwater level and topographic wetness index shows the lowest prediction rate, as the distribution of sinkhole occurrence shows a weak trend between each class. However, both of the conditioning factors indicate specific condition that has a high occurrence, which is represented by value of 6.10-7.15 for the TWI and groundwater level of 2.72 m-3.22 m from the surface, which indicate the most suitable setting for the cavities growth.

### 6.3. Analytical Hierarchy Process (AHP) Model

For the quality assurance and comparison, the frequency ratio model will be integrated with the analytical hierarchy process model by using the same parameter, weight and ranking or score to reduce the uncertainty of the AHP Model (Gao et al., 2021). The AHP method was proposed by Saaty (1977) for complex decision making. The AHP method is largely dependent on the knowledge, experience and intuition of the expert that ranks the criteria (Dweiri & Al-Oqla, 2006; Ho, 2008 in Taheri et al., 2015) and involves heuristic approach. Thus, to minimize the error involving inconsistency, the same ranking or weight of each conditioning factors and criterion have to be referred to quantitative methods such as frequency ratio.

This statistical method also involves the use of pair-wise comparison developed by Saaty (1981) to avoid complicated multi-factor comparison (Gao, 2021). The results of pair-wise comparison and normalized comparison matrix are shown in Table 6.2 and Table 6.3.

All the conditioning factors will be overlay-weighted into a sinkhole susceptibility index map as follows:

$$\text{Sinkhole susceptibility index} = (n_1.sc_1) + (n_2.sc_2) + \ldots + (n_n.sc_n)$$

where '*n*' indicates normalize weightage for each conditioning factors while '*sc*' indicate standardize score given for each sub-criteria or classes. The value of consistency ratio is to be kept below 10% and were processed using function in ArcGIS software to produce final susceptibility map Figure 6.3(B).

**Table 6.2** Pair-wise comparison matrix for each criteria.

| **Criterion** | Geology | LULC | Slope | Elevation | Landform | GW Alkalinity | Fault Distance | TWI | GW Level |
|---|---|---|---|---|---|---|---|---|---|
| Geology | 1 | 2 | 3 | 3 | 3 | 5 | 5 | 7 | 7 |
| LULC | 1/2 | 1 | 3 | 3 | 3 | 4 | 5 | 6 | 7 |
| Slope | 1/3 | 1/3 | 1 | 1 | 1 | 3 | 4 | 5 | 5 |
| Elevation | 1/3 | 1/3 | 1 | 1 | 1 | 3 | 3 | 5 | 6 |
| Landform | 1/3 | 1/3 | 1 | 1 | 1 | 2 | 4 | 5 | 5 |

| Criterion | Geology | LULC | Slope | Elevation | Landform | GW Alkalinity | Fault Distance | TWI | GW Level |
|---|---|---|---|---|---|---|---|---|---|
| GW Alkalinity | 1/5 | 1/4 | 1/3 | 1/3 | 1/2 | 1 | 2 | 3 | 3 |
| Fault Distance | 1/5 | 1/5 | 1/4 | 1/3 | 1/4 | 1/2 | 1 | 2 | 3 |
| TWI | 1/7 | 1/6 | 1/5 | 1/5 | 1/5 | 1/3 | 1/2 | 1 | 2 |
| GW Level | 1/7 | 1/7 | 1/5 | 1/6 | 1/5 | 1/3 | 1/3 | 1/2 | 1 |

**Table 6.3** Normalized comparison matrix for each criteria derived from Table 6.2.

| Criterion | Normalized comparison matrix | | | | | | | | | Normalized Weightage (%) |
|---|---|---|---|---|---|---|---|---|---|---|
| | Geology | LULC | Slope | Elevation | Landform | GW Alkalinity | Fault Distance | TWI | GW Level | |
| Geology | 0.31 | 0.42 | 0.30 | 0.30 | 0.30 | 0.26 | 0.20 | 0.20 | 0.18 | 27.8 |
| LULC | 0.16 | 0.21 | 0.30 | 0.30 | 0.30 | 0.21 | 0.20 | 0.17 | 0.18 | 23 |
| Slope | 0.10 | 0.07 | 0.10 | 0.10 | 0.10 | 0.16 | 0.16 | 0.14 | 0.13 | 11.72 |
| Elevation | 0.10 | 0.07 | 0.10 | 0.10 | 0.10 | 0.16 | 0.12 | 0.14 | 0.15 | 11.51 |
| Landform | 0.10 | 0.07 | 0.10 | 0.10 | 0.10 | 0.10 | 0.16 | 0.14 | 0.13 | 11.11 |
| GW Alkalinity | 0.06 | 0.05 | 0.03 | 0.03 | 0.05 | 0.05 | 0.08 | 0.09 | 0.08 | 5.71 |
| Fault Distance | 0.06 | 0.04 | 0.03 | 0.03 | 0.02 | 0.03 | 0.04 | 0.06 | 0.08 | 4.14 |
| TWI | 0.04 | 0.04 | 0.02 | 0.02 | 0.02 | 0.02 | 0.02 | 0.03 | 0.05 | 2.76 |
| GW Level | 0.04 | 0.03 | 0.02 | 0.02 | 0.02 | 0.02 | 0.01 | 0.01 | 0.03 | 2.20 |

### 6.4. Discussion & Suggestion

For the comparison, both susceptibility index map generated are classified into 5 susceptible classes namely i) very low, ii) low, iii) intermediate, iv) high and v) very high. The classification is made by using quantile method for the FR model and natural breaks methods for

the AHP model. Quantile method is showing the lowest degree of exaggeration (Pradhan et al., 2014) which in this case, are depending on the index value of both final maps.

Validation assessment on both produced sinkhole susceptibility index map shows a different accuracy. For the very high classes, AHP model shows a 79.31% occurrence while for the FR Model shows 72.42% of occurrence (Table 6.4). Both maps shows that most of the Kinta Valley region are regarded to be from intermediate to very high possibilities of sinkhole occurrence.

Some exaggerated results were encountered for both maps. For instance, AHP Model shows more exaggerated classification than FR Model (Figure 6.3). The plain and low elevation terrain located in the northwest of the area show an intermediate-low class of sinkhole susceptibility, due to lithology which consists of granitic basement. This might happen due to the high prediction rate for lithology conditional factor compared to the other conditional factor, or the quality and reliability of the data itself. Hence, thorough quality check and assurance should be conducted before determining the conditional factors.

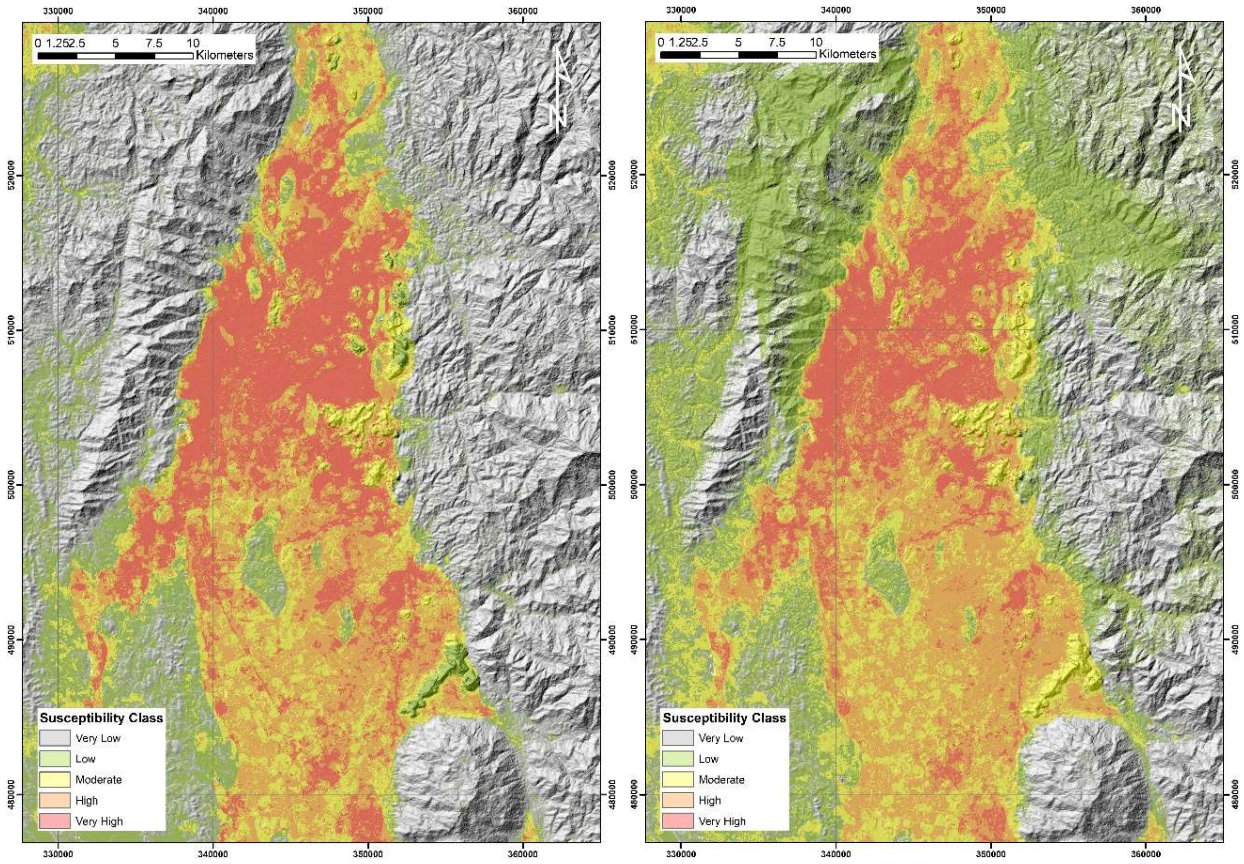


A B

***Figure 6.3*** *Sinkhole susceptibility map produced using (A) Frequency Ratio Method and (B) Analytical Hierarchy Process Method (AHP).*

**Table 6.4** Validation assessment for FR and AHP Model.

| Classes | FR Model | | AHP Model | |
|---|---|---|---|---|
| | **Occurrence** | **%** | **Occurrence** | **%** |
| Very low | 1 | 1.72 | 0 | 0 |
| Low | 3 | 3.45 | 2 | 8.62 |
| Intermediate | 0 | 0 | 2 | 8.62 |
| High | 8 | 13.79 | 12 | 20.69 |
| Very High | 46 | 79.31 | 42 | 72.42 |
| **Total** | **58** | **100.00** | **58** | **100.00** |

For the ground development in the area especially in Kinta Valley, specific site investigation are suggested to be implemented in the early stage of development such as planning stage, especially in the high-very high suscept area with the aim to i) recognize the subsurface site properties such as lithology, soil thickness, groundwater condition, underground karst morphology and the existence of cavities, ii) conclude suitable mitigation process that need to be conducted before any development. Recommended methods for site investigation include borehole and auger profiling, Macintosh Probe Test and need to be supported by geophysical methods such as resistivity, microgravity, and seismic reflection. The option for site investigation shall depend on the type of the development and size/scale of the development.

Some typical reclamation techniques practiced by the developers need to be avoided and reconsidered, such as i) lowering the water table and emplacement of fill material, ii) displacement method, as some of the slurry slime displaced by pushing in sandy fill are trapped within trough of the karstic limestone bedrock, and iii) containment method explained by Mohd Najib Abdul Rashid et al. (2015) as these methods are unsuitable to be practice in karst area. For the long term monitoring, two aspects need to be considered: i) groundwater condition (temperature, alkalinity, and groundwater level) including water level decline from the existing wells in the Kinta area and ii) regional ground subsidence from the satellite or raster data

# 7. CONCLUSION

Sinkhole geological hazard in Kinta Valley has been recorded since 1970 due to the rapid development, accelerated from the tin mining industries in the area. The geological factors proved to be the main conditioning factors for the sinkhole followed by land use/landcover, slope, elevation, and landform. In a regional scale, the sinkhole occurrence can be correlated to the climate change of the area, and most likely triggered from far-field earthquake and rainfall, although the location and magnitude of the sinkhole are almost unpredictable. Although there is no direct prevention can be made to reduce the hazard, wise development planning can reduce the risk and economic loss to the government and local communities.

# 8. FUTURE WORKS

For the future works, more research and study should be conducted to emphasize more accurate susceptibility by considering other conditioning factors that have significant effect on the sinkhole occurrence and updating the conditioning factors in more specific manners and higher resolution mapping. The list of potential factors that led to the sinkhole occurrence has been stated by Banks et al., (2020) and Taheri et al., (2015). Other statistical methods shall be used, such as logistic regression, which according to the Pradhan et al (2014), has been widely used for geological hazard prediction analysis.

For this study, only spatial data were used for analysis and temporal data, such as rainfall intensity and seismicity data shall be used to produce sinkhole hazard map. The sinkhole hazard map would be combined with the vulnerability map of Kinta Valley to produce sinkhole risk map, which are widely used in development's planning stage and decision making.

# CASE STUDY 2: ROCK FAILURE ASSESSMENT ON PALEO-COLLAPSE IN CASE THE PRASAT HIN PAN YOD TOURIST SITE, SATUN GEOPARK, THAILAND


## ABSTRACT

Rockfall and rockslide incident is currently the severe geohazard affecting marine tourism in Thailand. Lately, some tourist sites, located both in the Gulf of Thailand and the Andaman Sea, were prohibited to access. Prasat Hin Pan Yod, the study area developed from a paleo-collapse sinkhole on Koh Khao Yai island of Satun province, is now confronting unsafe caused by rockfall and rockslide hazards as well. The study applied the integration of simple multi-criteria in GIS, traditional stereographic projection analysis, and Slope Mass Rating (SMR) to determine rock mass instability of Ordovician limestone and to find a safe route entrancing the Prasat Hin Pan Yod tourist site. Various discontinuities on natural outcrop slope relating to geomorphological features were investigated and assessed the stability: sea cliff, sea cave, and a former broken block of the rockslide.

The study result shows the dominant wedge failure of rock fall can occur in many spots of the Prasat Hin Pan Yod tourist site. Small pieces of broken limestone hanging at high spots and also filling in rock niches are often found in the field investigation. Rock fragments splitting off rock face may fall away down whenever it is triggered by heavy rain or ground shaking. Direct toppling failure is the comparative subordinate of the rock fall hazard. Its negative impact is similar to wedge failure and difficulty to perform risk management as well. Planar failure and toppling failure seem to be low scores and rarely occur the two big severe events happened from that failure modes and revealed obviously field evidence of broken blocks. The precedent event was caused by toppling failure and the latest, February 20, 2021, was originated by planar failure. The traditional way is now not suitable for getting through the Prasat Hin Pan Yod chamber. Depending on the high SMR score and a few joint intersections causing the geohazard, a narrow strait located between the former broken block and sea cliff is determined as the new safe route for tourists. Moreover, Kayak should be adopted to use for moving over that narrow place and permit a one for in and out. The tourist numbers to visit attractive places should be controlled. For more safety, helmet is one of the simple essential tools for tourists and it will help them to protect the hanging rock fallen from sea cliffs or high places.



**Keywords:** RMR, SMR, Prasat Hin Pan Yod, Satun, Rock failure, Rockslide, Rockfall

# 1. INTRODUCTION

Rockfall and rockslide incidents have more frequently occurred in marine attractions of Thailand. Especially, during the southwest monsoon that affected the peninsular region. It causes the base rocks in southern Thailand which are dominant carbonate-rich rocks (ex. limestone, dolomite, and gypsum) that are easy to weather and erosion, so the karst topography is generally formed in this area. Coastal karst landforms are formed by the action of waves, currents, and tides. They are generally characterized by numerous caves and cavities, sinkholes, fissures, stacks, notch, arch, and underground streams. Most karst features are formed along with weaknesses in the rock mass, such as faults, joints, fractures, and bedding planes, that karst features decrease rock stability and lead to cause geohazard. Prasat Hin Pan Yod is one of famous coastal karst landforms in Thailand. The rockfall incident happened here on February 20, 2021. Fortunately, this incident did not cause people to die or be injured. However, spectacular karst morphology has been turned to be a dangerous area. Tourists and local people were not allowed to visit that place. People in Satun provincial area were indigent due to the loss of tourism revenue. Due to climate change and other triggering factors, particularly uncontrolled tourism, geohazard event trends are arising in Karst tourist sites.

As aforementioned, the Environmental Geology Division under the Department of Mineral Resources (DMR) has created a roadmap for geohazard risk reduction in Thailand's national park. Rock failure assessment and mapping in marine tourist places, particularly limestone islands, has been considered an urgent activity to identify the types of rockfall. All of the geohazard studying areas are not responsible by DMR, thus the mission has to obtain cooperation from different organizational departments and also local people. Moreover, the project on transboundary cooperation has to be launched in the border area.

# 2. OBJECTIVES

The objectives of this study are as follows:

i) To assess anticipated failure of rockfall and rockslide in the Prasat Hin Pan Yod area.

ii) To find the new comparatively safe route through the Prasat Hin Pan Yod.

## 3. STUDY AREA

Prasat Hin Pan Yod tourist site is located in the north part of Koh Khao Yai Island which is the limestone island in the Andaman Sea. The Khao Yai Island is a part of Mu Koh Petra National Park. The distance is about 3 kilometers far from Pak Bara Pier which is located in the administrative area of La Ngu district, Satun province, south of Thailand.

Prasat Hin Pan Yod is one of geosites within Satun Geopark where is The first UNESCO Global Geopark in Thailand. The Satun Geopark, was endorsed by the UNESCO Executive Board on April 17, 2018. The Geopark covers four districts: Thung Wa, La-Ngu, Manang, and part of Mueang Satun, and also consists of two national parks and one wildlife sanctuary. The Global Geopark is established by the concept of sites and landscapes of international geological significance, which are managed with a holistic concept of protection, education, and sustainable development.

## 4. GEOLOGY AND GEOHAZARD

Based on the lithological descriptions on the geological map scale 1:50,000 published by Sinsakul S., (1988) and Tiyapairach, S., (2004) (Figure 4.1), the Koh Khao Yai Island is abundantly covered by carbonate rocks, which can be classified into 2 parts. The lower part is medium to thick bedded dolomitic limestone with partly brown mudstone and the upper part is thicker to massive bedded. Locally, the northern part of Koh Khao Yai Islands where the Prasat Hin Pun Yod chamber is located is mainlyconsists of dark grey argillaceous limestone and stromatolitic limestone with dominant fossils (Fiugure 4.2) (ex. nautiloids, brachiopod, trilobite, and gastropod). Some fossils are occasionally found on the planar failure that is sub-parallel limestone bedding plane. Some experts documents such as Vongvanish (1990) and Meesook (2014), correlated the rocks in this area to Lae Tong Formation of Thung Song Group. Their paleo-environment deposition is interpreted as pelagic deeper water during Ordovician period. Thepju et al., (2017) classified onshore karst features in the Satun Geopark into 13 types which are (1) wall karst, (2) stromatolitic karst, (3) pinnacle, (4) cone and tower, (5) knob, (6) Karren or lapies, (7) stone forest, (8) polje, (9) sinkhole or doline, (10) karst spring or karst seepage, (11) karst waterfall, (12) karst lake and (13) cave. These features are mostly exokarst-subaerial occurring in the Lae Tong Formation and Rung Nok Formation of the Ordovician Thung Song Group. The Lae Tong

Formation is characterized by thin-bedded argillaceous limestone and interbedded with pinkish-brown shale at the lower sequence. The Rung Nok Formation, overlying the Lae Tong Formation with a gradual boundary, consists of dark grey to grey limestone, medium to thick-bedded limestone with stromatolitic interbedded with occasional stylolite and massive dolomite.

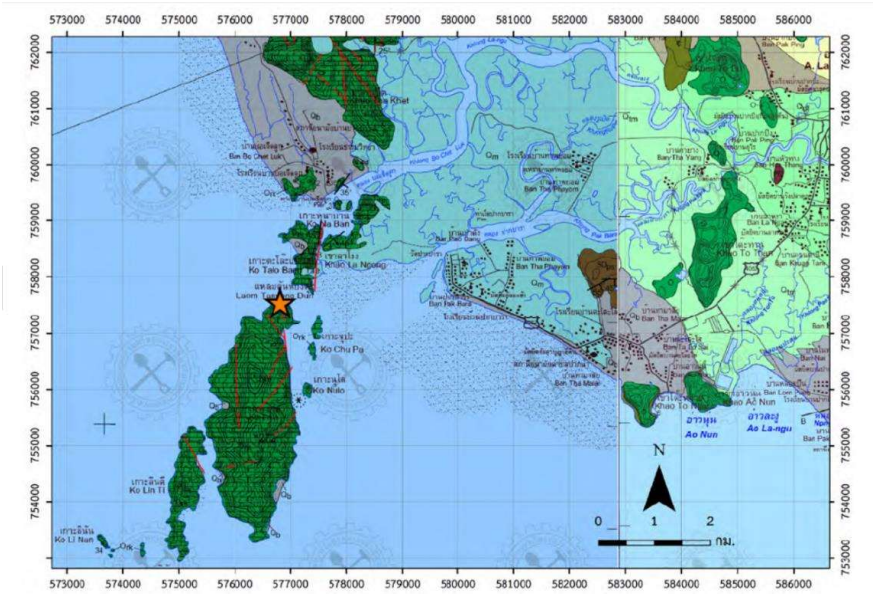


***Figure 4.1*** *Geological map of the Prasat Hin Pan Yod chamber (orange star), La-Ngu district, Satun province*

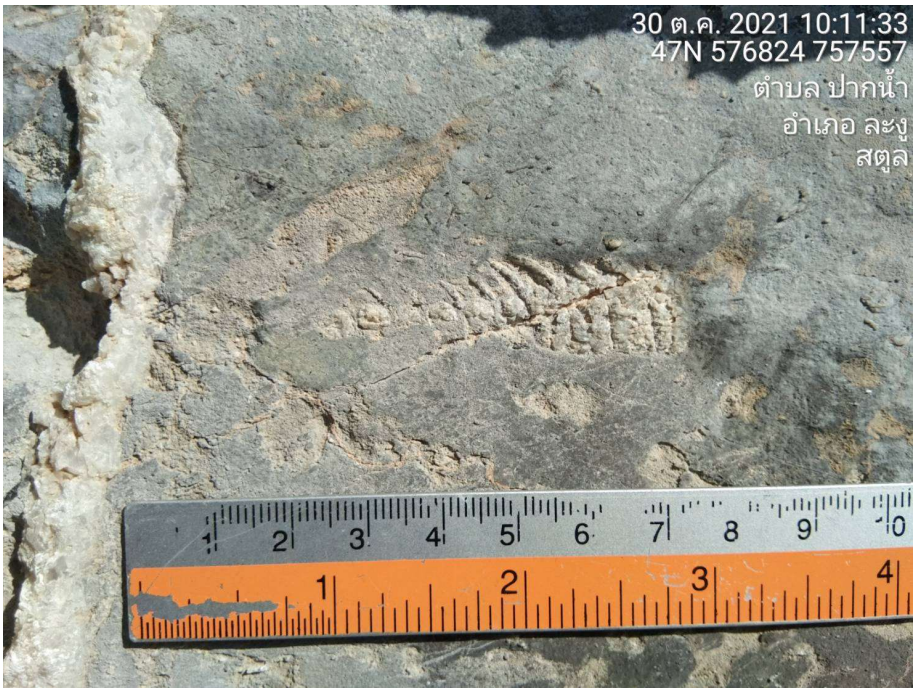


***Figure 4.2*** *Nautiloids on the top bedding of limestone in Prasat Hin Panyod.*

The Prasat Hin Pan Yod chamber is naturally a paleo-collapse sinkhole. Based on the sinkhole classification presented by Waltham et al., (2005), a collapse sinkhole is a roof collapse happening on unstable limestone beneath, particularly cavernous and high fracturing rock. The sinkhole originated on the hinge zone of a small asymmetry anticline whose fold axis is orientated nearly north-south (NNE-SSW) and gently plunged at 11º in a direction 014 (NNE). Limestone bedding planes have an average dip angle of 25 º in direction 320 (NW) and dip at 15 º in direction 035 (NE). A well-defined bimodal clustering on stereonet (Figure 4.3) shows the dominant strike directions of joint and fracture in limestone rock mass have approximately four directions The discontinuous plans are trending nearly north (NNW-SSE to NNE-SSW), northwest-southeast (NW-SE), northeast-southwest (NE-SW), and east-west (E-W). Thinner bedded limestones generally shows narrower spacing of joints and higher fracture density compares to massive limestones. Due to the southwest monsoon climate and sea process, the erosional karstic surface is well developed on strongly fractured limestone, particularly in the upper part of its succession as shown in Figure 4.4. According to karstic landforms, the imagination of people when they look at limestone pinnacles exposed on islands it resembles castle-like features with a thousand peaks.

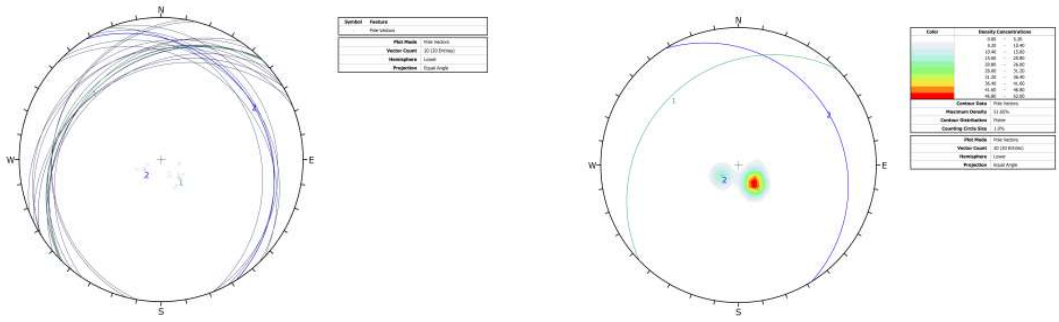

***Figure 4.3*** *Limestone anticline having a fold axis orientation in nearly north-south*


***Figure 4.4*** *The Prasat Hin Pan Yod (Tourism Authority of Thailand)*

There is a small chamber of formal sinkhole surrounded by spectacular limestone pinnacles and hides in the sea cliff. Its geometry is a small oval-shaped room with a longest of 20 meters and the shortest distance of 10 meters. As mentioned above, the Prasat Hin Pan Yod chamber is a paleo-collapse sinkhole located in the rocky intertidal zone of the island. By the action of currents and waves, sediments and other detrital material have entered the chamber via sea caves and deposited in a low-energy sinkhole hiding a sea cliff. The small beach will be exposed to air for only a short period when low tide. Tourists can enter in sightseeing site from March to Mid-May. Coastal massive limestone is no exception of strongly eroded by the action of the sea. Various karst types are generally found in the intertidal zone: notch, cave, cavity, stack, and column. Enlargement of cave size and connected passage networks has been still processed by both dissolution and erosion until the present time and invaded toward limestone chamber or collapse sinkhole. Cave passages lack the strength to span limestone overburden and create unsafety ground conditions for use.

Far from the Prasat Hin Pan Yod to the south direction of 150 meters, another rectangular-shaped formal collapse sinkhole with a long diameter of 150 meters across can be visible on remote sensing images. It has occurred on major joint/fault intersections having strike orientations on the north-south and northeast-southwest. The comparative size is larger than the others on the Google images (Figure 4.5). Because that area is shallowed by sediment deposit and covered by dense water grasses, which karstic characteristics can classify as the older age than a sinkhole of the

Prasat Hin Pan Yod. According to the karst engineering classification introduced by Waltham and Fookes (2003), the Prasat Hin Pan Yod can categorize as Complex to Extreme Karst. Besides specific lithology and geological structures, rock strength has been degraded by that various karst features leading to severe geohazard occurrence of the rock mass.

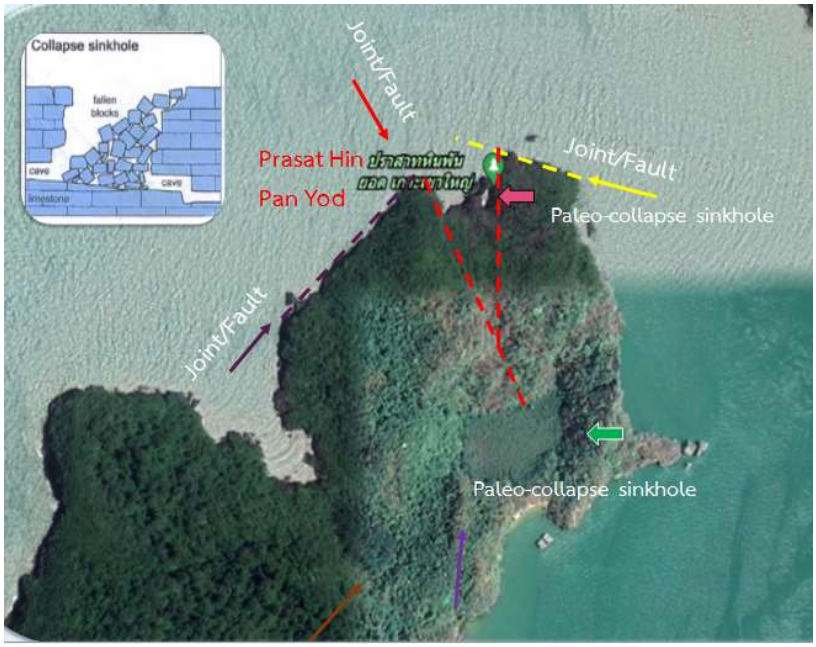


***Figure 4.5*** *Prasat Hin Pan Yod showing oval shaped collapse sinkhole that occurred next to an older rectangular shape (Blue arrow)*

In Satun provincial area, the geohazards at which have been concentrated by government organization and local people consists of landslides, sinkholes, earthquake, shoreline erosion, and tsunami. The five disasters have been interconnected and can cause ground instability on all scales. A physical and socio-economic impact might be both acute and chronic for a long time. Rockfall and rockslide is belonging to a type of landslide based on Varnes (1978) and Cruden and Varnes (1996). Landslide occurrences or slope movements have been subdivided into six categories: Fall, Topples, Slides (rotational and transitional), Lateral spreads, Flow, and Composites (combination of types). For each of these subdivisions, the materials are grouped as either rock, debris (predominantly coarse material), or earth (predominantly fine material). Rockfall is defined by free fall and very rapid movement that is caused by toppling failure and partly wedge failure at a steep slope. Rockslide is caused by planar rock failure and wedge failure in which part of the bedding plane or low angle fault penetrates through rock mass. The plane failure occurs when a structural discontinuity plane such as; the bedding plane, fault plane or preferred orientations of a

joint set dips or daylight towards the outcrop slope face at an angle smaller than the slope angle but greater than the friction angle of the discontinuity surface. Wedge failure may happen when the intersection line of two discontinuities planes generating wedge plunges in the same direction as outcrop slope face and the plunge angle is less than the slope angle but greater than friction angle along failure plane. Rock topples involve the forward rotation and movement of rock mass out of a slope. It generally occurs around an axis (or point) at or near the base of the block of rock. A toppling failure may occur when a steeply dipping discontinuities orients parallel to outcrop slope face and inclines into it. (Yoon et al., 2002; Siddique et al., 2015)

According to DMR (2020), landslide susceptibility in Satun province was assessed by the Frequency Ratio (FR) method in the GIS platform. Landslide susceptibility is classified into 5 levels, very low, low, medium, high, and very high. It is very useful for disaster risk management in mountainous areas. The disadvantage of a map cannot give more details on the small islands particularly the Prasat Hin Pan Yod area. Moreover, landslide types that following to the classification system of Varnes (1978) and Cruden and Varnes (1996) were not conducted.

The latest rockslide big event on February 20, 2021, occurred in the north part of Prasat Hin Pan Yod chamber, Koh Khao Yai Island as shown in Figure 4.6. The area is in an administrative area in Satun province.

***Figure 4.6*** *The latest rockslide big event happened on February 20, 2021*

Based on the DMR field evidence, the rockslide occurrence may briefly conclude in four parts:

First, erosion of fractured and cavernous limestone by sea, Due to the location placing at the narrow strait of Koh Khao Yai Island and Koh Khao Ta Lo Baen Tae, a strong waves and rapid currents can enter cave passages to hit unstable rock columns that partly support cave roof, Because of hydraulic power of the waves and compression of air within a confined space provide the fissures in rock mass widen and deepen and lead to having a broken column,

Second, as a result of the supporting column is being broken, the loss of rock strengths cannot carry limestone overburden at the upper part,

Third, the massive limestone volumes suddenly separated from the weakened sea cliff along major linear faults,

Fourth, the upper part slides through rock mass sub-parallel bedding plane / along low angle fault and falls in the north direction into the sea, hiding the traditional entrance of the chamber. The fragment block of the rockslide location is not far from the precedent rock topple. As mentioned above, the paleo-collapse sinkhole at the Prasat Hin Pan Yod can be a recurrence, particularly on the edge of the chamber.

Based on the orthophotos visual interpretation, geohazards in the Prasat Hin Pan Yod area have ever occurred at least 2 times: prior to the event on February 23, 2021, there was a precedent topple block sitting nearby the latest a rockslide. A huge block of limestone was broken along a major joint/fault and fallen to sea by a toppling failure mechanism as depicted in Figure 4.7. Rock fall and rockslide in the Prasat Hin Pan Yod will have happened in the near future.


***Figure 4.7*** *The older event occurred by topping failure (1) and the latest caused by planar failure (2)*

The tsunami, triggered by an earthquake with a magnitude of 9.1 to 9.3, was a big event on December 26, 2004. Local people along shoreline areas were affected by severe impact covering the four districts of Satun province: Muang, Tha Phae, La Ngu, and Thung Wa. Kidarn and Maihom (2021) delineated the preliminary area boundary of physical loss using the simple overlay technique in GIS. The total area was affected area covering about 5.12 square kilometers and the physical loss along Satun coasts was classified from medium to very high level of impacts. Only

the beach coast that was affected by Tsunami in Satun province had determined in the study. Even though rock mass along Satun coasts was happened by the energy generated from the tsunami and also storm surges, there have no research documents on rocky coast relating to the littoral sinkhole collapse in the Satun provincial area.

Sinkhole hazards naturally overspread in the Satun provincial area due to underlying limestone bedrock. The sinkhole potential map of Satun province was hurriedly produced after the big earthquake accompanied by the severe tsunami event in 2004 and the map was firstly published by DMR (2005). The mapping of sinkhole types relating to soil materials, especially dropout sinkholes, was the main task. The potential sinkhole area was delineated by the simple approach of limestone bedrock or mountain proximity. As a consequence, the limestone mountain is generally surrounded by areas of a high potential sinkhole. There have no collapse sinkholes both onshore and offshore represented on the map. To study rock failure, the sinkhole potential area classification must be studied in more detail.

According to Sinsakul et al, (2002), the Satun coastline erosion mapping was initially conducted by the DMR prior to 2002, and the mission of coastal management has been responsible by the Department of Marine and Coastal Resources (DMCR). To monitor shoreline erosion, Khundee et al., (2019) used the Real-Time Kinematic Global Navigation Satellite Systems (RTK-GNSS) method for the beach erosion investigation from the Pak Nam Bara to Ao Noon in the Mu Ko Petra National Park. Beach erosion is the topic study that is more focusing on Thailand. Many hardly structures are used to reduce the wave action of the sea. Erosion at rocky coasts has rarely been explored by organizations, so data is not adequate to support the study of limestone coast collapse.

Based on the intensity of the Mercalli scale, the seismic hazard map of Thailand published by DMR (2016) is categorized into 5 levels which are I-III, IV, V, VI, and VII In Satun province, the active faults have been never discovered, and the intensity of Satun is I-III which is classified as the lowest level. However, coastal karst terrain can be affected by the Klong Marui fault which is one of two major active strike-slip fault systems in southern Thailand. It extends in a northeast-southwest direction from Phuket towards Surat Thani province, and the distance from Satun provincial area to the Klong Marui fault zone is about 290 kilometers.

At coastal karst, tourists often take a time in an attractive place without realizing that there is danger from geohazards. Rock failure mode: a planar, wedge, or topple can cause rockslide or rockfall in high fractured limestone of marine karst terrain as the latest rockslide event happened on February 20, 2021. For the safety of tourists, rock mass stability and slope mass stability have to be investigated in the Satun Geopark and Thailand national Park. Moreover, recommendations or guidelines for rock reinforcement are introduced to reduce the opportunity of geohazard risk.

# 5. METHODOLOGY

Six processes were conducted for rock failure assessment (**Figure 5.1**). They are described below.

(1) Making of an orthophoto map obtained from drone flying, lineaments and boundary of limestone rock types can be extracted from the orthophoto by the method of visual interpretation.

(2) Mapping the sinkhole potential area of Satun province.

(3) Mapping Preliminary rock fall zonation by the multi-criteria analysis in GIS which the map using for field checking and determining rock stability study in detail.

(4) Collecting the data relating to rock mass discontinuity and clues of former rock fall, and to estimate Rock Mass Rating (RMR) values in field investigation.

(5) Slop Mass Rating (SMR) assessment, the first step is to assess the mode of failure that may be originated rock fall type and to evaluate the stability of outcrop slope due to discontinuity cutting on.

(6) Writing a report, presenting to the provincial office and local government, and giving recommendations for reducing rockfall impacts on tourist sites.

The equipments using in field investigation were geological hammer, compass (Breithaupt), tape measure or ruler, and Schmidt hammer. The Software used for data analysis and displays the imagery maps were Agisoft Metashape, DIPS, and ArcMap.

Field survey was took place at the end of the year 2021 from the coastal limestone outcrop that is considered as having a high potential area of geohazards at paleo-collapse sinkhole and may cause medium to high negative impact. The direct measurement or investigation in the field was composed of four data sets of primary data: photos obtained from drone flying, Rock Mass Rating ($RMR_b$) parameters, slope face orientation of outcrops, and various discontinuity in karstic limestone.

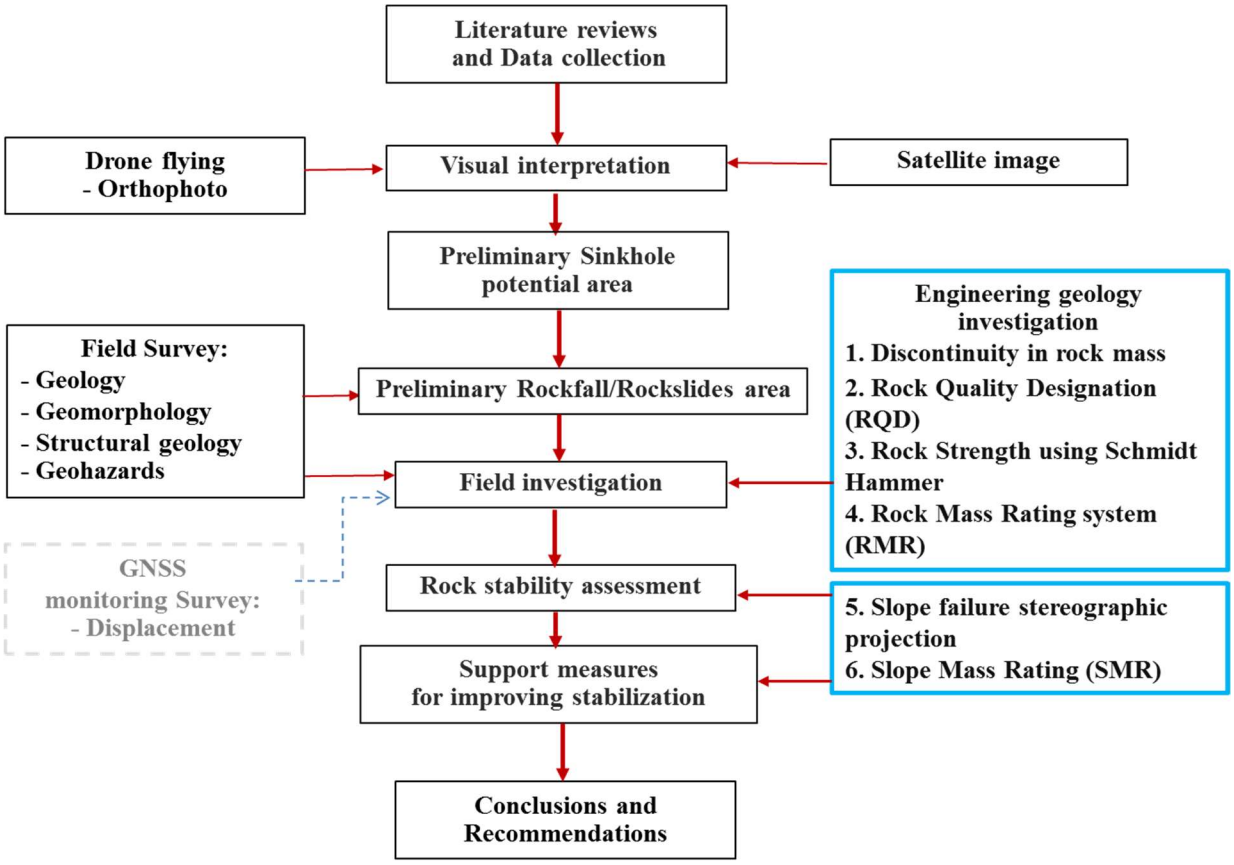


***Figure 5.1*** *Framework of activities*

### Rock Mass Rating (RMR)

The RMR is an effective geomechanics classification system for rocks mass (Bieniawski, 1974a, Bieniawski, 1974b; Bieniawski, 1976; Bieniawski, 1984; Bieniawski, 1989). Depending on practical knowledge, the seven parameters are basically used to classify a rock mass. They composed of uniaxial compressive strength of intact rock (R1), Rock Mass Quality or RQD (R2), Joint and discontinuity spacing (R3), Joint conditions (R4), Groundwater conditions (R5), and Orientation of discontinuities (R6). Each parameter is designed for specific score depending on specific engineering properties and the RMR ratings of Bieniawski are shown in Table 5.1

**Table 5.1** The rating of six parameters of RMR system

| **Strength of Intact Rock** | | | | | | | |
|---|---|---|---|---|---|---|---|
| **Uniaxial compressive strength (MPa)** | >250 | 100-250 | 50-100 | 25-50 | 5-25 | 1-5 | <1 |
| **Point load strength (MPa)** | 8 | 4-8 | 2-4 | 1-2 | - | - | - |
| **Rating 1** | 15 | 12 | 7 | 4 | 2 | 1 | 0 |
| **Rock Quality Designation** | | | | | | | |
| **Rock quality designation (%)** | 90-100 | | 75-90 | 50-75 | 25-50 | | <25 |
| **Rating 2** | 20 | | 17 | 13 | 8 | | 3 |
| **Spacing of Discontinuities** | | | | | | | |
| **Spacing of discontinuities (m)** | >2 | | 0.6-2 | 0.2-0.6 | 0.06-0.2 | | <0.06 |
| **Rating 3** | 20 | | 15 | 10 | 8 | | 5 |
| **Condition of Discontinuities** | | | | | | | |
| **Persistence (m)** | <1 | | 1-3 | 3-10 | 10-20 | | >20 |
| **Rating 4.1** | 6 | | 4 | 2 | **1** | | 0 |
| **Separation (mm)** | None | | <0.1 | 0.1-1 | 1-5 | | >5 |
| **Rating 4.2** | 6 | | 5 | 4 | **1** | | 0 |
| **Roughness of discontinuity surface** | Very rough | | Rough | Slightly rough | Smooth | | Slickensided |
| **Rating 4.3** | 6 | | 5 | 3 | **1** | | 0 |
| **Infillings (mm)** | None | | Hard filling | | Soft filling | | |
| | | | <5 | >5 | <5 | | >5 |
| **Rating 4.4** | 6 | | 4 | 2 | 2 | | 0 |
| **Weathering discontinuity surface** | Unweathered | | Slightly weathered | Moderately weathered | Highly weathered | | Decomposed |
| **Rating 4.5** | 6 | | 5 | 3 | **1** | | 0 |
| **Groundwater Condition** | | | | | | | |
| **Inflow per 10 m tunnel length (L/min)** | None | | <10 | 10-25 | 25-125 | | >125 |
| **Ratio of joint water pressure to major principal stress** | 0 | | 0-0.1 | 0.1-0.2 | 0.2-0.5 | | >0.5 |
| **General description** | Completely dry | | Damp | Wet | Dripping | | Flowing |
| **Rating 5** | 15 | | 10 | 7 | 4 | | 0 |

| **Joint Orientation** | | | | | | |
|---|---|---|---|---|---|---|
| **Assessment of Joint Orientation Effect on Tunnels** | | | | | | |
| **Strike perpendicular to tunnel axis** | | | | **Strike parallel to tunnel axis** | | **Irrespective of strike** |
| **Drive with dip** | | **Drive against dip** | | | | |
| **Dip 45-90°** | **Dip 20-45°** | **Dip 45-90°** | **Dip 20-45°** | **Dip 20-45°** | **Dip 45-90°** | **Dip 0-20°** |
| Very favorable | Favorable | Fair | Unfavorable | Fair | Very unfavorable | Fair |
| **Assessment of Joint Orientation Effect on Stability of Dam Foundation** | | | | | | |
| **Dip 0-10°** | **Dip 10-30° and Dip direction to** | | | **Dip 30-60°** | | **Dip 60-90°** |
| | **Upstream** | | **Downstream** | | | |
| Very favorable | Unfavorable | | Fair | Favorable | | Very unfavorable |

| **Rating 6** | | | | | |
|---|---|---|---|---|---|
| **Assessment for** | **Very favorable** | **Favorable** | **Fair** | **Unfavorable** | **Very unfavorable** |
| **Tunnels** | 0 | -2 | -5 | -10 | -12 |
| **Dam foundation** | 0 | -2 | -7 | -15 | -25 |
| **Slope*** | 0 | -5 | -25 | -50 | -60 |

Notes: *It is recommended to use slope mass rating.

A sum of each ratings values provide overall comprehensive index of rock mass quality or RMR value. The RMR value can be shown as the following equation,

$$RMR = R1+R2+R3+R4+R5+(-R6)$$

Each RMR parameter is explained as follows.

**Strength of intact rock (R1)**

The strength value can be obtained from the Uniaxial Compressive Strength (UCS) test. As consequence of the destructive rock testing in the Satun Geopark and Thailand national parks illegally conducted, UCS values in the field were measured rock hardness by using the Schmidt Hammer. The hardness rebound number of rock mass measured with the Schmidt hammer has a scale ranging from 0 to 100. The obtained value depends on the type of device used, the size of the media measured, and the position of the device when taking the hardness rebound number (Triana and Hermawan, 2020). The hardness rebound number of that nondestructive testing is converted into Uniaxial Compressive Strength with Mega Pascal (MPa) unit. For the Prasat Hin Pan Yod, the equation introduced by Tonnayopas (1994) was used in converting the hardness rebound number in order to get a more precise Uniaxial Compressive Strength, which the equation can be written as follows

$A_0=1+0.0065\times\rho\times SHR$

$A_0$= Linear regression correlation

$UCS = 10^{A_0}$

UCS = Uniaxial Compressive Strength

$\rho$ = Limestone density (equal to 2711 kg/m$^3$ or 0.027 MN/m$^2$)

SHR = Schmidt's Hammer Rebound value

**Rock quality designation (R2)**

The Rock Quality Designation (RQD) was proposed by Deere (1964) as a quick measure of estimating rock mass quality from core recovery along core axis. The traditional RQD is defined as the sum of the length of core pieces that are greater or equal to 10 centimeters divided by the total length of the core run as shown in the following equation.

$$\mathrm{RQD} = \frac{\text{sum of core pieces} \geq 10\ \text{cm}}{\text{total drill run}} . 100,$$

The traditional RQD method was directly used for the coastal limestone outcrop of the Prasat Hin Pan Yod. It is convenient to apply on the rocky coast during a short time of low tide. The RQD at outcrop can also be estimated using volumetric discontinuity count per one cubic meter of rock accompanied by the average joint spacing in meters for the number of joint sets (Palmström, 1982). Owing to gently dipping bedded limestone and moderately to steeply dipping joint plane, the vertical line profiles were preferred for estimating the RQD. Based on Bieniawski

(1989), the RQD classification and rating was shown in Table 5.2.

**Table 5.2** RQD and Rock quality**.**

| S. No. | RQD (%) | Rock quality |
|---|---|---|
| **1** | < 25 | Very poor |
| **2** | 25-50 | Poor |
| **3** | 50-75 | Fair |
| **4** | 75-90 | Good |
| **5** | 90-100 | Excellent |

**Spacing of discontinuities (R3)**

Discontinuities are composed of several types: bedding, joint, fault and shear zone weaken surface, cavity and cave. The frequency of discontinuities in rock mass was happened by geological force. For discontinuity spacing, the perpendicular distance between one discontinuity and another can be measured by distance tape, ruler and sight estimation. According to Bieniawski (1989) the spacing of discontinuities was categorized into five classes and the scores was assigned for each class as shown in Table 5.1.

**Discontinuity conditions (R4)**

Discontinuity conditions consist of roughness, separation, persistence, weathering, and infilling materials that appear on the surface. A careful judgment is essential to assess engineering rock conditions to numerical values. The obtained value may differ depending on the experience of the surveyor. The five discontinuity conditions are individually evaluated into a numeric value and combined to get the whole number. The discontinuity conditions and their rating are described by Bieniawski (1989) as shown in Table 5.1.

G**roundwater condition (R5)**

Groundwater condition is critical RMR parameter particularly karst topography. In case coastlines, the sea action giving high water pressure directly affects the strength of rock mass as well. Water flow rate measurement is trouble in the field. Fortunately, the general condition on

rock surfaces that proposal by Bieniawski (1989) : dry, humid, wet, dripping, and flowing as shown in Table 1, can be roughly applied the rating for coastal karst area.

**Discontinuity orientation (R6)**

The relation between discontinuity orientation and cave axis is influential factor to indicate the stability of cave. The unfavourable drive direction of cave may be caused unstable cave. However, Pantaweesak et al, (2017) suggested that the principle of discontinuity orientation is not suitable for estimating rock slope stability.

After the combination of these six parameters, the rating of RMR can be categorized into five classes which are very good (100–81), good (80–61), fair (60–41), poor (40–21), and very poor (<20). The design parameters and engineering properties of rock mass is depicted in Table 5.3.

**Table 5.3** Design parameters and engineering properties of rock mass.

| Properties of rock mass | RMR | | | | |
|---|---|---|---|---|---|
| | 100–81 (class I) | 80-61 (class II) | 60-41 (class III) | 40-21 (class IV) | <20 (class V) |
| Classification of rock mass | Very good | Good | Fair | Poor | Very poor |
| Average stand-up time | 20 years for 15 m span | 1 year for 10 m span | 1 week for 5 m span | 10 hours for 2.5 m span | 30 minutes for 1 m span |
| Cohesion of rock mass (MPa) | >0.4 | 0.3–0.4 | 0.2–0.3 | 0.1–0.2 | <0.1 |
| Internal friction angle of rock mass | >45º | 35–45º | 25–35º | 15–25º | <15º |
| Allowable bearing pressure (T/m$^2$) | 600–440 | 440–280 | 280–135 | 135–45 | 45–30 |
| Safe cut slope | >70º | 65º | 55º | 45º | <40º |
| Suggested supports for less than 10 meters tunnel | | | | | |
| Class | Support | | | | |
| I | No support required except for occasional spot bolting. | | | | |
| II | 20 mm diameter rock bolts with fully grouted in crown 3 m long spaced 2.5 m with wire mesh, shotcrete 50 mm in crown. | | | | |
| III | 20 mm diameter systematic rock bolts with fully grouted 4 m long spaced 1.5–2 m in crown and walls with wire mesh in crown, shotcrete 50–100 mm in crown and 30 mm in sides. | | | | |
| IV | 20 mm diameter systematic rock bolts with fully grouted 4–5 m long spaced 1–1.5 m in crown and wall with wire mesh, shotcrete 100–150 mm in crown and 100 mm in sides, Light-medium ribs spaced 1.5 m. | | | | |
| V | 20 mm diameter systematic rock bolts with fully grouted 5–6 m long spaced 1–1.5 m in crown and walls with wire mesh, shotcrete 150–200 mm in crown 150 mm in sides and 50 mm on face, Medium to heavy steel ribs spaced 0.75 m with steel lagging and forepoling. | | | | |

**Stereographic projection**

Stereographic projection is one of the most widely used methods used for evaluating rock slope stability. The method was carried out to determine rock failure styles: planar, wedge, and toppling that can be occur in discontinuous planes on both natural slope and artificial slope. Stereographic projection assesses the slope stability by using the pole position, measuring the strike and dip of discontinuities, such as joints or fault, and projecting the pole of discontinuity on the net. It does not analyze any other factors excluding orientation of discontinuity and the friction angle, but it can predict the stability of rock slope (Hoek and Bray, 1981).

Figure 5.2 is an example of a stability envelope diagram that shows the failure condition angle of sliding types, the great circle of discontinuity, face slope, and friction angle (⌀), and the potential sliding zone or daylight of planar, wedge, toppling envelope on the Schmidt net (Hoek and Bray, 1981).

Schmidt net or equal-area projection was used for the study area and analyzed by using DIPS v.7.0 software. Discontinuity in the rock mass, collecting in the field and analyzing in the software, was mainly composed of joint, fracture, fault and bedding. Orientation of discontinuity in rock mass was measured in term of dip direction/dip angle. The basic parameters directly relating to RMR value were designed for failure modeling in DIPS v.7.0 software: friction angle equal to 30 degrees, and also lateral limit angle equal to 20 degrees. In case without field RMR assessment, it has to use the RMR value of nearby stations due to the similarity of lithology and bedding.

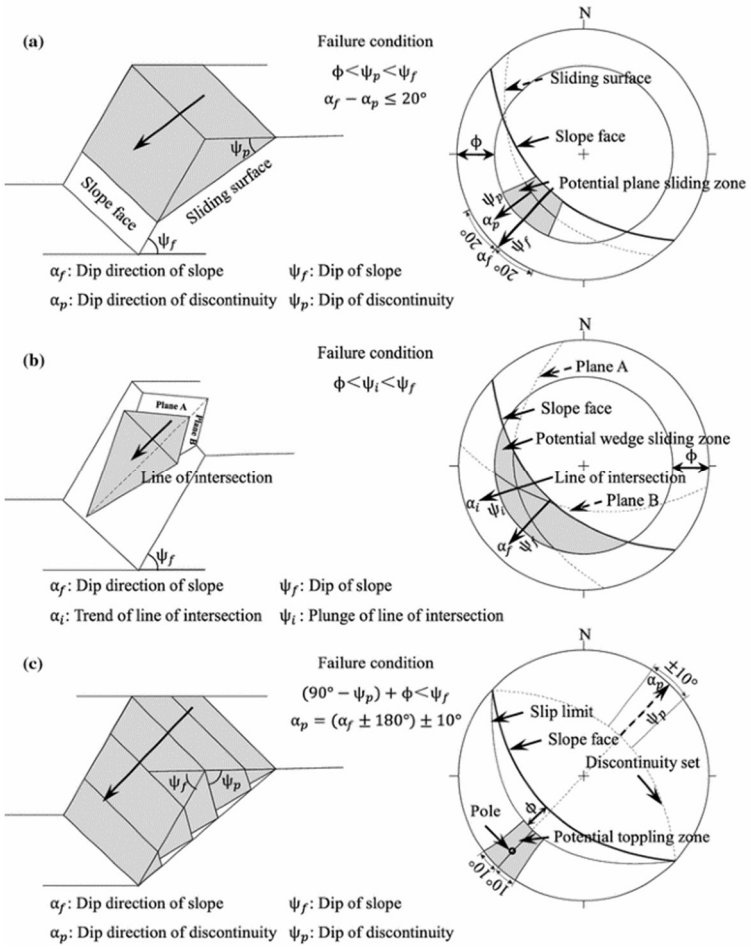


***Figure 5.2*** *Types of rock slope failure and stereographic projection of structural conditions (Hoek and Bray, 1981)*

**Slope Mass Rating (SMR)**

The SMR was developed by Romana (1985) for evaluating rock slope stability depending on the first five basic parameters of RMR ($RMR_b$) resulting from Bieniaski's rock mass classification as mentioned and then corrected by adjustment factors that related to correlation of discontinuity orientation with respect to face slope. To get SMR value, $RMR_b$ are evaluated with adjustment factors and can be written as following equation:

$$SMR = RMR_b + (F1*F2*F3) + F4$$

The adjustment factors (F1, F2, F3), as detailed description in Table 5.4 are specific scores given based on the orientation of the discontinuous plan on face slope (outcrop slope), and F4 is the correction factors for the method of excavation on an outcrops/slope. The adjustment factors/correction parameters for SMR as follows

F1 which depends on the parallelism between dip direction and slope dip;

F2 which depends on the steepness (or the dip angle) of discontinuity; bed, joint, fracture, fault, and shear/weaken plane;

F3 which depends on the relation of the discontinuity dip angle and the slope dip angle;

F4 is the correction factor that depends on the excavation method on slope as shown in Table 5.5.

**Table 5.4** Correction parameters for SMR classes (Romana,1985)

| Type of failure | | | Very favourable | Favourable | Normal | Unfavourable | Very unfavourable |
|---|---|---|---|---|---|---|---|
| P<br>T | A = | $\lvert\alpha_j-\alpha_s\rvert$<br>$\lvert\alpha_j-\alpha_s-180\rvert$ | >30° | 30-20° | 20-10° | 10-5° | <5° |
| P/T | $F_1$ | | 0.15 | 0.40 | 0.70 | 0.85 | 1.00 |
| P | B = | $\beta_j$ | <20° | 20-30° | 30-35° | 35-45° | >45° |
| P<br>T | $F_2$ | | 0.15<br>1.00 | 0.40 | 0.70 | 0.85 | 1.00 |
| P | C = | $\beta_j-\beta_s$ | >10° | 10-0° | 0° | 0-(-10°) | <(-10°) |
| T | | $\beta_j+\beta_s$ | <110° | 110-120° | >120° | - | - |
| P/T | $F_3$ | | 0 | -6 | -25 | -50 | -60 |
| FAILURE: P planar; T toppling. DIP DIRECTION: $\alpha_j$ discontinuity; $\alpha_s$ slope. DIP: $\beta_j$ discontinuity ; $\beta_s$: slope . | | | | | | | |

**Table 5.5** Values corresponding to the factor F4 (Romana,1985)

| Excavation method ($F_4$) | | | |
|---|---|---|---|
| Presplitting | +10 | Blasting or mechanical | 0 |
| Smooth blasting | +8 | Natural slope | +15 |
| Natural slope | +15 | | |

**Slope support guidelines**

According to SMR value, the recommendations of slope support measures can be determined for improving stabilization. Romana (1985) categorized SMR into 5 classes from very bad to very good as described in Table 5.6 and proposed slope support guideline based on SMR value as shown in Figure 5.3. The support measures can be groped into six different classes: No support, protection, reinforcement, concreting, drainage, and re-excavation. The greater value than 80 of SMR value defined as very good stability of slope having no support, whereas the lower level of stability will require a variety of reinforcement. Singh and Goel (2011) categorized SMR values in more detail and proposed various measures of stabilization for each SMR classes as given in Table 5.7. These slope support classification systems based on SMR values can give the first approximation during the reconnaissance investigation.

**Table 5.6** Explanations of SMR classes (Romana,1985).

| Classes | V | IV | III | II | I |
|---|---|---|---|---|---|
| SMR | 0-20 | 21-40 | 41-60 | 61-80 | 81-100 |
| Description | Very bad | Bad | Normal | Good | Very good |
| Stability | Completely unstable | Unstable | Partially stable | Stable | Completely stable |
| Failures | Big planar or soil-like | Planar or big wedges | Some joints or many wedges | Some blocks | None |
| Failure probability | 0.9 | 0.6 | 0.4 | 0.2 | 0 |

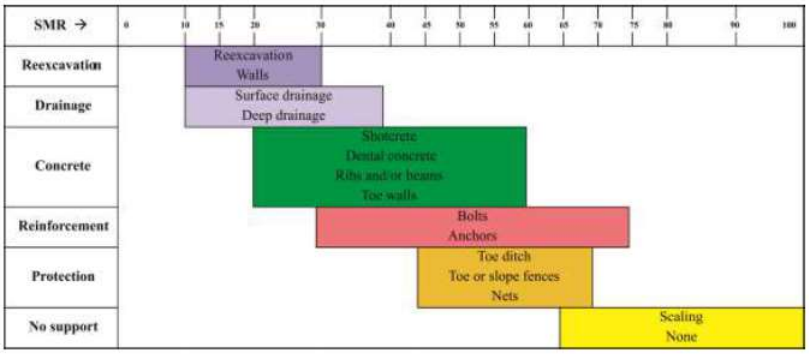


*Figure* 5.3 *Slope support guideline based on SMR (Romana, 1985)*

**Table 5.7** Suggested Supports for various classes (Singh and Goel, 2011)

| SMR classes | SMR values | Suggested supports |
|---|---|---|
| Ia | 91–100 | None |
| Ib | 81–90 | None, scaling is required |
| IIa | 71–80 | (None, toe ditch, or fence), spot bolting |
| IIb | 61–70 | (Toe ditch or fence nets), spot or systematic bolting |
| IIIa | 51–60 | (Toe ditch and/or nets), spot or systematic bolting, spot shotcrete |
| IIIb | 41–50 | (Toe ditch and/or nets), systematic bolting/ anchors, systematic shotcrete, toe wall and/or dental concrete |
| IVa | 31–40 | Anchors, systematic shotcrete, toe wall and/or concrete (or re-excavation), drainage |
| IVb | 21–30 | Systematic reinforced shotcrete, toe wall and/or concrete, re-excavation, deep drainage |
| Va | 11–20 | Gravity or anchored wall, re-excavation |

Less popular support measures are given in brackets.

# 6. RESULT AND DISCUSSION

## 6.1. Orthophoto map obtained from drone flying

The DJI Mavic 2 Pro, a lightweight Unmanned Aerial Vehicles (UAV) (Figure 6.1), was used for achieving the Koh Khao Yai image. The traverse line of drone was covered the north part of Koh Khao Yai islands where the Prasat Hin Pan Yod located. According to the time that taking photo was nearly at noon, it allowed dark shadow appeared along the edges of sea cliff, sea cave, and eastern side of the paleo-collapse sinkhole. The images obtained from UAV was totally 1,202 images covering 0.065 square kilometers. For orthophoto making, Agisoft Metashape software was adopted to conduct data processing. The output orthophoto had a Ground Sampling Distance (GSD) of 4.15 centimeters. For data quality control, the horizontal position value (East and North coordination) is quite precise, but its elevation or vertical axis is still high error. However, Orthophoto is very useful for the DMR surveying team to explore the orientation of rock mass discontinuity and to concentrate on unstable zone due to marine erosion.


***Figure 6.1*** *Lightweight drone released from the wooden fishing boat for rockfall exploration*

### 6.2. Mapping sinkhole potential area of Satun province

The first sinkhole potential map was published in 2005 by DMR, then it has been updated in 2022 by using the GIS system. The simple overlay technique of various relating factors was utilized for analysis. The five factors adopted for the improvement of sinkhole zoning have consisted of the density of lineament intersection, lineament density, distance to lineament, stream density, and distance to stream. Enhanced sinkhole potential area is classified into five levels which are very low, low, medium, high, and very high. All levels could be found on the Koh Kao Yai Islands. The grid cell resolution of result data is 30x30 meters. The high potential area is abundantly covered in the Koh Kao Yai Islands, particularly in the Prasat Hin Pan Yod sinkhole chamber (Figure 6.2). Types of the sinkholes as classified by Waltham et al., (2005) do not conduct by the DMR due to the scarcity of fundamental analysis data. However, an enhanced sinkhole potential map is still useful for limestone failure assessment in the Prasat Hin Pan Yod area.

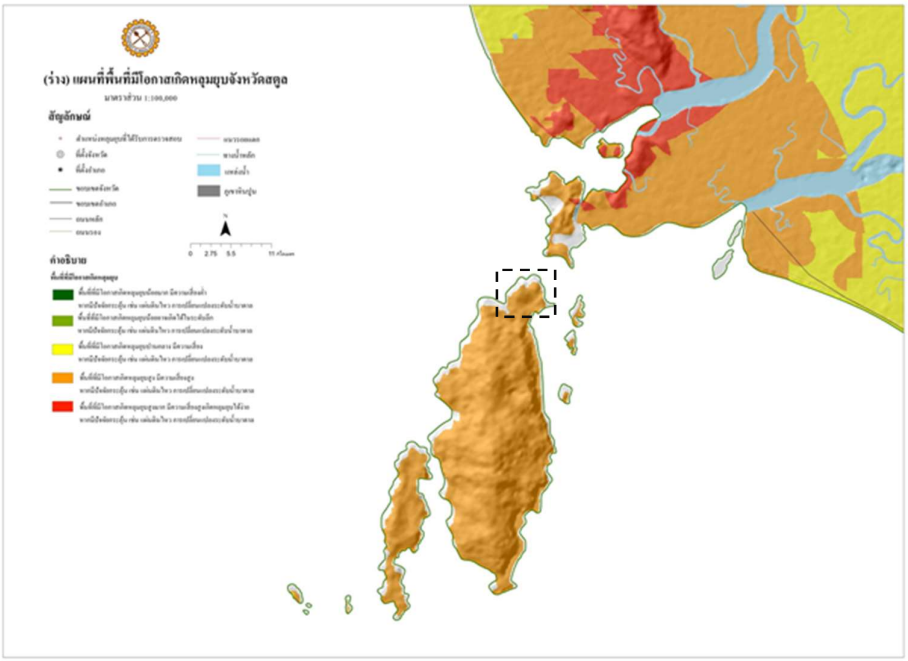

***Figure 6.2*** *High sinkhole potential covering the Prasat Hin Pan Yod chamber (Black dash rectangular shape) and the overall area of Koh Kao Yai Islands*

### 6.3. Rock fall hazard zonation

To examine the overview rock mass stability and select suitable locations for collecting field data, rock fall hazard zonation of the Prasat Hin Pan Yod chamber had mapped by using the approach of simple multi-criteria in GIS. The five basic factors were integrated to analyze and delineate rock fall hazard areas (Figure 6.3). They are consisting of density of lines (Figure

6.3A), density of intersection points (Figure 6.3B), Lineament proximity (Figure 6.3C), slope (Figure 6.3D), and aspect (Figure 6.3E).

The rock fall hazard zonation (Figure 6.5) resulted in a grid cell size of 5x5 meters and was categorized into 5 classes including very low, low, moderate, high, and very high. The map shows moderate to high level hazard seems to be happening along sea cliffs and at the entrance of tourist sites as well.

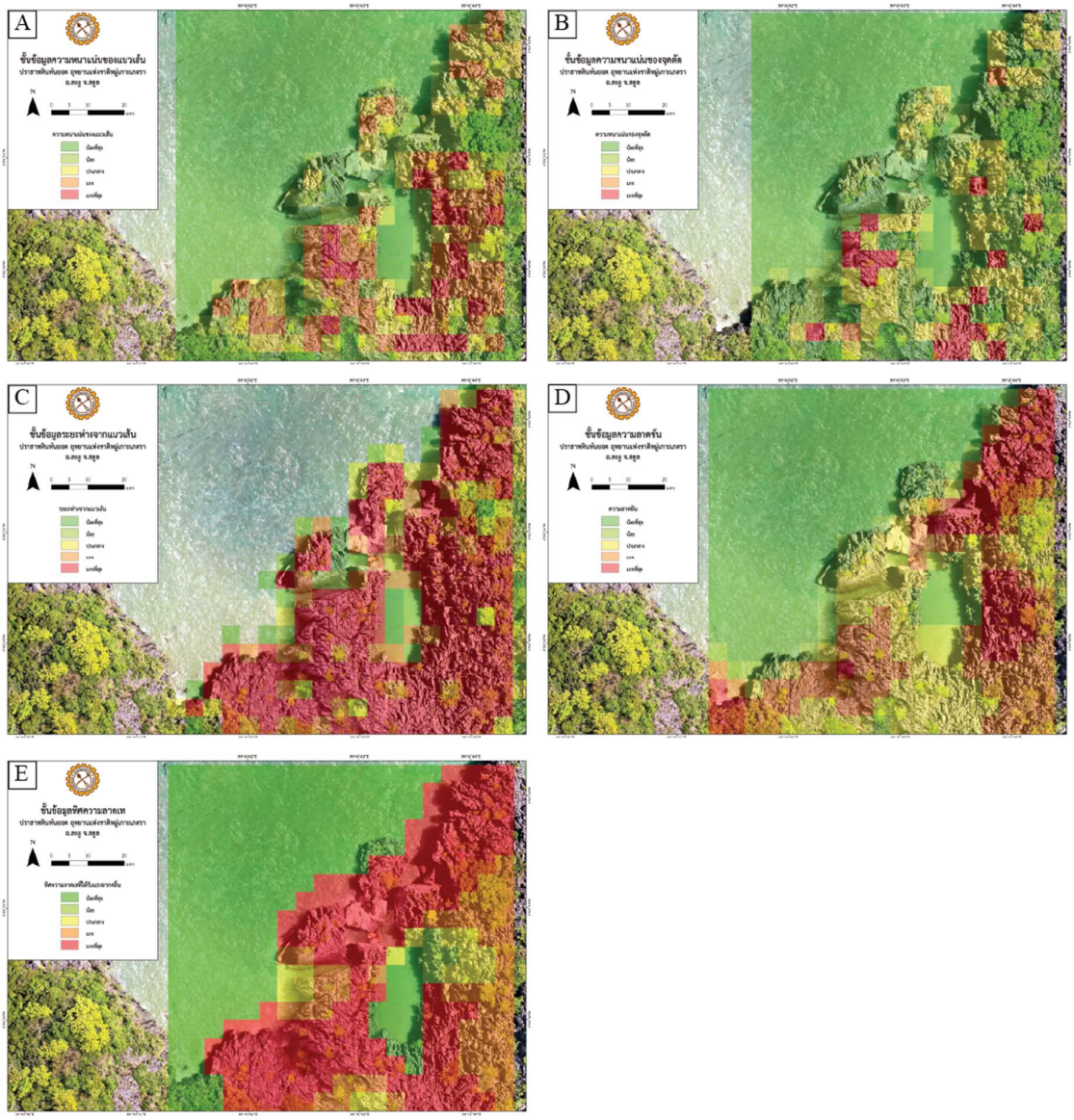


***Figure 6.3*** *Five factors for preliminary rock fall hazard mapping using GIS; (A) density of lines, (B) density of intersection points, (C) Lineament proximity, (D) slope, and (E) aspect.*

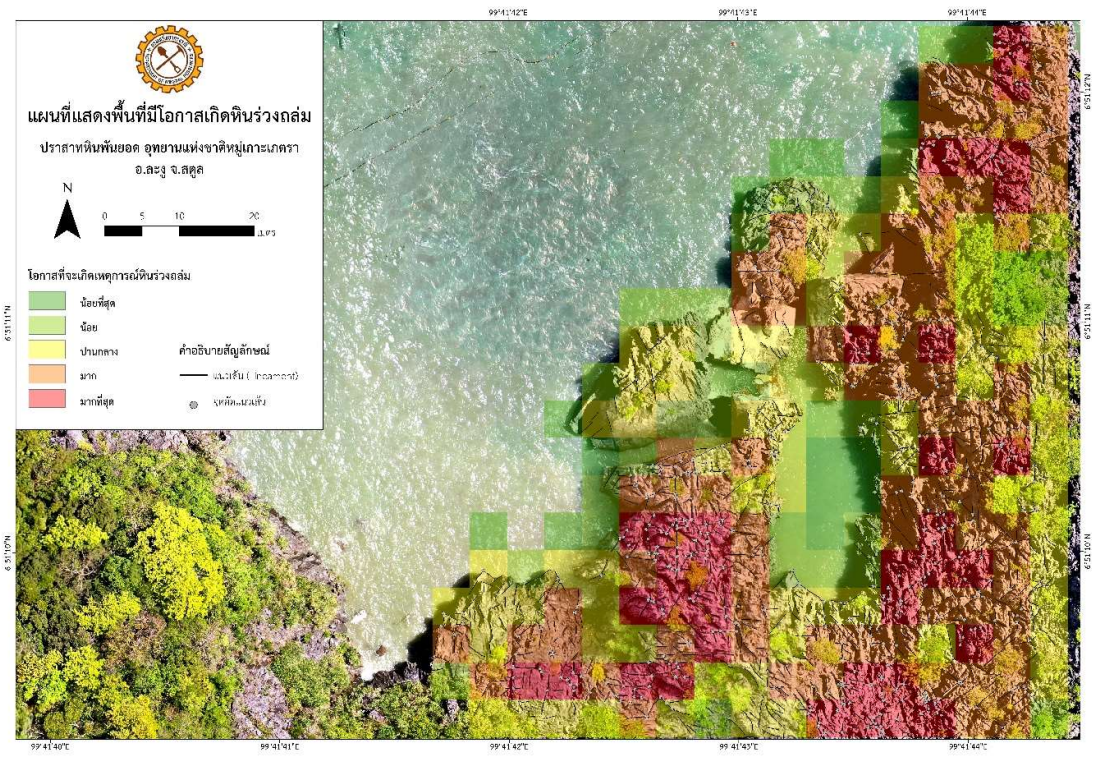


***Figure 6.4*** *preliminary rock fall hazard map, Prasat Hin Pan Yod tourist site, Satun province*

### 6.4. Rock Mass Rating (RMR) evaluation

The RMR values can be estimated through nine locations (Figure 6.5) distributed along the rim of the sinkhole chamber, a big broken block of limestone, and the new expected entrance of the tourist site. The RMR values ranged from 53 to 62. They are detailed in Table 6.1. The result shows that the RMR of bedded limestone has a lower value than massive limestone. Thinner bedding is stratigraphically overlying on the Massive limestone, so it is hard to explore unstable rock when rock mass locates in the high places of the Prasat Hin Pan Yod area.

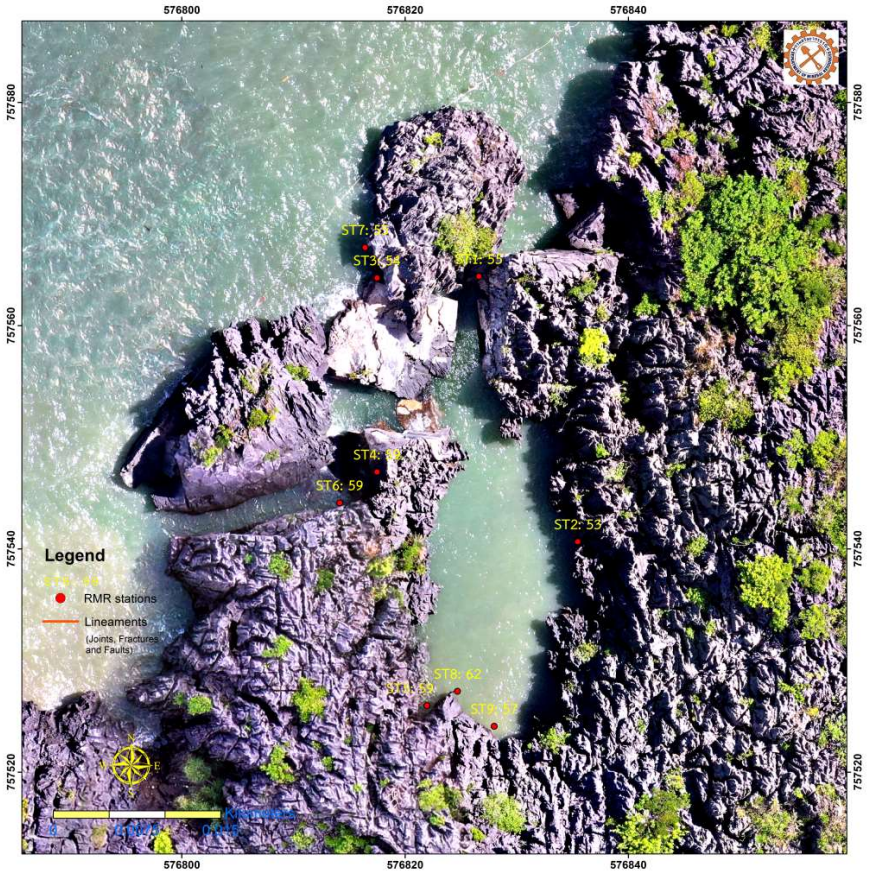


***Figure 6.5*** *showing stations of measured Rock Mass Rating overlying on orthophoto*

**Table 6.1** The summary of RMR value that obtained from the field investigation

| Station | UCS | RQD | joint spacing | Persistent | Aperture | joint roughness | Filling | Weathering | GW | Discontinuity orientation | RMR |
|---|---|---|---|---|---|---|---|---|---|---|---|
| **1** | 54.29 | 75.38 | 117.78 cm | 4.87 m | 20-30 mm | rough | none | moderate | Flowing | none | **55** |
| | 7 | 17 | 15 | 2 | 0 | 5 | 6 | 3 | 0 | 0 | |
| **2** | 54.83 | 95.68 | 60,80, 100cm | 6.05 m | 5-10 mm | rough | none | moderate | Flowing | Dip 0-20 irrespective of strike | **53** |
| | 7 | 20 | 15 | 2 | 0 | 5 | 6 | 3 | 0 | -5 | |
| **3** | 61.78 | 75.38 | 118.78cm | 10.69 m | 20-30 mm | rough | none | moderate | Flowing | none | **54** |
| | 7 | 17 | 15 | 1 | 0 | 5 | 6 | 3 | 0 | 0 | |
| **4** | 63.39 | 95.7 | 65 cm | 3 m | 20 mm | very rough | none | moderate | Flowing | none | **59** |
| | 7 | 20 | 15 | 2 | 0 | 6 | 6 | 3 | 0 | 0 | |
| **5** | 56.84 | 92.09 | 60 cm | 3,10 m | 5mm | rough | none | moderate | tidal | none | **59** |
| | 7 | 20 | 15 | 2 | 1 | 5 | 6 | 3 | 0 | 0 | |
| **6** | 61.78 | 93 | 110 cm | 3 m | 12 mm | very rough | none | modeatre | Flowing | none | **59** |
| | 7 | 20 | 15 | 2 | 0 | 6 | 6 | 3 | 0 | 0 | |
| **7** | 61.24 | 75.38 | 70 cm | 10 m | 10 mm | rough | none | moderate | Flowing | none | **55** |
| | 7 | 17 | 15 | 2 | 0 | 5 | 6 | 3 | 0 | | |
| **8** | 54.83 | 91.48 | 60, 100 cm | 3 m | 5 mm | very rough | none | moderate | tidal | none | **62** |
| | 7 | 20 | 15 | 4 | 1 | 6 | 6 | 3 | 0 | 0 | |
| **9** | 58.23 | 96.91 | 64 cm | 12.6m | 1 0mm | rough | none | moderate | tidal | none | **57** |
| | 7 | 20 | 15 | 1 | 0 | 5 | 6 | 3 | 0 | 0 | |

### 6.5. Rock failure analysis using Stereographic projection

The result of rock failure analysis using stereographic projection was shown in Table 6.2 and the failure model of some investigating stations were stereographically illustrated in Figure 6.6 to Figure 6.9. The study was found that the wedge failure of rock fall has more potential and happens more frequently than toppling and planar, respectively. After field checking, Wedge failure was found that it tends to be occurred small event of rock fall with small block pending in cavity and mainly caused unsafely in tourist site. For toppling failure, oblique toppling and direct toppling have the same situation as planar failure but will be happened in particularly locality. Planar failure can be occurred the lowest potential of rock fall, but big events with huge block can be happened in the recent time, for example, the Rock fall/Rock slide event of the Prasat Hin Pan Yod area in February 23, 2021.

The making of stereographic projection from the discontinuous planes on natural outcrop slope was used for modeling of rock mass failures or rock fall types that can occur in a planar, wedge, or toppling. The rock mass failures were next used to calculate the SMR adjustment factors.

**Table 6.2** The summary of rock failure analysis using stereographic projection

| Station | No. | Face slope (Dip direction/Dip angle) | Failure mode | | | | | |
|---|---|---|---|---|---|---|---|---|
| | | | Planar (%) | Wedge (%) | Toppling (%) | | | |
| | | | | | Direct | Oblique | Flexural | Base plane |
| 1 | 1A | 003/85 | 0 | 25.15 | 15.2 | 9.36 | 0 | 0 |
| | 1B | 355/88 | 0 | 42.69 | 16.96 | 9.36 | 0 | 21.05 |
| | 1C | 087/88 | 26.32 | 59.06 | 10.53 | 12.87 | 0 | 36.84 |
| | 1D | 317/89 | 10.53 | 50.88 | 2.92 | 25.15 | 0 | 10.53 |
| | 1E | 233/78 | 21.05 | 35.09 | 21.64 | 34.5 | 10.53 | 21.05 |
| 2 | 2A | 325/80 | 0 | 1.11 | 11.11 | 47.78 | 21.43 | 0 |
| | 2B | 255/83 | 14.29 | 40 | 5.56 | 13.33 | 0 | 14.29 |
| | 2C | **225/84** | 21.43 | 64.44 | 10 | 4.44 | 0 | 21.43 |
| | 2D | 353/85 | 0 | 3.33 | 18.89 | 50 | 21.43 | 7.14 |
| 3 | 3A | 020/89 | 20 | 46.67 | 0 | 0 | 0 | 40 |
| | 3B | **095/89** | 33.33 | 32.38 | 10.48 | 1.9 | 6.67 | 40 |
| | 3C | 328/87 | 6.67 | 35.24 | 0.95 | 9.52 | 0 | 26.67 |
| | 3D | 122/87 | 0 | 18.1 | 13.33 | 3.81 | 6.67 | 6.67 |
| 4 | 4A | **260/78** | 12.5 | 45 | 12.5 | 17.5 | 18.75 | 18.75 |
| 5 | 5A | 062/85 | 0 | 0 | 0 | 10 | 0 | 20 |
| 6 | 6A | 004/81 | 0 | 1.9 | 3.33 | 39.52 | 4.76 | 14.29 |
| | 6B | 163/72 | 0 | 0.95 | 8.1 | 33.81 | 28.57 | 0 |
| | 6C | 337/81 | 0 | 5.24 | 0 | 26.67 | 0 | 14.29 |
| 7 | 7A | 245/78 | 9.09 | 22.92 | 35.04 | 12.12 | 12.12 | 9.09 |
| | 7B | 264/83 | 6.06 | 18.75 | 17.23 | 9.28 | 3.03 | 6.06 |
| | 7C | 324/77 | 9.09 | 21.97 | 0.57 | 4.55 | 24.24 | 18.18 |
| | 7D | **222/77** | 9.09 | 17.61 | 29.92 | 13.26 | 18.18 | 9.09 |
| | 7E | 290/82 | 9.09 | 23.67 | 4.92 | 4.92 | 12.12 | 12.12 |
| | 7F | 110/82 | 12.12 | 42.8 | 6.63 | 10.23 | 12.12 | 21.21 |
| 8 | 8A | 034/85 | 0 | 17.65 | 5.88 | 13.07 | 0 | 22.22 |
| 9 | 9A | 022/85 | 10 | 22.22 | 4.44 | 22.22 | 0 | 30 |

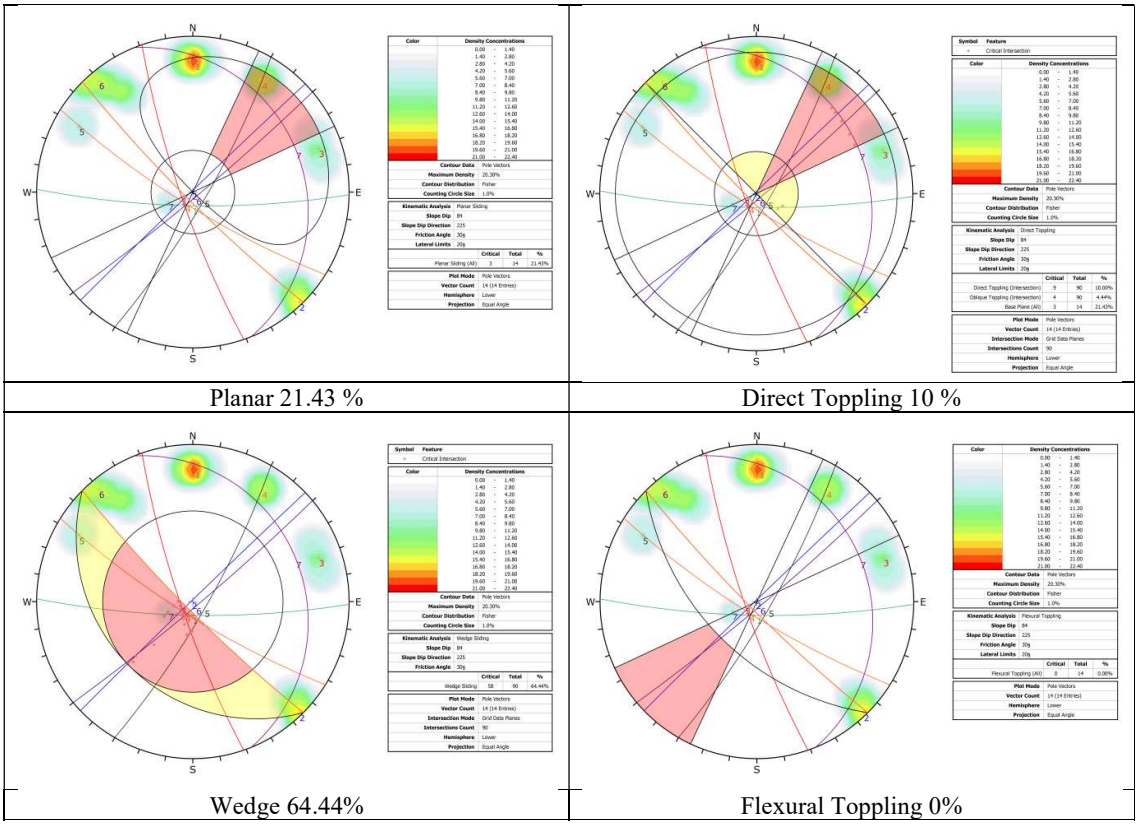


***Figure 6.1*** *showing stereographic projection of the station 2C*

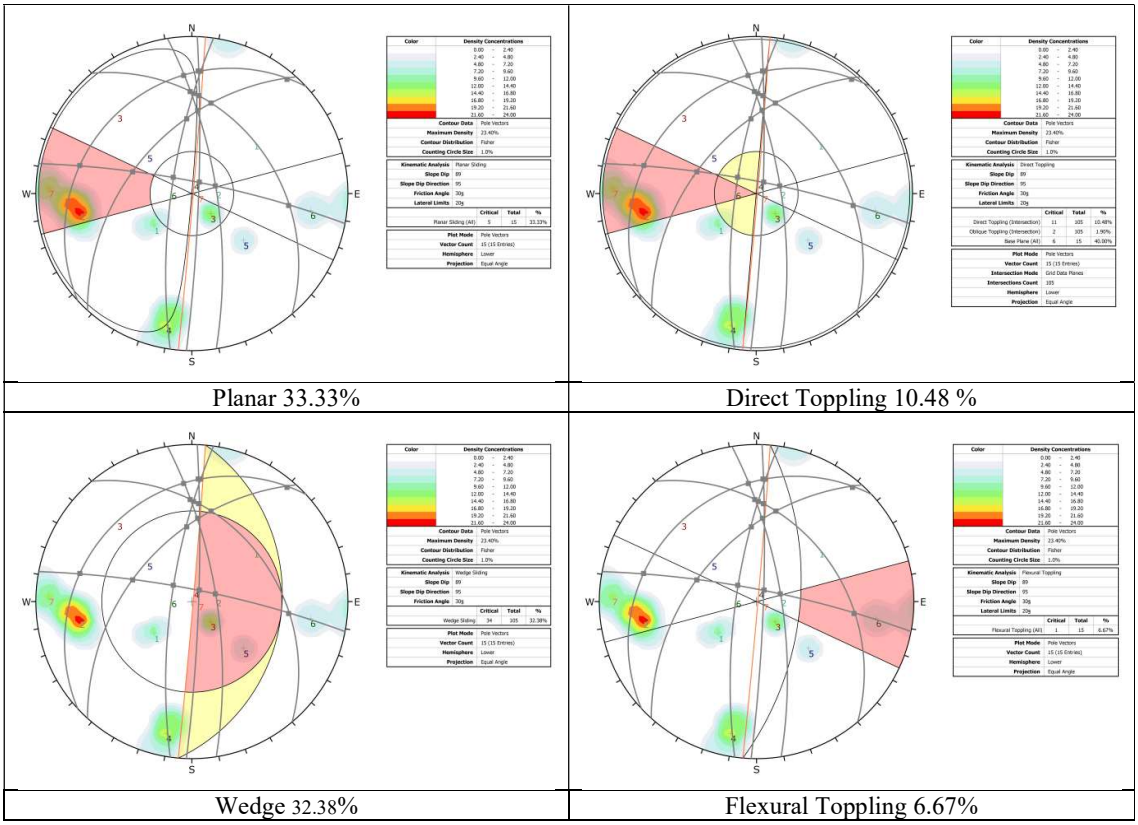


***Figure 6.2*** *showing stereographic projection of the station 3B*

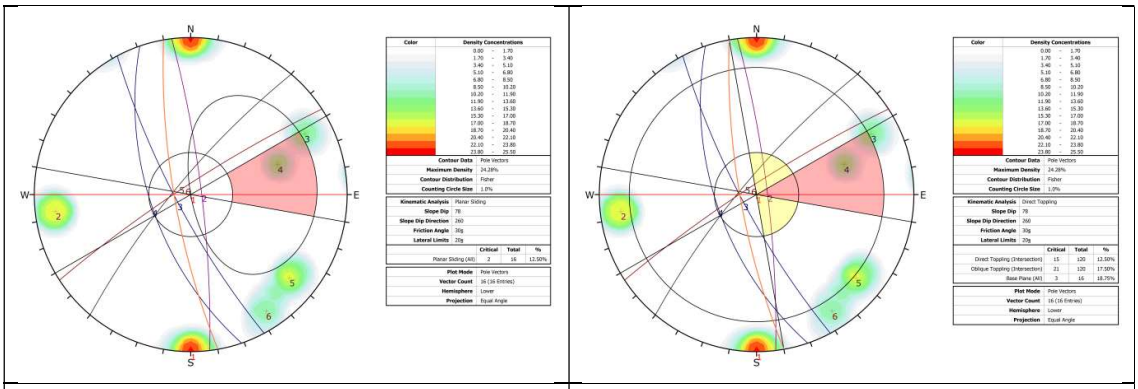

Planar 12.5%



Direct Toppling 12.5 %

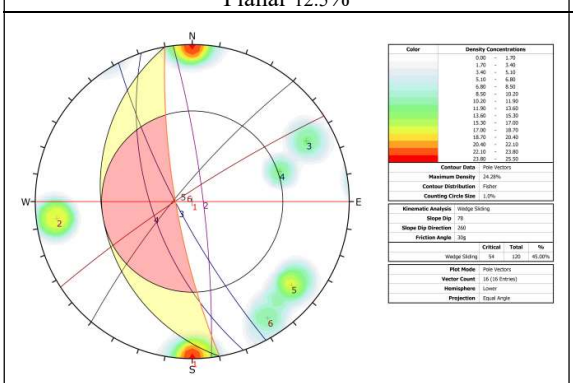

Wedge 45%

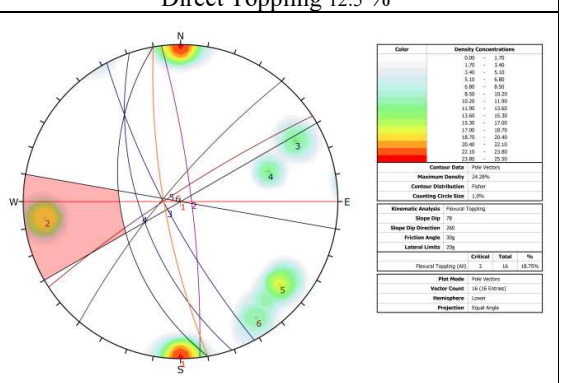

Flexural Toppling 18.75%

***Figure 6.6*** *showing stereographic projection of the station 4A*

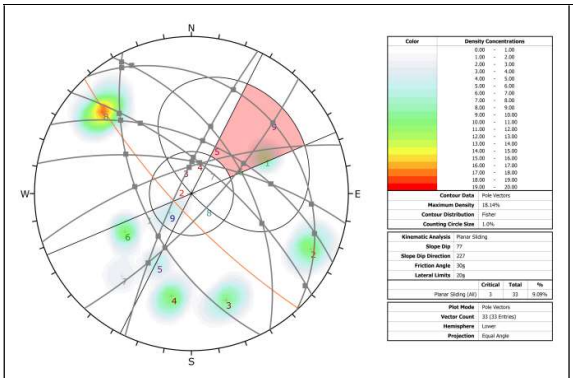

Planar 9.09 %

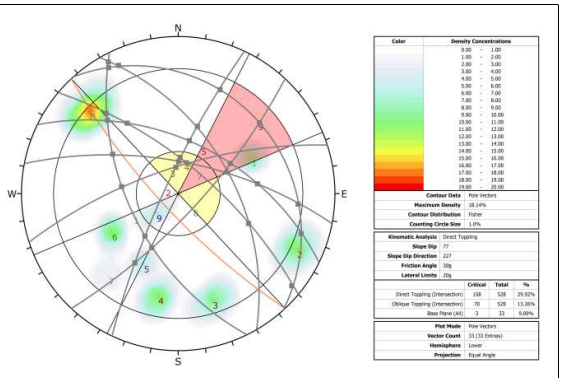

Direct Toppling 29.92 %

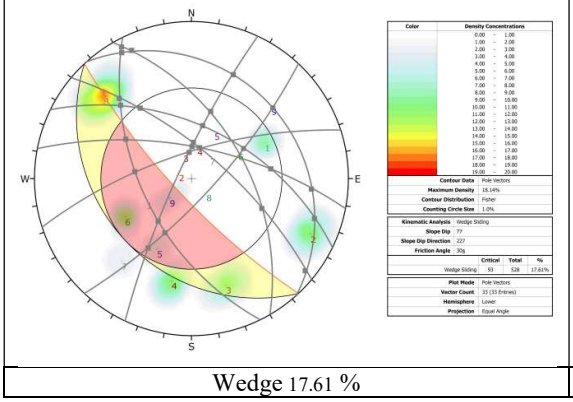

Wedge 17.61 %

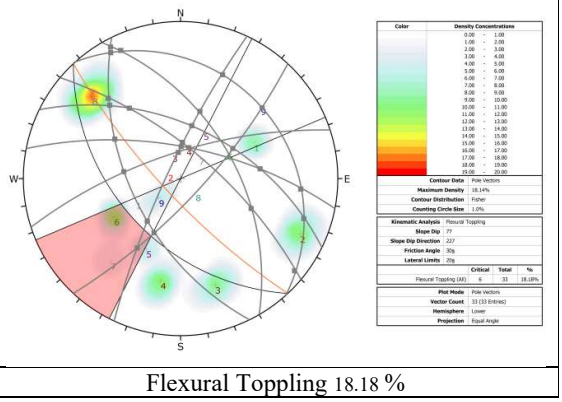

Flexural Toppling 18.18 %

***Figure 6.7*** *showing stereographic projection of the station 7D*

### 6.6. Slope Mass Rating (SMR) assessments

The SMR assessment in the Prasat Hin Pan Yod area can be divided into 4 sub-areas with a totally 26 of the SMR stations as shown in Figure 6.10

1) The area of rock slide in February, 23, 2021 that nowadays hiding the Prasat Hin Panyod entrance, in which was represented by the stations of 1A to1E, 3A to 3D, and 7A to 7F

2) The strait locating between linearly sea cliff and the former huge topple of rock mass, in which was illustrated by the stations of 4A, and 6A to 6C

3) A high eroded sea cave with clues of former rock fall and thin column supporting with high potential hazard, which representative stations was composed of 2A to 2C

4) A small beach within the Prasat Hin Pan Yod chamber that exposed whenever low tide, the representative stations were 8A and 9A

Slope Mass Rating (SMR) were calculated and classified according to Romana (1985). The SMR assessment in detail of station 2A and station 4A was partly shown in Table 6.3 and Table 6.4, respectively. The overall result of the 26 station was depicted in Table 6.5, and was shortly summarized in Table 6.6

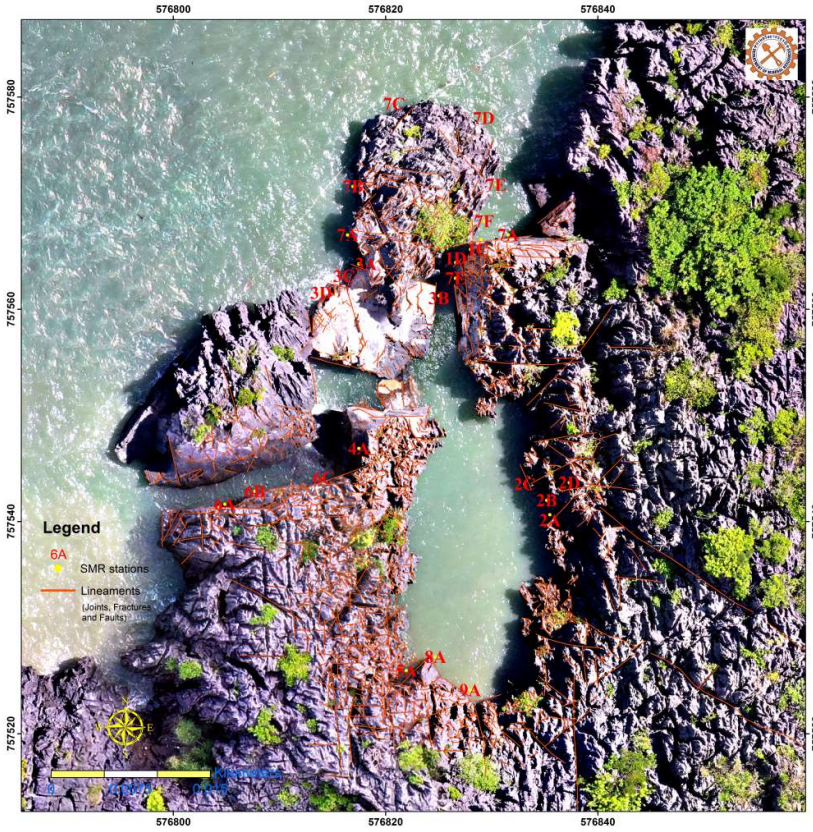

***Figure 6.8*** *showing stations of Slope Mass Rating (SMR) assessment*

**Table 6.3** Some of the evaluating result of Slope Mass Rating (SMR) at the station 2A

| Failure mode | Face slope | joint sets | Trend | Plunge | RMR | F1 | F2 | F3 | F4 | F1F2F3+F4 | SMR | Class | Stability |
|---|---|---|---|---|---|---|---|---|---|---|---|---|---|
| Planar | 225/84 | 120/80 | - | - | 53 | 105 | 80 | -4 | Natural | 7.5 | 60.5 | Normal | Partially stable |
| | | | | | | 0.15 | 1 | -50 | 15 | | | | |
| | 225/84 | 318/89 | - | - | 53 | 91 | 89 | 5 | Natural | 14.1 | 67.1 | Good | Stable |
| | | | | | | 0.15 | 1 | -6 | 15 | | | | |
| | 225/84 | 140/86 | - | - | 53 | 85 | 86 | 2 | Natural | 14.1 | 67.1 | Good | Stable |
| | | | | | | 0.15 | 1 | -6 | 15 | | | | |
| | 225/84 | 68/19 | - | - | 53 | 157 | 19 | -65 | Natural | 13.65 | 66.65 | Good | Stable |
| | | | | | | 0.15 | 0.15 | -60 | 15 | | | | |
| Wedge | 225/84 | 251/88, 316/89 | 232 | 80 | 53 | 7 | 80 | -4 | Natural | -27.5 | 25.5 | Bad | Unstable |
| | | | | | | 0.85 | 1 | -50 | 15 | | | | |
| | 225/84 | 251/81, 140/86 | 210 | 78 | 53 | 15 | 78 | -6 | Natural | -20 | 33 | Bad | Unstable |
| | | | | | | 0.7 | 1 | -50 | 15 | | | | |
| | 225/84 | 251/81, 212/80 | 223 | 80 | 53 | 2 | 80 | -4 | Natural | -35 | 18 | Very Bad | Completely unstable |
| | | | | | | 1 | 1 | -50 | 15 | | | | |
| | 225/84 | 251/81, 120/80 | 184 | 68 | 53 | 41 | 68 | -16 | Natural | 6 | 59 | Normal | Partially stable |
| | | | | | | 0.15 | 1 | -60 | 15 | | | | |
| | 225/84 | 251/81, 181/80 | 212 | 78 | 53 | 13 | 78 | -6 | Natural | -20 | 33 | Bad | Unstable |
| | | | | | | 0.7 | 1 | -50 | 15 | | | | |
| | 225/84 | 316/89, 140/86 | 227 | 39 | 53 | 2 | 39 | -45 | Natural | -45 | 8 | Very Bad | Completely unstable |
| | | | | | | 1 | 1 | -60 | 15 | | | | |
| | 225/84 | 316/89, 212/80 | 231 | 79 | 53 | 6 | 79 | -5 | Natural | -27.5 | 25.5 | Bad | Unstable |
| | | | | | | 0.85 | 1 | -50 | 15 | | | | |
| | 225/84 | 181/80, 140/86 | 210 | 79 | 53 | 15 | 79 | -5 | Natural | -20 | 33 | Bad | Unstable |
| | | | | | | 0.7 | 1 | -50 | 15 | | | | |
| | 225/84 | 181/80, 316/89 | 230 | 75 | 53 | 5 | 75 | -9 | Natural | -27.5 | 25.5 | Bad | Unstable |
| | | | | | | 0.85 | 1 | -50 | 15 | | | | |
| Direct Toppling | 225/84 | 181/80 | - | - | 53 | 224 | 1 | 164 | Natural | 11.25 | 64.25 | Good | Stable |
| | | | | | | 0.15 | 1 | -25 | 15 | | | | |
| | 225/84 | 120/80 | - | - | 53 | 285 | 1 | 164 | Natural | 11.25 | 64.25 | Good | Stable |
| | | | | | | 0.15 | 1 | -25 | 15 | | | | |
| | 225/84 | 316/89 | - | - | 53 | 89 | 1 | 173 | Natural | 11.25 | 64.25 | Good | Stable |
| | | | | | | 0.15 | 1 | -25 | 15 | | | | |
| | 225/84 | 140/86 | - | - | 53 | 265 | 1 | 170 | Natural | 11.25 | 64.25 | Good | Stable |
| | | | | | | 0.15 | 1 | -25 | 15 | | | | |
| Flexural Toppling | 225/84 | 120/80 | - | - | 53 | 285 | 1 | 164 | Natural | 11.25 | 64.25 | Good | Stable |
| | | | | | | 0.15 | 1 | -25 | 15 | | | | |
| | 225/84 | 316/89 | - | - | 53 | 89 | 1 | 173 | Natural | 11.25 | 64.25 | Good | Stable |
| | | | | | | 0.15 | 1 | -25 | 15 | | | | |
| | 225 | 140/89 | - | - | 53 | 265 | 1 | 173 | Natural | 11.25 | 64.25 | Good | Stable |
| | | | | | | 0.15 | 1 | -25 | 15 | | | | |

**Table 6.4** Some of the evaluating result of Slope Mass Rating (SMR) at the station 4A

| Failure mode | Face slope | joint sets | Trend | Plunge | RMR | F1 | F2 | F3 | F4 | F1F2F3+F4 | SMR | Class | Stability |
|---|---|---|---|---|---|---|---|---|---|---|---|---|---|
| Planar | 260/78 | 360/90 | - | - | 59 | 100 | 90 | 12 | Natural | 15 | 74 | Good | Stable |
| | | | | | | 0.15 | 1 | 0 | 15 | | | | |
| | 260/78 | 083/82 | - | - | 59 | 177 | 82 | 4 | Natural | 14.1 | 73.1 | Good | Stable |
| | | | | | | 0.15 | 1 | -6 | 15 | | | | |
| | 260/78 | 327/83 | - | - | 59 | 67 | 83 | 5 | Natural | 14.1 | 73.1 | Good | Stable |
| | | | | | | 0.15 | 1 | -6 | 15 | | | | |
| Wedge | 260/78 | 310/79, 327/83 | 262 | 74 | 59 | 2 | 74 | -4 | Natural | -35 | 24 | Bad | Unstable |
| | | | | | | 1 | 1 | -50 | 15 | | | | |
| | 260/78 | 360/90, 251/61 | 270 | 60 | 59 | 10 | 60 | -18 | Natural | -36 | 23 | Bad | Unstable |
| | | | | | | 0.85 | 1 | -60 | 15 | | | | |
| | 260/78 | 251/61, 327/83 | 250 | 61 | 59 | 10 | 61 | -17 | Natural | -36 | 23 | Bad | Unstable |
| | | | | | | 0.85 | 1 | -60 | 15 | | | | |
| | 260/78 | 242/79, 310/79 | 276 | 77 | 59 | 16 | 77 | -1 | Natural | -20 | 39 | Bad | Unstable |
| | | | | | | 0.7 | 1 | -50 | 15 | | | | |
| | 260/78 | 251/61, 310/79 | 240 | 61 | 59 | 20 | 61 | -17 | Natural | -27 | 32 | Bad | Unstable |
| | | | | | | 0.7 | 1 | -60 | 15 | | | | |

| | | | | | | | | | | | | | |
|---|---|---|---|---|---|---|---|---|---|---|---|---|---|
| | 260/78 | 242/79, 327/83 | 271 | 78 | 59 | 11 | 78 | 0 | Natural | -2.5 | 56.5 | Normal | Partially stable |
| | | | | | | 0.7 | 1 | -25 | 15 | | | | |
| | 260/78 | 242/79, 251/61 | 327 | 23 | 59 | 67 | 23 | -55 | Natural | 11.4 | 70.4 | Good | Stable |
| | | | | | | 0.15 | 0.4 | -60 | 15 | | | | |
| Direct Toppling | 260/78 | 360/90 | - | - | 59 | 80 | 1 | 168 | Natural | 11.25 | 70.25 | Good | Stable |
| | | | | | | 0.15 | 1 | -25 | 15 | | | | |
| | 260/78 | 083/82 | - | - | 59 | 357 | 1 | 160 | Natural | 11.25 | 70.25 | Good | Stable |
| | | | | | | 0.15 | 1 | -25 | 15 | | | | |
| | 260/78 | 327/83 | - | - | 59 | 357 | 1 | 161 | Natural | 11.25 | 70.25 | Good | Stable |
| | | | | | | 0.15 | 1 | -25 | 15 | | | | |
| | 260/78 | 310/79 | - | - | 59 | 130 | 1 | 157 | Natural | 11.25 | 70.25 | Good | Stable |
| | | | | | | 0.15 | 1 | -25 | 15 | | | | |
| Flexural Toppling | 260/78 | 360/90 | - | - | 59 | 80 | 1 | 168 | Natural | 11.25 | 70.25 | Good | Stable |
| | | | | | | 0.15 | 1 | -25 | 15 | | | | |
| | 260/78 | 327/83 | - | - | 59 | 113 | 1 | 161 | Natural | 11.25 | 70.25 | Good | Stable |
| | | | | | | 0.15 | 1 | -25 | 15 | | | | |
| | 260/78 | 251/61 | - | - | 59 | 189 | 1 | 139 | Natural | 11.25 | 70.25 | Good | Stable |
| | | | | | | 0.15 | 1 | -25 | 15 | | | | |
| | 260/78 | 310/79 | - | - | 59 | 130 | 1 | 157 | Natural | 11.25 | 70.25 | Good | Stable |
| | | | | | | 0.15 | 1 | -25 | 15 | | | | |

Station 1A to 1E is the former entrance of the Prasat Hin Pan Yod concealed from a huge block of the rockslide. Stations 1A to 1E had an SMR value of 27.5-70.1275, which was classified as bad to good as shown in Table 6.5. The dominant SMR values were categorized as a good class. There were two intersections of joint sets of wedge failure, and one of the joint planes of toppling failure was classified as a normal class. Additionally, two points intersections of joint sets had an SMR score of 27.5, which was classified as low class. For such the representative SMR, wedge failure of rock fall type has so higher potential to have occurred in stations 1A to 1E. The three intersections as shown in Table 6.6, plunging to nearly north (NNE) nearly east, and also southwest (SW) may be originated from wedge failure of rock fall type. As mentioned, the tourist route for the inner chamber should not pass stations 1A, 1C, and 1E

Station 2A is a place of the sea cave that locating beneath a massive limestone roof and supported by a thin column. The evidence of a former rock fall had two big blocks, as shown in Figure 6.9. Due to the high energy of currents and waves, rock collapse might have occurred in nearly future. The SMR value's wedge failure shown in Table 6.3 and Table 6.5, was categorized as bad and very bad. The SMR value was 8-18 and 25.5-33, respectively. Wedge failure of rock fall type has a higher potential to have occurred than planar and toppling failure. Moreover, bedding rock fall blocks is one of the high potential hazards, and it is difficult to determine by the SMR approach.

Station 3A-3D is the lower part of the broken rock that remained from the rockslide event in February 2021. The SMR value was range 18-69 as shown in Table 6.5, and it was

almost categorized as a good class and normal class. The SMR value of direct toppling failure was partly categorized as very bad (two values) to bad (one value), meanwhile, four SMR value of wedge failure was classified as a bad class. The very bad to bad SMR class of direct toppling failure had a joint plan dipping to the east (E). The bad SMR class of wedge failure had five intersects of joint sets plunging to the northwest (NW) and nearly north (NEE) as shown in Table 6.6, and it may be caused by wedge failure of rock fall type. Although the SMR value of planar failure is classified as a normal class, rockslide can be occurred as well particularly, in case of repeatedly column supporting broken. For safety, the tourist route should not pass station 3A-3D getting through the Prasat Hin Panyod chamber.

Station 4A had SMR value of 23-74, which is classified as bad to good as shown in Figure 6.12. The five intersects of joint sets was classified as bad class and the details of SMR assessment was shown in Table 6.4 and Table 6.5. The intersection of joint sets plunge to west and southwest that shows potential wedge failure of rock fall hazard type as shown in Table 6.6. Tourist may be slightly affected by small piece of rock wedge that pending at high place. Fortunately, distance passing station 4A and getting through is quite short (not over 3 meters).


***Figure 6.9*** *station 2A and station 4A*

Station 5A had SMR value of 70.25-74 as shown in Table 6.5 and Table 6.6, and all SMR values were classified as good class. It can be said that limestone rock mass having stable and safety for tourist.

Station 6A to 6C had SMR score of 56.65-73.1 as shown in Table 6.5 and Table 6.6,

which all SMR values were classified as normal to good class. There was none of bad to very bad. However, rock fall hazard may be originated by both direct and oblique toppling.

Station 7A to 7F is the huge block of planar rockslide that occurred by column supporting broken in the event of February 2021. The investigated stations had SMR values of 19-70 as shown in Table 6.5, which were classified as very bad to good. The dominant SMR values were categorized as a good class. Two intersections of joint sets of wedge failure had SMR value of 19, which were categorized as a very bad class. There were five intersections of joint sets of wedge failure, which were classified as a bad class (28-34.3). Furthermore, four intersections of joint sets of wedge failure and one joint plan of direct toppling were classified as a normal class, which still had partially stable. The rock movement direction was mainly plunging west to northwest (W-NW) and southeast to southwest (SE-SW) as shown in Table 6.6. As mentioned, tourists should not close up the huge block of planar rockslide located nearby sea cliff because of rock fall, particularly small wedge shape hanging on the high place.

Station 8A had SMR score of 35-7.77 as shown in Table 6.5, which the dominant values were classified as good class as shown in Table 6.6. There was only one intersects of joint sets that classified as bad class. Rock fall hazard may be caused by wedge failure. Because of intersection of joint sets plunging to northeast (NE), tourist should be aware pieces of rock wedge that pending at high place in the Prasat Hin Pan Yod chamber.

Station 9A had SMR score of 29.5-69.6 as shown in Table 6.5. The SMR value was mostly classified as good class. There was only one joint plan dipping to nearly north (NNE) as shown in Table 6.6, planar failure may be originated rock fall in the Prasat Hin Pan Yod chamber.

### 6.7. Support guidelines for stabilization

According to Table 6.7, Most SMR values are classified the rock slope as good class. Some SMR values have lower than 10 due to error of under estimation or rock failure occurred already. No slope having an SMR value below 10 exist in natural. SMR value below 20 may cause the rock slope failure very quickly. Detailed studies should be carried out where an SMR value is less than 40 (or IVa to Va) because tourists site are in danger and rock slope should be stabilized by the integration of various measures: bolting/anchors, shotcrete, diversion drains and removal of rock fragment at high place as following in Table 5.7. In National Park and Satun Geopark, a safe slope angle should be determined to increase SMR to 60.

**Table 6.5** The result of SMR assessment in the Prasat Hin Panyod chamber

| Station | No. | RMR | Face slope | Failure analysis of Stereonet analysis | | | SMR | | | | A number of SMR class in failure mode | | | | |
|---|---|---|---|---|---|---|---|---|---|---|---|---|---|---|---|
| | | | | Failure modes | % | Number of joint or intersection | Range | | Mode | | Very Bad | Bad | Normal | Good | Very good |
| | | | | | | | min | max | SMR value | SMR class | 0-20 | 21-40 | 41-60 | 61-80 | 81-100 |
| 1 | 1A | | 003/85 | Planar | 0 | 0 | | | | | | | | | |
| | | | | Wedge | 25.15 | 5 | 27.5 | 69.1 | none | Good | 0 | 1 | 0 | 4 | 0 |
| | | | | Direct Toppling | 15.2 | 8 | 52.5 | 66.25 | 66.25 | Good | 0 | 0 | 1 | 7 | 0 |
| | | | | Oblique Toppling | 9.36 | | | | | | | | | | |
| | | | | Flexural Toppling | 0 | 0 | | | | | | | | | |
| | 1B | | 355/88 | Planar | 0 | 0 | | | | | | | | | |
| | | | | Wedge | 42.69 | 7 | 52.5 | 68.65 | 62.5 | Good | 0 | 0 | 1 | 6 | 0 |
| | | | | Direct Toppling | 16.96 | 5 | 66.25 | 66.25 | 66.25 | Good | 0 | 0 | 0 | 5 | 0 |
| | | | | Oblique Toppling | 9.36 | | | | | | | | | | |
| | | | | Flexural Toppling | 0 | 0 | | | | | | | | | |
| | 1C | | 087/88 | Planar | 26.32 | 2 | 61 | 66.25 | none | Good | 0 | 0 | 0 | 2 | 0 |
| | | | | Wedge | 59.06 | 3 | 27.5 | 66.25 | none | Good | 0 | 1 | 0 | 2 | 0 |
| | | | | Direct Toppling | 10.53 | 4 | 66.25 | 66.25 | 66.25 | Good | 0 | 0 | | 4 | 0 |
| | | | | Oblique Toppling | 12.87 | | | | | | | | | | |
| | | | | Flexural Toppling | 0 | 0 | | | | | | | | | |
| | 1D | | 317/89 | Planar | 10.53 | 2 | 61 | 62.5 | none | Good | 0 | 0 | 0 | 2 | 0 |
| | | | | Wedge | 50.88 | 5 | 50 | 62.5 | 61 | Good | 0 | 0 | 1 | 4 | 0 |
| | | | | Direct Toppling | 2.92 | 5 | 66.25 | 66.25 | 66.25 | Good | 0 | 0 | 0 | 5 | 0 |
| | | | | Oblique Toppling | 25.15 | | | | | | | | | | |
| | | | | Flexural Toppling | 0 | 0 | | | | | | | | | |
| | 1E | 55 | 233/78 | Planar | 21.05 | 1 | 70.1275 | 70.1275 | 70.1275 | Good | 0 | 0 | 0 | 1 | 0 |
| | | | | Wedge | 35.09 | 3 | 27.5 | 61 | 61 | Good | 0 | 1 | 0 | 2 | 0 |
| | | | | Direct Toppling | 21.64 | 8 | 66.25 | 66.25 | 66.25 | Good | 0 | 0 | 0 | 8 | 0 |
| | | | | Oblique Toppling | 34.5 | 1 | 66.25 | 66.25 | 66.25 | Good | 0 | 0 | 0 | 1 | 0 |
| | | | | Flexural Toppling | 10.53 | | | | | | | | | | |
| 2-JO | 2A | 53 | 325/80 | Planar | 0 | 0 | | | | | | | | | |
| | | | | Wedge | 1.11 | 2 | 59 | 64.25 | 59, 64.25 | Normal, Good | 0 | 0 | 1 | 1 | 0 |
| | | | | Direct Toppling | 11.11 | 13 | 64.25 | 64.25 | 64.25 | Good | 0 | 0 | 0 | 13 | 0 |
| | | | | Flexural Toppling | 21.43 | 1 | 64.25 | 65.25 | 66.25 | Good | 0 | 0 | 0 | 1 | 0 |
| | | | | Oblique Toppling | 47.78 | | | | | | | | | | |
| | 2B | | 255/83 | Planar | 14.29 | 3 | 60.5 | 67.1 | none | Good | 0 | 0 | 1 | 0 | 2 |
| | | | | Wedge | 40 | 9 | 48 | 60.5 | 60.5 | Normal | 0 | 0 | 9 | 0 | 0 |
| | | | | Direct Toppling | 5.56 | 6 | 64.25 | 64.25 | 64.25 | Good | 0 | 0 | 0 | 6 | 0 |
| | | | | Oblique Toppling | 13.33 | | | | | | | | | | |
| | | | | Flexural Toppling | 0 | 0 | | | | | | | | | |
| | 2C | | 225/84 | Planar | 21.43 | 4 | 60.5 | 67.1 | 67.1 | Good | 0 | 0 | 1 | 3 | 0 |
| | | | | Wedge | 64.44 | 9 | 8 | 59 | 25.5 | Bad | 2 | 6 | 1 | 0 | 0 |
| | | | | Direct Toppling | 10 | 4 | 64.25 | 64.25 | 64.25 | Good | 0 | 0 | 0 | 4 | 0 |
| | | | | Oblique Toppling | 4.44 | | | | | | | | | | |
| | | | | Flexural Toppling | 0 | 0 | | | | | | | | | |
| | 2D | | 353/85 | Planar | 0 | 2 | 60.5 | 60.5 | 60.5 | Normal | 0 | 0 | 2 | 0 | 0 |
| | | | | Wedge | 3.33 | 4 | 59 | 66.65 | 59, 66.65 | Normal, Good | 0 | 0 | 2 | 2 | 0 |
| | | | | Direct Toppling | 18.89 | 6 | 64.25 | 64.25 | 64.25 | Good | 0 | 0 | 0 | 6 | 0 |
| | | | | Oblique Toppling | 50 | 2 | 64.25 | 65.25 | 66.25 | Good | 0 | 0 | 0 | 2 | 0 |
| | | | | Flexural Toppling | 21.43 | | | | | | | | | | |
| 3 | 3A | 54 | 020/89 | Planar | 20 | 3 | 60 | 61.5 | 60 | Good | 0 | 0 | 2 | 1 | 0 |
| | | | | Wedge | 46.67 | 15 | 34 | 67.65 | 52.5 | Normal | 0 | 3 | 7 | 5 | 0 |
| | | | | Direct Toppling | 0 | 4 | 65.25 | 65.25 | 65.25 | Good | 0 | 0 | 0 | 4 | 0 |
| | | | | Flexural Toppling | 0 | 0 | | | | | | | | | |
| | | | | Oblique Toppling | 0 | 0 | | | | | | | | | |
| | 3B | | 095/89 | Planar | 33.33 | 4 | 60 | 65.4 | 60 | Normal | 0 | 0 | 2 | 2 | 0 |
| | | | | Wedge | 32.38 | 14 | 45 | 67.65 | 65.4, 67.65 | Good | 0 | 0 | 3 | 11 | 0 |
| | | | | Direct Toppling | 10.48 | 9 | 9 | 60 | 60 | Normal | 2 | 1 | 6 | 0 | 0 |
| | | | | Flexural Toppling | 6.67 | 6 | 60 | 60 | 60 | Normal | 0 | 0 | 6 | 0 | 0 |
| | | | | Oblique Toppling | 1.9 | | | | | | | | | | |
| | 3C | | 328/87 | Planar | 6.67 | 1 | 61.35 | 61.35 | 61.35 | Good | 0 | 0 | 0 | 1 | 0 |
| | | | | Wedge | 35.24 | 9 | 27 | 65.4 | 65.4 | Good | 0 | 1 | 2 | 6 | 0 |
| | | | | Direct Toppling | 0.95 | 5 | 65.25 | 66.25 | 67.25 | Good | 0 | 0 | 0 | 5 | 0 |
| | | | | Oblique Toppling | 9.52 | | | | | | | | | | |
| | | | | Flexural Toppling | 0 | 0 | | | | | | | | | |
| | 3D | | 122/87 | Planar | 0 | 0 | | | | | | | | | |
| | | | | Wedge | 18.1 | 4 | 59.4 | 67,65 | none | Normal, Good | 0 | 0 | 2 | 2 | 0 |
| | | | | Direct Toppling | 13.33 | 11 | 47.75 | 69 | 65.25 | Good | 0 | 0 | 4 | 7 | 0 |
| | | | | Oblique Toppling | 3.81 | | | | | | | | | | |
| | | | | Flexural Toppling | 6.67 | 4 | 65.25 | 68.1 | 65.25 | Good | 0 | 0 | 0 | 4 | 0 |
| 4 | 4A | 59 | 260/78 | Planar | 12.5 | 3 | 73.1 | 74 | 73.1 | Good | 0 | 0 | 0 | 3 | 0 |
| | | | | Wedge | 45 | 7 | 23 | 70.4 | 23 | Bad | 0 | 5 | 1 | 1 | 0 |
| | | | | Direct Toppling | 12.5 | 4 | | | | | | | | | |
| | | | | Oblique Toppling | 17.5 | | 70.25 | 71.25 | 72.25 | Good | 0 | 0 | 0 | 4 | 0 |
| | | | | Flexural Toppling | 18.75 | 4 | 70.25 | 70.25 | 70.25 | Good | 0 | 0 | 0 | 4 | 0 |
| 5 | 5A | 59 | 062/85 | Planar | 0 | 0 | | | | | | | | | |
| | | | | Wedge | 0 | 0 | | | | | | | | | |
| | | | | Direct Toppling | 0 | 0 | | | | | | | | | |
| | | | | Oblique Toppling | 10 | 3 | 70.25 | 74 | 70.25 | Good | 0 | 0 | 0 | 3 | 0 |
| | | | | Flexural Toppling | 0 | 0 | | | | | | | | | |
| 6 | 6A | 59 | 004/81 | Planar | 0 | 0 | | | | | | | | | |
| | | | | Wedge | 1.9 | 11 | 66.5 | 73.1 | 73.1 | Good | 0 | 0 | 0 | 11 | 0 |
| | | | | Direct Toppling | 3.33 | 15 | 52.75 | 70.25 | 70.25 | Good | 0 | 0 | 2 | 0 | 0 |
| | | | | Oblique Toppling | 39.52 | | | | | | | | | | |
| | | | | Flexural Toppling | 4.86 | 3 | 70.25 | 74 | 70.25 | Good | 0 | 0 | 0 | 3 | 0 |
| | 6B | | 163/72 | Planar | 0 | 0 | | | | | | | | | |
| | | | | Wedge | 0.95 | 4 | 73.1 | 74 | 74 | Good | 0 | | 0 | 4 | 0 |
| | | | | Direct Toppling | 8.1 | 16 | 52.75 | 70.25 | 70.25 | Good | 0 | 0 | 4 | 12 | 0 |
| | | | | Oblique Toppling | 33.81 | | | | | | | | | | |
| | | | | Flexural Toppling | 28.57 | 2 | 70.25 | 70.25 | 70.25 | Good | 0 | | 0 | 2 | 0 |
| | 6C | | 337/81 | Planar | 0 | 0 | | | | | | | | | |
| | | | | Wedge | 5.24 | 5 | 65 | 73.1 | 66.5 | Good | 0 | 0 | 0 | 5 | 0 |
| | | | | Direct Toppling | 0 | 0 | | | | | | | | | |
| | | | | Oblique Toppling | 26.67 | 15 | 70.25 | 70.25 | 70.25 | Good | 0 | 0 | 0 | 15 | 0 |
| | | | | Flexural Toppling | 0 | 0 | | | | | | | | | |
| 7-JO | 7A | 55 | 245/78 | Planar | 9.09 | 6 | 61 | 66.4 | 61 | Good | 0 | 0 | 0 | 6 | 0 |
| | | | | Wedge | 22.92 | 11 | 46 | 68.5 | 68.5 | Good | 0 | 0 | 1 | 10 | |
| | | | | Direct Toppling | 35.04 | 7 | 66.25 | 70 | 66.25 | Good | 0 | 0 | 0 | 7 | 0 |
| | | | | Oblique Toppling | 12.12 | | | | | | | | | | |
| | | | | Flexural Toppling | 12.12 | 4 | 66.25 | 66.25 | 66.25 | Good | 0 | 0 | 0 | 4 | 0 |
| | 7B | | 264/78 | Planar | 6.06 | 6 | 61 | 66.4 | 61 | Good | 0 | 0 | 0 | 6 | 0 |
| | | | | Wedge | 18.75 | 8 | 28 | 66.4 | 61,62.35,66. | Good | 0 | 1 | 0 | 7 | 0 |
| | | | | Direct Toppling | 17.23 | 8 | 66.25 | 70 | 66.25 | Good | 0 | 0 | 0 | 8 | 0 |
| | | | | Oblique Toppling | 9.28 | | | | | | | | | | |
| | | | | Flexural Toppling | 3.03 | 3 | 66.25 | 66.25 | 66.25 | Good | 0 | 0 | 0 | 3 | 0 |
| | 7C | | 324/77 | Planar | 9.09 | 3 | 61 | 62.5 | 61 | Good | 0 | 0 | 0 | 3 | 0 |
| | | | | Wedge | 21.97 | 12 | 28 | 68.65 | 62.5 | Good | 0 | 1 | 2 | 9 | 0 |
| | | | | Direct Toppling | 0.57 | 6 | 66.25 | 67.25 | 68.25 | Good | 0 | 0 | 0 | 6 | 0 |
| | | | | Oblique Toppling | 4.55 | | | | | | | | | | |
| | | | | Flexural Toppling | 24.24 | 10 | 66.25 | 70 | 66.25 | Good | 0 | 0 | 0 | 10 | 0 |
| | 7D | | 227/77 | Planar | 9.09 | 7 | 61 | 69.1 | 62.5 | Good | 0 | 0 | 0 | 7 | 0 |
| | | | | Wedge | 17.61 | 5 | 19 | 62.35 | none | Good | 1 | 1 | 1 | 2 | 0 |
| | | | | Direct Toppling | 29.92 | 8 | 61 | 61 | 61 | Good | 0 | 0 | 0 | 8 | 0 |
| | | | | Oblique Toppling | 13.26 | | | | | | | | | | |
| | | | | Flexural Toppling | 18.18 | 5 | 61 | 61 | 61 | Good | 0 | 0 | 0 | 5 | 0 |
| | 7E | | 290/82 | Planar | 9.09 | 5 | 61 | 66.4 | 61 | Good | 0 | 0 | 0 | 5 | 0 |
| | | | | Wedge | 23.67 | 12 | 28 | 62.35 | 61 | Good | 0 | 2 | 0 | 10 | 0 |
| | | | | Direct Toppling | 4.92 | 9 | 66.25 | 70 | 66.25 | Good | 0 | 0 | 0 | 9 | 0 |
| | | | | Oblique Toppling | 4.92 | | | | | | | | | | |
| | | | | Flexural Toppling | 12.12 | 6 | 66.25 | 66.25 | 66.25 | Good | 0 | 0 | 0 | 6 | 0 |
| | 7F | | 110/82 | Planar | 12.12 | 4 | 61 | 61 | 61 | Good | 0 | 0 | 0 | 4 | 0 |
| | | | | Wedge | 42.8 | 12 | 19 | 68.65 | 61 | Good | 1 | 0 | 1 | 10 | 0 |
| | | | | Direct Toppling | 6.63 | 8 | 48.75 | 66.25 | 67.25 | Good | 0 | | 2 | 6 | 0 |
| | | | | Oblique Toppling | 10.23 | | | | | | | | | | |
| | | | | Flexural Toppling | 12.12 | 10 | 66.25 | 70 | 66.25 | Good | 0 | 0 | 0 | 10 | 0 |
| 8 | 8A | 62 | 034/85 | Planar | 0 | 0 | | | | | | | | | |
| | | | | Wedge | 17.65 | 5 | 35 | 75.65 | none | Good | 0 | 1 | 0 | 4 | 0 |
| | | | | Direct Toppling | 5.88 | 4 | 73.25 | 77 | 73.25 | Good | 0 | 0 | 0 | 4 | 0 |
| | | | | Oblique Toppling | 13.07 | | | | | | | | | | |
| | | | | Flexural Toppling | 0 | 0 | | | | | | | | | |
| 9 | 9A | 57 | 022/85 | Planar | 10 | 3 | 29.5 | 69.6 | none | Good | 0 | 1 | 0 | 2 | 0 |
| | | | | Wedge | 12.12 | 3 | 63 | 68.4 | 63 | Good | 0 | 0 | 0 | 3 | 0 |
| | | | | Direct Toppling | 4.44 | 3 | 68.25 | 68.25 | 69.25 | Good | 0 | 0 | 0 | 3 | 0 |
| | | | | Oblique Toppling | 22.22 | | | | | | | | | | |
| | | | | Flexural Toppling | 0 | 0 | | | | | | | | | |

**Table 6.6** The summary of SMR, failure mode, critical joints and intersections

| Station | No. | Face slope | Failures | Intersection point | joint sets | RMR | SMR | SMR class | SMR stability |
|---|---|---|---|---|---|---|---|---|---|
| 1 | 1A | 003/85 | Wedge | 031/85 | 086/87,323/88 | 55 | 60 | Normal | Partially stable |
| | | | Wedge | 010/80 | 086/87,045/80 | 55 | 27.5 | Bad | Unstable |
| | | | Direct Toppling | none | 171/59 | 55 | 52.5 | Normal | Partially stable |
| | 1B | 355/88 | Wedge | 341/88 | 360/88,323/88 | 55 | 52.5 | Normal | Partially stable |
| | 1C | 087/88 | Wedge | 081/78 | 360/88,045/80 | 55 | 27.5 | Bad | Unstable |
| | 1D | 317/89 | Wedge | 341/88 | 360/88,323/88 | 55 | 50 | Normal | Partially stable |
| | 1E | 233/78 | Wedge | 238/69 | 224/70,323/88 | 55 | 27.5 | Bad | Unstable |
| 2 | 2A | 325/80 | Wedge | 045/55 | 316/89,120/80 | 53 | 59 | Normal | Partially stable |
| | 2B | 255/83 | Wedge | 232/80 | 251/88,316/89 | 53 | 48 | Normal | Partially stable |
| | | | Wedge | 227/39 | 316/89,140/86 | 53 | 47.6 | Normal | Partially stable |
| | | | Wedge | 231/79 | 316/89,212/80 | 53 | 48 | Normal | Partially stable |
| | | | Wedge | 230/75 | 181/80,316/89 | 53 | 49 | Normal | Partially stable |
| | 2C | 225/84 | Wedge | 232/80 | 251/88,316/89 | 53 | 25.5 | Bad | Unstable |
| | | | Wedge | 210/78 | 251/81,140/86 | 53 | 33 | Bad | Unstable |
| | | | Wedge | 223/80 | 251/81,212/80 | 53 | 18 | Very Bad | Completely unstable |
| | | | Wedge | 212/78 | 251/81,181/80 | 53 | 33 | Bad | Unstable |
| | | | Wedge | 227/39 | 316/89,140/86 | 53 | 8 | Very Bad | Completely unstable |
| | | | Wedge | 231/79 | 316/89,212/80 | 53 | 25.5 | Bad | Unstable |
| | | | Wedge | 210/79 | 181/80,140/86 | 53 | 33 | Bad | Unstable |
| | | | Wedge | 230/75 | 181/80,316/89 | 53 | 25.5 | Bad | Unstable |
| | 2D | 353/85 | Wedge | 045/55 | 120/80,316/89 | 53 | 59 | Normal | Partially stable |
| | | | Wedge | 062/72 | 120/80,140/86 | 53 | 59 | Normal | Partially stable |
| 3 | 3A | 020/89 | Planar | none | 278/75 | 54 | 60 | Normal | Partially stable |
| | | | Planar | none | 312/48 | 54 | 60 | Normal | Partially stable |
| | | | Wedge | 311/72 | 011/81,278/75 | 54 | 60 | Normal | Partially stable |
| | | | Wedge | 072/72 | 011/81,081/72 | 54 | 60 | Normal | Partially stable |
| | | | Wedge | 290/46 | 011/81, 312/48 | 54 | 60 | Normal | Partially stable |
| | | | Wedge | 033/80 | 011/81,092/85 | 54 | 34 | Bad | Unstable |
| | | | Wedge | 012/29 | 312/48,050/35 | 54 | 52.2 | Normal | Partially stable |
| | | | Wedge | 004/34 | 312/48,081/72 | 54 | 39.6 | Bad | Unstable |
| | | | Wedge | 005/34 | 312/48, 092/85 | 54 | 39.6 | Bad | Unstable |
| | | | Wedge | 004/26 | 050/35, 092/85 | 54 | 52.2 | Normal | Partially stable |
| | | | Wedge | 001/25 | 050/35,278/75 | 54 | 52.2 | Normal | Partially stable |
| | | | Wedge | 000/26 | 081/72, 278/75 | 54 | 52.2 | Normal | Partially stable |
| | 3B | 095/89 | Planar | none | 312/48 | 54 | 60 | Normal | Partially stable |
| | | | Planar | none | 278/75 | 54 | 60 | Normal | Partially stable |
| | | | Wedge | 097/26 | 011/81,050/35 | 54 | 45 | Normal | Partially stable |
| | | | Wedge | 072/72 | 011/81,081/72 | 54 | 60 | Normal | Partially stable |
| | | | Wedge | 311/72 | 011/81278/75 | 54 | 60 | Normal | Partially stable |
| | | | Direct Toppling | none | 312/48 | 54 | 60 | Normal | Partially stable |
| | | | Direct Toppling | none | 317/20 | 54 | 60 | Normal | Partially stable |
| | | | Direct Toppling | none | 011/81 | 54 | 60 | Normal | Partially stable |
| | | | Direct Toppling | none | 278/75 | 54 | 9 | Very Bad | Completely unstable |
| | | | Direct Toppling | none | 092/85 | 54 | 60 | Normal | Partially stable |
| | | | Flexural Toppling | none | 050/35 | 54 | 60 | Normal | Partially stable |
| | | | Flexural Toppling | none | 011/81 | 54 | 60 | Normal | Partially stable |
| | | | Flexural Toppling | none | 081/72 | 54 | 60 | Normal | Partially stable |
| | 3C | 328/87 | Wedge | 290/46 | 011/81,312/48 | 54 | 60 | Normal | Partially stable |
| | | | Wedge | 311/72 | 011/81,278/75 | 54 | 27 | Bad | Unstable |
| | | | Wedge | 072/72 | 081/72,011/81 | 54 | 60 | Normal | Partially stable |
| | 3D | 122/87 | Wedge | 072/72 | 081/72,011/81 | 54 | 60 | Normal | Partially stable |
| | | | Wedge | 097/26 | 050/35,011/81 | 54 | 59.4 | Normal | Partially stable |
| | | | Direct Toppling | none | 312/48 | 54 | 47.75 | Normal | Partially stable |
| | | | Direct Toppling | none | 278/75 | 54 | 59 | Normal | Partially stable |
| 4 | 4A | 260/78 | Wedge | 262/74 | 310/79,327/83 | 59 | 24 | Bad | Unstable |
| | | | Wedge | 270/60 | 360/90,251/61 | 59 | 23 | Bad | Unstable |
| | | | Wedge | 250/61 | 251/61,327/83 | 59 | 23 | Bad | Unstable |
| | | | Wedge | 276/77 | 242/79,310/79 | 59 | 39 | Bad | Unstable |
| | | | Wedge | 240/61 | 251/61,310/79 | 59 | 32 | Bad | Unstable |
| | | | Wedge | 271/78 | 242/79,327/83 | 59 | 56.5 | Normal | Partially stable |
| 5 | 5A | 062/65 | Oblique Toppling | none | Almost | 59 | 70.25 to 74 | Good | Stable |
| 6 | 6A | 004/81 | Wedge | none | Almost | 59 | 66.5 to 73.1 | Good | Stable |
| | | | Direct Toppling | none | Almost | 59 | 64 to 70.25 | Good | Stable |
| | | | Direct Toppling | none | 193/76 | 59 | 52.75 | Normal | Partially stable |
| | | | Direct Toppling | none | 196/80 | 59 | 56.5 | Normal | Partially stable |
| | | | Flexural Toppling | none | Almost | 59 | 70.25 to 74 | Good | Stable |
| | 6B | 163/72 | Planar | none | Almost | 59 | 71.6 to 74 | Good | Stable |
| | | | Direct Toppling | none | Almost | 59 | 70.25 | Good | Stable |
| | | | Direct Toppling | none | 335/86 | 59 | 52.75 | Normal | Partially stable |
| | | | Direct Toppling | none | 327/88 | 59 | 56.5 | Normal | Partially stable |
| | | | Direct Toppling | none | 356/86 | 59 | 56.5 | Normal | Partially stable |
| | | | Flexural Toppling | none | Almost | 59 | 70.25 | Good | Stable |
| | 6C | 337/81 | Wedge | none | Almost | 59 | 65.5 to 73.1 | Good | Stable |
| | | | Direct Toppling | none | Almost | 59 | 70.25 | Good | Stable |
| 7 | 7A | 245/78 | Wedge | 218/52 | 244/55,295/80 | 55 | 46 | Normal | Partially stable |
| | 7B | 264/78 | Wedge | 277/50 | 244/55,342/71 | 55 | 28 | Bad | Unstable |
| | 7C | 324/77 | Wedge | 324/32 | 026/53,040/69 | 55 | 28 | Bad | Unstable |
| | | | Wedge | 316/24 | 244/55,026/53 | 55 | 49.6 | Normal | Partially stable |
| | | | Wedge | 301/38 | 244/55,011/67 | 55 | 49.6 | Normal | Partially stable |
| | 7D | 227/77 | Wedge | 218/52 | 244/55,295/80 | 55 | 19 | Very Bad | Unstable |
| | | | Wedge | 206/48 | 244/55,133/75 | 55 | 46 | Normal | Partially stable |
| | | | Wedge | 212/35 | 295/80,133/75 | 55 | 34.3 | Bad | Unstable |
| | 7E | 290/82 | Wedge | 277/50 | 244/55,342/71 | 55 | 28 | Bad | Unstable |
| | | | Wedge | 301/38 | 244/55,011/67 | 55 | 34.3 | Bad | Unstable |
| | 7F | 110/82 | Wedge | 083/36 | 011/67,026/53 | 55 | 49.6 | Normal | Partially stable |
| | | | Wedge | 113/38 | 060/52,040/69 | 55 | 19 | Very Bad | Unstable |
| | | | Direct Toppling | none | 295/80 | 55 | 48.75 | Normal | Partially stable |
| | | | Direct Toppling | none | 277/50 | 55 | 52.5 | Normal | Partially stable |
| 8 | 8A | 034/85 | Wedge | 053/51 | 345/73,128/78 | 62 | 35 | Bad | Unstable |
| | | | Wedge | none | Almost | 62 | 68 to 75.65 | Good | Stable |
| | | | Direct Toppling | none | Almost | 62 | 73.25 to 77 | Good | Stable |
| 9 | 9A | 022/85 | Planar | none | 014/81 | 57 | 29.5 | Bad | Unstable |
| | | | Wedge | none | Almost | 57 | 63 to 68.4 | Good | Stable |
| | | | Direct Toppling | none | Almost | 57 | 68.25 | Good | Stable |

**Table 6.7** Support measures for stabilization based on Singh and Goel (2011)

| Station | No. | Face slope | Failures | Intersection point | joint sets | RMR | SMR | SMR class | SMR stability | Suggested Supports |
|---|---|---|---|---|---|---|---|---|---|---|
| 1 | 1A | 003/85 | Wedge | 031/85 | 086/87,323/88 | 55 | 60 | Normal | Partially stable | IIIa |
| | | | Wedge | 010/80 | 086/87,045/80 | 55 | 27.5 | Bad | Unstable | IVb |
| | | | Direct Toppling | none | 171/59 | 55 | 52.5 | Normal | Partially stable | IIIa |
| | 1B | 355/88 | Wedge | 341/88 | 360/88,323/88 | 55 | 52.5 | Normal | Partially stable | IIIa |
| | 1C | 087/88 | Wedge | 081/78 | 360/88,045/80 | 55 | 27.5 | Bad | Unstable | IVb |
| | 1D | 317/89 | Wedge | 341/88 | 360/88,323/88 | 55 | 50 | Normal | Partially stable | IIIb |
| | 1E | 233/78 | Wedge | 238/69 | 224/70,323/88 | 55 | 27.5 | Bad | Unstable | IVb |
| 2 | 2A | 325/80 | Wedge | 045/55 | 316/89,120/80 | 53 | 59 | Normal | Partially stable | IIIa |
| | 2B | 255/83 | Wedge | 232/80 | 251/88,316/89 | 53 | 48 | Normal | Partially stable | IIIb |
| | | | Wedge | 227/39 | 316/89,140/86 | 53 | 47.6 | Normal | Partially stable | IIIb |
| | | | Wedge | 231/79 | 316/89,212/80 | 53 | 48 | Normal | Partially stable | IIIb |
| | | | Wedge | 230/75 | 181/80,316/89 | 53 | 49 | Normal | Partially stable | IIIb |
| | 2C | 225/84 | Wedge | 232/80 | 251/88,316/89 | 53 | 25.5 | Bad | Unstable | IVb |
| | | | Wedge | 210/78 | 251/81,140/86 | 53 | 33 | Bad | Unstable | IVa |
| | | | Wedge | 223/80 | 251/81,212/80 | 53 | 18 | Very Bad | Completely unstable | Va |
| | | | Wedge | 212/78 | 251/81,181/80 | 53 | 33 | Bad | Unstable | IVa |
| | | | Wedge | 227/39 | 316/89,140/86 | 53 | 8 | Very Bad | Completely unstable | Error/failure |
| | | | Wedge | 231/79 | 316/89,212/80 | 53 | 25.5 | Bad | Unstable | IVb |
| | | | Wedge | 210/79 | 181/80,140/86 | 53 | 33 | Bad | Unstable | IVa |
| | | | Wedge | 230/75 | 181/80,316/89 | 53 | 25.5 | Bad | Unstable | IVb |
| | 2D | 353/85 | Wedge | 045/55 | 120/80,316/89 | 53 | 59 | Normal | Partially stable | IIIa |
| | | | Wedge | 062/72 | 120/80,140/86 | 53 | 59 | Normal | Partially stable | IIIa |
| 3 | 3A | 020/89 | Planar | none | 278/75 | 54 | 60 | Normal | Partially stable | IIIa |
| | | | Planar | none | 312/48 | 54 | 60 | Normal | Partially stable | IIIa |
| | | | Wedge | 311/72 | 011/81,278/75 | 54 | 60 | Normal | Partially stable | IIIa |
| | | | Wedge | 072/72 | 011/81,081/72 | 54 | 60 | Normal | Partially stable | IIIa |
| | | | Wedge | 290/46 | 011/81, 312/48 | 54 | 60 | Normal | Partially stable | IIIa |
| | | | Wedge | 033/80 | 011/81,092/85 | 54 | 34 | Bad | Unstable | IVa |
| | | | Wedge | 012/29 | 312/48,050/35 | 54 | 52.2 | Normal | Partially stable | IIIa |
| | | | Wedge | 004/34 | 312/48,081/72 | 54 | 39.6 | Bad | Unstable | IVa |
| | | | Wedge | 005/34 | 312/48, 092/85 | 54 | 39.6 | Bad | Unstable | IVa |
| | | | Wedge | 004/26 | 050/35, 092/85 | 54 | 52.2 | Normal | Partially stable | IIIa |
| | | | Wedge | 001/25 | 050/35,278/75 | 54 | 52.2 | Normal | Partially stable | IIIa |
| | | | Wedge | 000/26 | 081/72, 278/75 | 54 | 52.2 | Normal | Partially stable | IIIa |
| | 3B | 095/89 | Planar | none | 312/48 | 54 | 60 | Normal | Partially stable | IIIa |
| | | | Planar | none | 278/75 | 54 | 60 | Normal | Partially stable | IIIa |
| | | | Wedge | 097/26 | 011/81,050/35 | 54 | 45 | Normal | Partially stable | IIIb |
| | | | Wedge | 072/72 | 011/81,081/72 | 54 | 60 | Normal | Partially stable | IIIa |
| | | | Wedge | 311/72 | 011/81278/75 | 54 | 60 | Normal | Partially stable | IIIa |
| | | | Direct Toppling | none | 312/48 | 54 | 60 | Normal | Partially stable | IIIa |
| | | | Direct Toppling | none | 317/20 | 54 | 60 | Normal | Partially stable | IIIa |
| | | | Direct Toppling | none | 011/81 | 54 | 60 | Normal | Partially stable | IIIa |
| | | | Direct Toppling | none | 278/75 | 54 | 9 | Very Bad | Completely unstable | Error/failure |
| | | | Direct Toppling | none | 092/85 | 54 | 60 | Normal | Partially stable | IIIa |
| | | | Flexural Toppling | none | 050/35 | 54 | 60 | Normal | Partially stable | IIIa |
| | | | Flexural Toppling | none | 011/81 | 54 | 60 | Normal | Partially stable | IIIa |
| | | | Flexural Toppling | none | 081/72 | 54 | 60 | Normal | Partially stable | IIIa |
| | 3C | 328/87 | Wedge | 290/46 | 011/81,312/48 | 54 | 60 | Normal | Partially stable | IIIa |
| | | | Wedge | 311/72 | 011/81,278/75 | 54 | 27 | Bad | Unstable | IVb |
| | | | Wedge | 072/72 | 081/72,011/81 | 54 | 60 | Normal | Partially stable | IIIa |
| | 3D | 122/87 | Wedge | 072/72 | 081/72,011/81 | 54 | 60 | Normal | Partially stable | IIIa |
| | | | Wedge | 097/26 | 050/35,011/81 | 54 | 59.4 | Normal | Partially stable | IIIa |
| | | | Direct Toppling | none | 312/48 | 54 | 47.75 | Normal | Partially stable | IIIb |
| | | | Direct Toppling | none | 278/75 | 54 | 59 | Normal | Partially stable | IIIa |
| 4 | 4A | 260/78 | Wedge | 262/74 | 310/79,327/83 | 59 | 24 | Bad | Unstable | IVb |
| | | | Wedge | 270/60 | 360/90,251/61 | 59 | 23 | Bad | Unstable | IVb |
| | | | Wedge | 250/61 | 251/61,327/83 | 59 | 23 | Bad | Unstable | IVb |
| | | | Wedge | 276/77 | 242/79,310/79 | 59 | 39 | Bad | Unstable | IVa |
| | | | Wedge | 240/61 | 251/61,310/79 | 59 | 32 | Bad | Unstable | IVa |
| | | | Wedge | 271/78 | 242/79,327/83 | 59 | 56.5 | Normal | Partially stable | IIIa |
| 5 | 5A | 062/65 | Oblique Toppling | none | Almost | 59 | 70.25 to 74 | Good | Stable | IIa |
| 6 | 6A | 004/81 | Wedge | none | Almost | 59 | 66.5 to 73.1 | Good | Stable | IIb to IIa |
| | | | Direct Toppling | none | Almost | 59 | 64 to 70.25 | Good | Stable | IIb |
| | | | Direct Toppling | none | 193/76 | 59 | 52.75 | Normal | Partially stable | IIIa |
| | | | Direct Toppling | none | 196/80 | 59 | 56.5 | Normal | Partially stable | IIIa |
| | | | Flexural Toppling | none | Almost | 59 | 70.25 to 74 | Good | Stable | IIa |
| | 6B | 163/72 | Planar | none | Almost | 59 | 71.6 to 74 | Good | Stable | IIa |
| | | | Direct Toppling | none | Almost | 59 | 70.25 | Good | Stable | IIb |
| | | | Direct Toppling | none | 335/86 | 59 | 52.75 | Normal | Partially stable | IIIa |
| | | | Direct Toppling | none | 327/88 | 59 | 56.5 | Normal | Partially stable | IIIa |
| | | | Direct Toppling | none | 356/86 | 59 | 56.5 | Normal | Partially stable | IIIa |
| | | | Flexural Toppling | none | Almost | 59 | 70.25 | Good | Stable | IIb |
| | 6C | 337/81 | Wedge | none | Almost | 59 | 65.5 to 73.1 | Good | Stable | IIb to IIa |
| | | | Direct Toppling | none | Almost | 59 | 70.25 | Good | Stable | IIb |
| 7 | 7A | 245/78 | Wedge | 218/52 | 244/55,295/80 | 55 | 46 | Normal | Partially stable | IIIb |
| | 7B | 264/78 | Wedge | 277/50 | 244/55,342/71 | 55 | 28 | Bad | Unstable | IVb |
| | 7C | 324/77 | Wedge | 324/32 | 026/53,040/69 | 55 | 28 | Bad | Unstable | IVb |
| | | | Wedge | 316/24 | 244/55,026/53 | 55 | 49.6 | Normal | Partially stable | IIIb |
| | | | Wedge | 301/38 | 244/55,011/67 | 55 | 49.6 | Normal | Partially stable | IIIb |
| | 7D | 227/77 | Wedge | 218/52 | 244/55,295/80 | 55 | 19 | Very Bad | Unstable | Va |
| | | | Wedge | 206/48 | 244/55,133/75 | 55 | 46 | Normal | Partially stable | IIIb |
| | | | Wedge | 212/35 | 295/80,133/75 | 55 | 34.3 | Bad | Unstable | IVa |
| | 7E | 290/82 | Wedge | 277/50 | 244/55,342/71 | 55 | 28 | Bad | Unstable | IVb |
| | | | Wedge | 301/38 | 244/55,011/67 | 55 | 34.3 | Bad | Unstable | IVa |
| | 7F | 110/82 | Wedge | 083/36 | 011/67,026/53 | 55 | 49.6 | Normal | Partially stable | IIIb |
| | | | Wedge | 113/38 | 060/52,040/69 | 55 | 19 | Very Bad | Unstable | Va |
| | | | Direct Toppling | none | 295/80 | 55 | 48.75 | Normal | Partially stable | IIIb |
| | | | Direct Toppling | none | 277/50 | 55 | 52.5 | Normal | Partially stable | IIIa |
| 8 | 8A | 034/85 | Wedge | 053/51 | 345/73,128/78 | 62 | 35 | Bad | Unstable | IVa |
| | | | Direct Toppling | none | Almost | 62 | 73.25 to 77 | Good | Stable | IIa |
| 9 | 9A | 022/85 | Planar | none | 014/81 | 57 | 29.5 | Bad | Unstable | IVb |
| | | | Wedge | none | Almost | 57 | 63 to 68.4 | Good | Stable | IIb |
| | | | Direct Toppling | none | Almost | 57 | 68.25 | Good | Stable | IIb |

# 7. CONCLUSIONS AND RECOMMENDATIONS

Preliminary rock fall zonation mapping is useful for field investigation. For the better quality of mapping, Field data and more parameters relating to rock fall occurrence have to be added to GIS analysis. Paleo-collapse sinkhole at coastal zone can be recurrent at the place having weakened or cavernous rockmass and high force of the sea process. The new collapse often happens at the rime of sinkhole chamber by various failure mechanisms: planar, wedge, and topple, and the event show as rockslide and rockfall.

The rockfall is defined as the one of the major geohazards in the Prasat Hin Pan Yod area. It is mainly caused by the wedge failure mechanism. Topple and planar failure is subordinate to rockfall and rockslide hazards.

The former route getting through the chamber (stations of 1A to1E, 3A to 3D, and 7A to 7F) should be avoided due to having high potential rock fall of wedge failure. Toppling and planar failure have a lower potential to be originated rock fall hazards. The rock fall hazard is expected to have occurred in small events, but it is high frequency

The line of stations 4A and 6A to 6C are said to be the safest new route to getting through the chamber. However, the wedge failure of rock fall can occur within a short distance of a sea cliff (about 3 meters). A helmet, one of the simple tools, can protect tourists from fallen rock which it is pending on sea cliffs or high places. For the linear strait, the route is narrow, and slightly strong waves in some time, kayak carrying tourists passing should be controlled and permit a one for in and out.

A limitation of the tourist number is essential for the Prasat Hin Pan Yod chamber. Tourists can spend their time in the sinkhole chamber, but they must be aware of the rockfalls of wedge failures, and avoid visitation near sea caves that it locates beneath massive limestone.

# 8. THE FUTURE WORK

Because the Prasat Hin Pan Yod has located nearby a strait, the strong wave and currents in the monsoon period can cause the broken block to movement, titling, or more fracturing. Rock mass stability and slope mass stability still need long-term site investigation and monitoring at the sea cliffs and the rim of the sinkhole chamber; therefore, Real-time kinematic (RTK) surveying will use for detecting rock displacement.

# BIBLIOGRAPHY


Ahmad Khairut , T., Ahmad, K., & Rodeano, R. (2018). An Overview of Sinkhole Geohazard Incidence Recorded in The Kinta Valley Area, Perak. *ASM Sc. J., 11, Special Issue 2, 2018 for SANREM*, pp. 19-28.

Al-Kouri, O., Al-Rawashdeh, S., Sadoun, B., Pradhan, B., & others. (2013). Geospatial modeling for sinkholes hazard map based on GIS \& RS data. *Journal of geographic information system 2013*, pp. 584-592.

Anua, N., & Zabidi, H. (2018). Petrography and Geochemistry of Kinta Valley Palaeozoic Carbonate Rock. In *Journal of Physics: Conference Series (Vol. 1082, No. 1)* (p. 012095). IOP Publishing.

Augarde, C. E., Lyamin, A. V., & Sloan, S. W. (2003). Prediction of undrained sinkhole collapse. *Journal of Geotechnical and Geoenvironmental Engineering, 129(3)*, pp. 198 – 205.

Bacic, M., Kovacecic, M. H., Libric, L., & Zuzul, P. (2021). Sinkholes induced by the Petrinja M6.2 earthquake and guidelines for their remediation. *1st Croatian Conference on Earthquake Engineering (1CroCEE)*, pp. 341 – 351.

Banks, V. J., Arnhardt, C., Ramli, Z., Ahmad, F., & Pereira, J. (2020). Sinkhole susceptibility mapping in the Kuala Lumpur and the need for a buried karst database. In *National Cave and Karst Research Institute Symposium 8*.

Bieniawski, Z. (1973). Engineering classification of jointed rock masses. *Civil Engineering= Siviele Ingenieurswese, 1973*(12), 335-343.

Bieniawski, Z. (1974a). Estimating the strength of rock materials. *Journal of South African Institute of Minerals and Metallurgy, 74*, 312-320.

Bieniawski, Z. (1974b). Geomechanics Classification of Rock Masses and Its Application in Tunneling. *3rd Congress of the International Society of Rock Mechanics* (pp. 27-32). Washington DC: Denever National Academy of Sciences.

Bieniawski, Z. (1976). Rock mass classification in rock engineering. *Proceedings of Symposium on Exploration for Rock Engineering*, *1*, pp. 97-106. Balkema, Rotterdam.

Bieniawski, Z. (1984). *Rock mechanics design in mining and tunneling*.

Bieniawski, Z. (1988). *The rock mass rating (RMR) system (geomechanics classification) in engineering practice, Rock Classification Systems for Engineering Purposes*. ASTM International.

Bieniawski, Z. (1989). *Engineering rock mass classifications: a complete manual for engineers and geologists in mining, civil, and petroleum engineering*. John Wiley & Sons.

Brady, B., & Brown, E. (2006). *Rock mechanics: for underground mining*. Springer science & business media.

Cruden, D. (1993). Cruden, DM, Varnes, DJ, 1996, Landslide Types and Processes, Transportation Research Board, US National Academy of Sciences, Special Report, 247: 36-75. *Landslides Eng. Pract*, 20-47.

Deere, D., & Miller, R. (1966). *Engineering classification and index properties for intact rock*. Illinois Univ At Urbana Dept Of Civil Engineering.

DMR. (2005). *Sinkhole potential map of Thailand*. Environmental Geology Division. Bangkok: Department of Mineral Resources.

DMR. (2016). *Seismic hazard map of Thailand*. Environmental Geology Division. Bangkok: Department of Mineral Resource.

DMR. (2020). *Landslide susceptibility map of Thailand*. Environmental Geology Division. Bangkok: Department of Mineral Resources.

Doctor, K. Z. (2008). GIS and Spatial Statistical Methods for Determining Sinkhole Potential in Frederick Valley, Maryland. *Conference: U.S. Geological Survey Karst Interest Group ProceedingsAt*. Bowling Green, KentuckyVolume: U.S. Geological Survey Scientific Investigations Report 2008-5023.

Elmahdy, S., & Mostafa, M. (2013). Natural hazards susceptibility mapping in Kuala Lumpur, Malaysia: an assessment using remote sensing and geographic information system (GIS). *Geomatics, Natural hazards and risk, 4*(1), 71-91.

Gao, R., Wang, C., Liang, Z., Han, S., & Li, B. (2021). A research on susceptibility mapping of multiple geological hazards in Yanzi river basin, China. *ISPRS International Journal of Geo-Information,10(4)*, p. 218.

Goel, R., & Singh, B. (2011). *Engineering rock mass classification: tunnelling, foundations and landslides*. Elsevier.

Goodman, R. (1989). *Introduction to rock mechanics* (2nd ed.). New York, United States of America: Wiley & Sons.

Gupta, R. (2003). *Remote sensing geology* (2nd ed.). New York, United States of America: Springer.

Hoek, E., & Bray, J. (1981). *Rock slope engineering* (3rd ed.). London: CRC Press, Institute of Mining and Metallurgy.

Khundee, S., Kererattanasathian, V., Hongsaban, N., Khlonkratoke, A., Maihom, P., & Tewa, C. (2019). *Coastal changes along the Petra Beach to Ao Noon Bay, La-ngu District, Satun Province*. Environmental Geology Division. Bangkok: Department of Mineral Resources.

Kidarn, P., & Maihom, P. (2021). *Application of Geographic Information System to Study physical loss levels in the area affected by the tsunami in Satun province*. Environmental Geology Division. Bangkok: Department of Mineral Resources, Bangkok.

Kong, T. B. (2002). *Environmental Geology of Limestone in Malaysia : Geology*. Retrieved from http://www.karst.edu.cn/public/upload/b20170609/igcp448/2002/3-2-7.pdf

Krahenbuhl, R. (1991). Magmatism, tin mineralization and tectonics of the Main Range, Malaysia Peninsula: consequences for the plate tectonic model for Southeast Asia based on Rb-Sr, K-Ar and fission track data. *Geological Society of Malaysia Bulletin, No. 29*, pp. 1-100.

Manzano, L., Lucero, A. R., Mula, E., Garas, K. L., Ondona, A., Leido, L., . . . Avellana, R. (2013). Post-Earthquake Subsidence Of Karst In Southwestern Bohol. *An Introduction. Training on Disaster Risk Reduction: The Role of DOST Regional Offices, December 10 – 12*. Quezon City.: PHIVOLCS Auditorium.

Markland, J. T. (1972). A useful technique for estimating the stability of rock slopes when the rigid wedge slide type of failure is expected. *Interdepartmental Rock Mechanics Project* (p. 10). London: Imperial College of Science and Technology.

Marto, A., Tan, C., Kasim, F., & Mohd Yunus, N. (2013). Seismic impact in peninsular Malaysia. *Proceedings of the 5th International Geotechnical Symposium*. Incheon, Seoul, Korea.

Meesook, A. (2014). *Lithostratigraphy, Faunal assemblages, Biodiversity, Paleocology and Environment of Deposition of the Cambrian-Permian Rocks in Satun Province, Peninsular Thailand Technical report contract No. 39/2557*. Bureau of Geological surve. Bangkok: Department of Mineral Resources.

Meng, C. C., Pubellier, M., Abdeldayem, A., & Sum, C. W. (December, 2016). Deformation styles and structural history of the Paleozoic limestone, Kinta Valley, Perak, Malaysia. In *Bulletin of the Geological Society of Malaysia, Volume 62* (pp. 37 – 45). Geological Society of Malaysia (GSM).

Meng, C., & Pubellier, M. (2015). Geological Structures of the Kinta Valley Revisited Using Drainage Anomalies. In M. Awang, B. Negash, N. Md Akhir, & L. Lubis (Ed.), *ICIPEG 2014* (pp. 267-276). Singapore: Springer.

Meng, C., Sautter, B., Pubellier, M., Menier, D., Chow, W., & Askury, A. (2015). *Geological Features Of The Kinta Valley: Platform, Vol 10 No 2*.

Mohd, H., Mohd, H., Mohd, I., Nor, K., Mohd, H., Kamarul, I., . . . Aditya, S. (2021). Hujan Asid: Satu Kajian Awal Di Ipoh, Perak. *sian Journal of Environment, History and Heritage June 2021, Vol. 5, Issue. 1*, 25-39.

Muhammad, R. (2018). The Extreme Karstification of the Kinta Valley, West Malaysia. *Proceedings of the 15th Sinkhole Conference*, (pp. 297 - 306).

Muhammad, R., Al-kouri, O., Yassin, R., & Lat, C. (2011). Geophysical reconnaissance of karst sinkhole occurrences in Jeram, Kinta Valley, West Malaysia after the 2004 Indian Ocean earthquake. *Asian Trans-Disciplinary Karst Conference*. Yogyakarta.

Oh, H.-J., & Pradhan, B. (2011). Application of a neuro-fuzzy model to landslide-susceptibility mapping for shallow landslides in a tropical hilly area. *Computers & Geosciences 37*, 1264–1276.

Omar, M. Z., & Main, R. (2011). *The Impact of Acid Rain on Historical Buildings in Kuala Lumpur, Malaysia. Design Principles and Practices: An International Journal Volume 5, Issue 6*.

Ozdemir, A. (2015). Susceptibility Mapping Using a Frequency Ratio Method and GIS Technology near Karapinar, Konya-Turkey. *Proceedia Earth and Planetary Science 15*, 502 – 506.

Palmström, A. (1982). Volumetric Joint Count – A successful and Simple Measure of The Degree of Rock Mass Jointing. *4th International Congress*. *4*, pp. 221-228. New Delhi: International Association of Engineering Geology.

Pantaweesak, P., Sontamino, P., Tonnayopas, D., & Vattanasak, H. (2017). PSU-RSR v. 1: An initial android application for estimating rock mass stability. *Proceedings of Coal Mining and Utilization for Sustainable Development International Conference*, (pp. 23-24).

Pradhan, B., & Lee, S. (2010). Delineation of landslide hazard areas on Penang Island, Malaysia, by using frequency ratio, logistic regression, and artificial neural network models. *Environ Earth Sci, 60*(5), 1037–1054.

Pradhan, B., Abokharima, M., Jebur, M., & Tehrany, M. (2014). Land subsidence susceptibility mapping at Kinta Valley (Malaysia) using the evidential belief function model : GIS. *Nat Hazards, 73*(2), 1019–1042.

Rajah, S. (1979). The Kinta Tinfield, Malaysia. *Geological Society of Malaysia Bulletin 11*, 111 – 136.

Rashid, M., Ahmad, H., Jamil, S., Yahaya, N., & Othman, M. (2015). A Review of Ex-Mining Land Reclamation as Construction Project Activities: Focusing in City of Ipoh. *Proceedings of Postgraduate Conference on Global Green Issues (Go Green)* (pp. 333 – 339). Perak, Malaysia: UiTM.

Romana, M. (1985). New adjustment ratings for application of Bieniawski classification to slopes. *Proceedings of the international symposium on role of rock mechanics*, (pp. 49-53). Zacatecas, Mexico.

Rosdi, M., Othman, A., Abdul, M., & Yusoff, Z. (2017). SINKHOLE SUSCEPTIBILITY HAZARD ZONES USING GIS AND ANALYTICAL HIERARCHICAL PROCESS (AHP): A CASE STUDY OF KUALA LUMPUR AND AMPANG JAYA. *International Archives of the Photogrammetry, Remote Sensing & Spatial Information Sciences, 42*, 145-151.

Saaty, T. (1977). A scaling method for priorities in hierarchical structures. *Journal of mathematical psychology, 15*(3), 234-281.

Saaty, T. (1980). *The analytic hierarchy process (AHP) for decision making* (Vols. 1-69). Kobe, Japan.

Siddique, T., Masroor Alam, M., Mondal, M., & Vishal, V. (2015). Slope mass rating and kinematic analysis of slopes along the national higway-58 near Jonk, Rishikesh, India. *Journal of Rock Mechanics and Geotechnical Engineering, 7*, 600-606.

Singh, B., & Goel, R. (2011). *Engineering rock mass classification: tunnelling, foundations and landslides*. Elsevier.

Sinsakul, S. (1988). *Geological map of Amphoe Langu (4922 I) map sheet*. Bangkok: Department of Mineral Resources.

Sinsakul, S., Tiyapairach, S., Chaimanee, N., & Aramprayoon, B. (2002). *Coastal change along the Andaman Sea coast of Thailand*. Geological Survey Division. Bangkok: Department of Mineral Resource.

Suntharalingam, T. (1968). *Upper Palaeozoic stratigraphy of the West of Kampar, Perak*. Geological Society of Malaysia (GSM).

Taheri, K., Gutierrez, F., Mohseni, H., Raeisi, E., & Taheri, M. (2015). Sinkhole susceptibility mapping using the analytical hierarchy process (AHP) and magnitude–frequency relationships: A case study in Hamadan province, Iran. *Geomorphology, 234*, 64–79.

Tan, Y., & Chow, C. (2012). FOUNDATION DESIGN AND CONSTRUCTION PRACTICE IN LIMESTONE AREA IN MALAYSIA. pp. 21-43.

Tangang, F., Juneng, L., Salimun, E., Sei, K., & Halimatun, M. (2012). Climate change and variability over Malaysia: gaps in science and research information. *Sains Malaysiana, 41*(11), 1355-1366.

Thepju, W., Yamansabedean, N., & Bamrungsong, P. (2017). Karst features in Satun Geopark, Satun province. *DMR-CCOP-TNCU Technical Seminar on " Biostratigraphy and Karst Morphology of Satun Aspiring Geopark*, (pp. 50-59). Bangkok, Thailand.

Tiyapairach, S. (2004). *Geological map of Ban Pak Bara (4922 IV) map sheet*. Bangkok, Thailand: Department of Mineral Resources.

Tonnayopas, D., Charitgnam, T., & Chaowanontakit, S. (1994). Correlation between Compressive strength value in rock mass and intact rock. *5th Mining conference 24-25 Nov 1994* (pp. 3-134-3-148). Mineral Industry and Energy for Economic Development, Department of Mining and Metallurgical Engineering, Faculty of Engineering, Prince of Songkla University.

Triana, K., & Hermawan, K. (2020). Slope mass rating-based analysis to assess rockfall hazard on Yogyakarta Southern Mountain, Indonesia. *Geoenvironmental Disasters, 7*, 1-14.

United Nations. (2015). Transforming our world: The 2030 agenda for sustainable development.

Varnes, D. (1978). Slope Movement Types and Processes. In R. Schuster, & R. Krizek, *Landslides, Analysis and Control, Transportation Research Board, Special Report No. 176* (pp. 11-33). Washington D.C.: National Academy of Sciences.

Waltham, A., & Fookes, P. (2003). Engineering classification of karst ground conditions. *Quarterly Journal of Engineering Geology and Hydrogeology, 36*(2), 101-118.

Waltham, T., Bell, F., Culshaw, M., Knez, M., & Slabe, T. (2005). *Sinkholes and subsidence: karst and cavernous rocks in engineering and construction* (Vol. 382). UK: Springer.

Wong, C., Venneker, R., Uhlenbrook, S., Jamil, A., & Zhou, Y. (2009). Variability of rainfall in Peninsular Malaysia. *Hydrology and Earth System Sciences Discussions, 6*(4), 5471-5503.

Wongvanish, T. (1990). Lithostratigraphy, sedimentology, and diagenesis of the Ordovician carbonates, Southern Thailand. 215. University of Tasmania, unpublished Ph.D. thesis.

Wyllie, D., & Mah, C. (2004). *Rock slope engineering* (4th ed.). UK: CRC Press.

Xiaomin, Q., Shuo-Sheng, W., & Yan, C. (2020). Sinkhole susceptibility assessment based on morphological, imagery, and contextual attributes derived from gis and imagery data. *Journal of Cave and Karst Studies, 82*(1), 1-17.

Yassin, R., Muhammad, R., & Hj-Taib, S. (2013). Integrated Techniques To Identify Consequences Of Sinkhole Hazards For Constructing Housing Complexes On Carbonate Karst Terrains In Perak. *Peninsular Malaysia, 2*(7).

Yassin, R., Muhammad, R., & Taib, S. (2014). Determine Sinkholes and overburden thicknesses in selected covered carbonate Karst Terrains (Kinta valley), Perak, Malaysia by combining Wenner ER Tomography, geological and satellite images techniques. *Journal of Geography and Geology, 6*(4), 199.

Yoon, W., Jeong, U., & Kim, J. (2002). Kinetic analysis for sliding failure of multi-faced rock slopes. *Engineering geology, 67*(1-2), 51-61.

Yunus, A. R., Chow , W. S., & Jamaluddin, O. (2003). Sinkholes in the Bukit Chuping area, Kangar, Perlis. *Geological Society of Malaysia. Bulletin 46*, pp. 87 – 92.

Zhou, W., Beck, B. F., & Adams, A. L. (2003). Sinkhole risk assessment along highway I-70 near Frederick, Maryland. *Ninth Multidisciplinary Conference on Sinkholes and the Engineering and Environmental Impacts of Karst September 6-10, 2003*. Huntsville, Alabama, United States.